

## ABSTRACT

ACKETT, RYAN WAYNE. Evaluation of Drought-Tolerant Bermudagrass Response to Water-Saving Irrigation Scheduling Methods. (Under the direction of Dr. Chadi Sayde).

New, drought tolerant turfgrass cultivars have the potential to reduce water usage while maintaining desirable turfgrass aesthetics. The response of visual quality of TifTuf hybrid bermudagrass (*Cynodon dactylon* x *C. transvaalensis*) to varying levels of deficit irrigation and frequency was measured by three assessment methods. Two of the methods, the visual assessment and the hand-held NDVI meter methods, are conventionally used in the turfgrass industry. A third method was developed to overcome the two main limitations that the conventional methods suffer from i.e. high labor input requirements, and low temporal resolution. For that, a stationary mounted camera system was proposed as an alternative imagery collection method, and an algorithm was developed to independently measure the NDVI of twenty-four turfgrass plots within view of the camera. Solar position during a single day was determined to strongly predict diurnal shifts in turfgrass NDVI ( $R^2 = 0.87$ ), and turfgrass mowing direction was also determined to have a significant effect on NDVI (p-value = 0.0063). The NDVI calculated from the developed model proved a good predictor of ground truthing data ( $R^2 = 0.71$ ).

In response to varying levels of deficit irrigation treatments, only the mean visual quality of unirrigated TifTuf bermudagrass was significantly lower than that of the highest quality treatment (80% ET) as measured by three methods of assessing turf quality. Overirrigation (120% ET) also resulted in significantly lower mean quality than the highest quality treatment as measured by camera-based NDVI. Unirrigated turfgrass experienced the highest number of days below acceptable quality (18-31 days during a 90 day period), while the 40% ET treatment

experienced 5 days of unacceptable quality measured only by NDVI meter. From all sources, the unirrigated turfgrass received 55.8 mm less water over 90 days than the 100% ET treatment, while the 40% ET treatment received 38.8 mm less water than the 100% ET treatment. Water savings achieved by deficit irrigation during this study by the 80% ET, 60% ET, 40% ET, and 0% ET treatments were, respectively: 29.8 mm, 58.6 mm, 90.7 mm, and 159 mm.

The ability of NDVI measurements determined either by the developed camera system or the hand-held NDVI system, as well as the commonly used soil moisture sensing to predict water stress during a drought was also evaluated. Of the three, soil moisture was the strongest predictor of water stress coefficient ( $R^2 = 0.87$ ), while the camera-based NDVI ( $R^2 = 0.63$ ) outperformed handheld NDVI measurements ( $R^2 = 0.53$ ). The sensitivity of sensors to early signs of stress were also determined through progressive partial regression to determine the no-effect ranges of each sensor data to the water stress coefficient. Again, soil moisture outperformed other sensors, with a significant response to water stress over its full range. The camera system responded significantly to declining water stress below a coefficient of 0.37, while handheld meter measurements responded significantly only to water stress coefficients below 0.24. From limited data, visual quality ratings were determined to decline significantly below stress coefficients of 0.34.

© Copyright 2022 by Ryan Wayne Ackett

All Rights Reserved

Evaluation of Drought-Tolerant Bermudagrass Response to Water-Saving Irrigation Scheduling  
Methods

by  
Ryan Wayne Ackett

A thesis submitted to the Graduate Faculty of  
North Carolina State University  
in partial fulfillment of the  
requirements for the degree of  
Master of Science

Biological and Agricultural Engineering

Raleigh, North Carolina  
2022

APPROVED BY:

---

Dr. Chadi Sayde

---

Dr. Grady Miller

---

Dr. Sierra Young

## **DEDICATION**

To my parents, Wayne and Jennifer, for a lifetime of support, and to Onyx, whom I could not have done this without.

## **BIOGRAPHY**

Ryan Ackett was born in St. Petersburg, Florida to Wayne and Jennifer Ackett. Ryan discovered his love for agriculture and water resources in college, where he discovered he could apply engineering skills to global challenges of food production and resource management.

After completing undergraduate studies at the University of Florida, Ryan worked as the supervisor of research and development on a citrus farm in South Florida. After three years of growth and learning in the field, he returned to school to pursue research at North Carolina State University. There Ryan was offered the chance to pursue a master's degree and his passion of sustainable agricultural water management research with Dr. Chadi Sayde. Ryan was able to develop as a researcher and reignite his enthusiasm for solving big problems. After graduating, Ryan hopes to continue on his path as a researcher building a resilient and sustainable food system.

## TABLE OF CONTENTS

List of Tables .....	vii
List of Figures .....	ix
Chapter One: Literature Review .....	1
Turfgrass Visual Quality and Water Saving Irrigation Strategies .....	2
Vegetation Indices and Assessing Turfgrass Visual Quality .....	5
Chapter Two: A automated assessment of turfgrass visual quality using a pole mounted camera system .....	11
Abstract .....	12
Introduction .....	12
Materials and Methods .....	15
Site Description and Camera Installation .....	15
Image Acquisition .....	19
Image Processing .....	22
Data Verification and Cleaning .....	33
Analysis and Modeling .....	36
Solar Azimuth Correction .....	37
Model Development .....	42
Model Validation .....	50
Discussion of Data Collection Methods .....	51

Conclusion .....	54
Chapter 3: Response of TifTuf Bermudagrass to Irrigation Frequency and Deficit Irrigation ....	56
Abstract.....	57
Introduction.....	57
Materials and Methods.....	59
Site Description .....	59
Experimental Design .....	60
Visual Quality Assessments .....	63
Zone Application Rate.....	64
Irrigation Runtime Calculations .....	66
Results and Discussion .....	70
Water Management.....	70
Site Management, Challenges, and Effect on Data .....	75
Visual Ratings of Turf Quality .....	77
Relating NDVI Assessment Methods to Quality Ratings .....	77
Significance of Turfgrass Quality Differences Between Irrigation Treatments.....	84
Acceptability of Turfgrass Quality Within Treatments by Each Method .....	86
Unirrigated Turfgrass Quality .....	93
Unirrigated Turfgrass Stress Recovery.....	95
Overirrigated Turfgrass Quality .....	96

Comparison of Turfgrass Quality Assessment by Each Method.....	99
Conclusions.....	106
Chapter 4: Early Detection of Turfgrass Water Stress.....	109
Abstract.....	110
Introduction.....	110
Materials and Methods.....	113
Analysis and Results.....	115
Data Cleaning.....	115
Soil Moisture Deficit and Water Stress.....	120
TCM 500 NDVI Sampling and Stress Coefficient.....	127
Imagery Based NDVI and Stress Coefficient.....	131
Summary of Predictive Models.....	136
Early Detection of Water Stress.....	136
Summary of Water Stress Detection Sensitivity.....	141
Conclusions.....	143
References.....	146

## LIST OF TABLES

### Chapter Two

Table 2.1: Linear regressions of the average NDVI and solar azimuth.....	40
Table 2.2: Partial effects tests of all initial model predictors and interactions .....	47
Table 2.3: Parameter estimates of all initial model predictors and interactions .....	48
Table 2.4: Partial effects test results of the first revised model .....	48
Table 2.5: Partial effects test results of the final model.....	49

### Chapter Three

Table 3.1: Average irrigation, effective rainfall, and soil moisture of treatments .....	72
Table 3. 2: Pairwise difference comparison of turfgrass quality under varying irrigation treatments, as assessed by visual quality ratings, TCM 500 NDVI measurements, and imagery-based NDVI .....	84
Table 3.3: Estimated days of unacceptable turfgrass quality measured by three assessment methods during a 90 day period.....	88
Table 3.4: Average standard error of NTEP turfgrass quality ratings over a three month period across irrigation treatments by three assessment methods .....	102

### Chapter Four

Table 4.1: AVONA table of the final model using TCM 500 as the predictor of water stress coefficient .....	130
Table 4.2: ANOVA of the final model using camera-based NDVI as the predictor of water stress coefficient (Equation 6) .....	135
Table 4. 3: Fitness of models using sensor data to predict the water stress coefficient of turfgrass.....	136

Table 4. 4: Summary of breaking points defining no-effect areas of turfgrass sensors and  
water stress coefficient..... 142

## LIST OF FIGURES

### Chapter Two

Figure 2.1: Pole Mounted camera system installed at the field site.....	17
Figure 2.2: Camera system electronics installation .....	19
Figure 2.3: Flow chart of the image processing algorithm developed.....	24
Figure 2.4: Camera imagery after colored circles were drawn around identified keypoints .....	26
Figure 2.5: Matching keypoints between the template image (right) and the image to be registered (left) .....	27
Figure 2.6: Two registered images with blue shading drawn over pixels within plot boundaries. The left image represents successful registration and plot area identification, while the right image represents registration resulting in misalignment of plot areas .....	34
Figure 2.7: Histogram of the pixels within one plot from one red and one NIR image, before and after exposure correction. ....	35
Figure 2.8: Diurnal changes in the average NDVI across all plots.....	38
Figure 2.9: Linear regressions of the NDVI of turfgrass calculated from imagery taken at different solar positions.....	39
Figure 2.10: Residuals by predicted plot of the initial model.....	45
Figure 2.11: Normal quantile plot of the initial model.....	45
Figure 2.12: Studentized residuals plot of the initial model .....	46
Figure 2.13: Normal plot of effects included in the initial model .....	46
Figure 2. 14: Actual NDVI of plots measured by TCM 500 versus the predicted NDVI using imagery and the developed model .....	50

### Chapter Three

Figure 3.1: Experimental design and field site diagram .....	63
Figure 3.2: Cumulative potential evapotranspiration and water received by turfgrass plots in each treatment .....	71
Figure 3.3: Average volumetric soil moisture of turfgrass plots in each treatment.....	73
Figure 3.4: Box and whisker plot of soil moisture measurements throughout the experimental period.....	74
Figure 3.5: Average NTEP visual ratings of turfgrass of each treatment.....	77
Figure 3.6: TCM 500 NDVI of turfgrass under irrigation treatments .....	78
Figure 3.7: Camera-based NDVI of turfgrass under irrigation treatments .....	78
Figure 3.8: Visual quality and TCM 500 NDVI of turfgrass plots measured on the same day ....	79
Figure 3.9: Distribution of TCM 500 NDVI measurements of turfgrass with varying rated visual qualities.....	81
Figure 3.10: Median NDVI of turfgrass plots with visual quality rated between 4 and 8.....	81
Figure 3.11: Estimated average turfgrass visual quality by TCM 500 NDVI measurements .....	83
Figure 3.12: Estimated average visual turfgrass quality by camera-based NDVI measurements.....	83
Figure 3.13: Least squared means of visual quality of turfgrass treatments.....	85
Figure 3.14: Least squared means of TCM 500 NDVI of turfgrass treatments.....	86
Figure 3.15: Least squared means of imagery-based NDVI of turfgrass treatments .....	86
Figure 3.16: Daily estimated visual quality ratings of turfgrass treatments . .....	91
Figure 3.17: Daily estimated visual quality of turfgrass treatments .....	92

Figure 3.18: Daily estimated visual quality of turfgrass treatments by camera-based NDVI .....	93
Figure 3.19: Estimated visual quality of unirrigated turfgrass by three assessment methods and soil moisture content over time .....	94
Figure 3.20: Estimated visual quality of overirrigated turfgrass by three assessment methods and soil moisture content over time .....	97
Figure 3.21: Low density and dollar spot observed in overirrigated turfgrass in Plot 7 and Plot 8 .....	98
Figure 3.22: Visual quality and standard error of turfgrass plots irrigated at 100% ET four times weekly .....	101
Figure 3.23: Visual quality and standard error of unirrigated turfgrass plots.....	105

## **Chapter Four**

Figure 4.1: Original dataset of average water stress coefficients of three unirrigated turfgrass plots .....	117
Figure 4.2: Cleaned dataset of average water stress coefficients of three unirrigated turfgrass plots .....	120
Figure 4.3: Volumetric water content of topsoil in three unirrigated turfgrass plots .....	121
Figure 4.4: Daily turfgrass water stress coefficient and predawn soil volumetric water content .....	122
Figure 4.5: Daily turfgrass water stress coefficient and predawn soil moisture depletion .....	124
Figure 4.6: Normal quantile plot of second order linear model using soil moisture depletion as the predictor of water stress coefficient .....	125
Figure 4.7: Studentized residuals plot of second order linear model using soil moisture depletion as the predictor of water stress coefficient .....	125

Figure 4.8: Residuals plot of second order linear model using soil moisture depletion as the predictor of water stress coefficient .....	125
Figure 4.9: Actual by predicted plot of the final model using soil moisture depletion as the predictor of water stress coefficient (Equation 4) .....	127
Figure 4.10: Daily water stress coefficient and TCM 500 NDVI of unirrigated turfgrass plots .....	128
Figure 4.11: Normal quantile plot of second order linear model using TCM 500 NDVI as the predictor of water stress coefficient.....	129
Figure 4.12: Studentized residuals plot of second order linear model using TCM 500 NDVI as the predictor of water stress coefficient .....	129
Figure 4.13: Residuals versus predicted plot of second order linear model using TCM 500 NDVI as the predictor of water stress coefficient .....	129
Figure 4.14: Actual by predicted plot of the final model using TCM 500 as the predictor of water stress coefficient (Equation 5) .....	131
Figure 4.15: Daily water stress coefficient and camera-based NDVI of unirrigated turfgrass plots .....	132
Figure 4.16: Studentized residuals plot of second order linear model using camera-based NDVI as the predictor of water stress coefficient .....	133
Figure 4.17: Residuals by predicted plot of second order linear model using camera-based NDVI as the predictor of water stress coefficient .....	133
Figure 4.18: Normal quantile plot of second order linear model using camera-based NDVI as the predictor of water stress coefficient .....	134

Figure 4.19: Actual by predicted plot of the final model using camera-based NDVI as a predictor for water stress coefficient (Equation 6) .....	135
Figure 4. 20: Breaking point defining the no-effect range between the water stress coefficient and visual quality ratings of turfgrass .....	138
Figure 4.21: Breaking point defining the no-effect range between the water stress coefficient and TCM 500 measurements of NDVI of turfgrass .....	139
Figure 4.22: Breaking point defining the no-effect range between the water stress coefficient and pole mounted camera-based NDVI of turfgrass .....	140
Figure 4.23: Attempt to identify a breaking point defining a no-effect range between the water stress coefficient and soil moisture depletion of turfgrass.....	141

## **CHAPTER ONE: LITERATURE REVIEW**

## **Turfgrass Visual Quality and Water Saving Irrigation Strategies**

Turfgrasses are a significant agricultural crop in the United States. In 2005 it was estimated that managed turfgrasses combine to cover a total land area of 163,812 km<sup>2</sup> in the continental United States, a land area three times greater than that devoted to the next largest irrigated crop and equivalent to 1.9% of its total terrestrial surface area (Milesi et al., 2005). Turfgrasses are highly concentrated in urban population centers, where they comprise the primary pervious land cover (Milesi et al., 2005). In these areas, turfgrasses may serve as ground covers in residential lawns, corporate and industry grounds, parks and sporting grounds, golf courses, education center campuses, and more. These urban areas where turfgrasses are ubiquitous are also home to more than 80% of the total US population according to the 2010 US Census. What's more, the trend of low density urbanization characteristic of suburban sprawl in American cities creates disproportionately more land for turfgrass cover in urban landscapes (Nemani et al., 2009).

Turfgrasses are distinct from pasture and native grasses in that they are specially selected for certain aesthetic and traffic qualities, and as such are dominated by a small number of mostly nonnative species and require comparatively intensive management investments (Robbins et al., 2001; Thompson & Kao-Kniffin, 2017). Monoculture lawns as thought of today in fact originated in 16th century England as status symbols for landed elite, who could afford to devote resources and land into a crop which does not produce food (Bormann et al., 2001). To this day, well-manicured lawns contribute to improved land and home values (Henry, 1999).

As often nonnative species, turfgrasses require irrigation in most areas that they are grown in the United States (Nemani et al., 2009). In the warm south, the most common turfgrass species are bermudagrass, centipedegrass, and St. Augustinegrass (Thompson & Kao-Kniffin,

2017). Because of turfgrasses' concentration in population centers, their irrigation can comprise a major portion of total area freshwater usage. Turfgrass water consumption can range widely between climate regions in the US. A study of twelve cities in different climactic regions found outdoor residential water use, which is primarily lawn irrigation, to range from 22-38% of total residential water usage in cities with cool climates, to 59-67% in warm and dry climates (Opitz et al., 1999). Haley et al. estimated that turfgrass irrigation accounted for 64% of all residential water use across central Florida (Haley et al., 2007). These findings closely relate to a study of residential lawns in Utah which found lawn irrigation responsible for 61% of total homeowner water use during the turfgrass growing season (Reza Aurasteh et al., 1984). Residential water usage also makes up a majority of all total public water use, indicating that lawn irrigation alone comprises a substantial portion of total public-supply water use (Haley et al., 2007).

These high and spatially concentrated water usage rates necessary to maintain aesthetic turf can come at ecological costs and put strain on municipal water supplies. In order to mitigate high irrigation water consumption, water management districts are often forced to place limitations on lawn irrigation such as frequency and time of day restrictions, even in regions with high average annual rainfall (Haley et al., 2007; Ozan & Alsharif, 2013). Increasing lawn irrigation water use Tampa, Florida in combination with low flow in the St. Johns River have contributed to local water supplies being exhausted (Ozan & Alsharif, 2013). However, the efficacy of such lawn irrigation policies is uncertain. Investigations into the response in water usage following the implementation of water ordinances have shown that irrigation usage may not decrease (Ozan & Alsharif, 2013). Many factors work against the efficacy of such regulations, including negligible fines and small enforcement budgets. Additionally, there are significant social and financial pressures to prioritize the visual quality of one's lawn over

ordinance compliance. A fine might be considered a small price to pay to maintain or increase property values, which have been shown to be linked to a healthy and attractive green lawn (Henry, 1999). Homeowners are highly conscious of this relationship between lawn quality and home value, and not only take care to maintain their own lawns but also put pressure on neighboring homeowners to do the same (Clayton, 2007; Robbins et al., 2001; Sisser et al., 2016). In the American culture, luscious lawns are often considered to hold not just investment value but moral value. A healthy lawn is perceived as a social responsibility to one's neighbors and a general sign of a responsible and upstanding citizen (Harris & Brown, 1996; Robbins et al., 2001). While one's water consumption is not socially conspicuous, the state of one's lawn certainly is, which may help to explain the prioritization of lawn quality over local irrigation restrictions.

Between the strong desire for homeowners to maintain attractive lawns and the need for water management districts to sustainably manage local supplies lies the potential for turfgrasses and irrigation strategies which together can maintain healthy visual appearance under reduced water consumption. Drought causes stress to turfgrass which may manifest in decreased visual quality, with symptoms including browning leaf blades, wilting, firing, and decreased green cover area (Jespersen et al., 2019). Turfgrasses may possess one or several physiological traits that help to maintain higher quality while experiencing a water deficit. The two general strategies of drought tolerance traits can be categorized as drought avoidance, by which grasses develop the ability to continue to better maintain water content in dry conditions, and drought tolerance, by which grasses may better maintain metabolic activity under dry conditions (Katuwal et al., 2020). Through these strategies, turfgrasses may avoid drought stress or the symptoms of drought stress which negatively impact visual quality. Thus, by developing and selecting these

turfgrass varieties capable of using one or both of these strategies, lawn owners might better satisfy both the social and cultural desire for a lush green lawn while reducing water consumption and alleviating stress on local municipalities.

However, even with the use of drought tolerant turfgrass varieties, there remains at least one more hurdle to clear before the benefits of water savings may be achieved. Unlike other crops, a significant portion of those who grow turfgrasses are not professionals but do so recreationally. Because of strong motivations to maintain a green lawn, homeowners have often been shown to excessively irrigate, likely as a result of taking a ‘better safe than sorry’ approach to inputs and a lack of comprehension of the consequences of overirrigation. The majority of homeowners studied over five years in Alberta, Canada were found to have overirrigated when compared to evapotranspiration estimated by the Jensen Haise method (Berg et al., 1996). Nine homes studied in central Florida over a three year period were found to have applied an average of 2.4 times the amount of water required (Haley et al., 2007). A study of ten homeowners with solid set irrigation systems found homeowners to apply 38% more water than required, although poor distribution uniformity meant that much of the lawn area was still underwatered (Reza Aurasteh et al., 1984).

### **Vegetation Indices and Assessing Turfgrass Visual Quality**

Implicit in the supposition that strong evidence of acceptable visual quality of turfgrass under water saving irrigation strategies will change management decisions toward using these strategies is the ability to reliably and objectively measure turfgrass visual quality. The traditional method of assessing visual quality is for a trained person to rate areas of turfgrass on a number system according to a set of standards. One such standard is the National Turfgrass

Evaluation Program (NTEP), in which turfgrass is rated on a scale from 1 to 9, where 1 represents the lowest visual quality, 9 represents the highest visual quality, and 5 represents minimally acceptable visual quality (Morris & Shearman, 1998). However, such a method is inherently subjective and prone to bias and inaccuracies (Keskin et al., 2003). Over any given surface area, turfgrass cover will be comprised of many different plants, and leaves within even a single plant will be of different heights and colors. Turfgrass quality is therefore highly spatially heterogeneous, and rating a given area involves making quick estimations about what percentages of the area is of better and worse qualities and assigning an average. Ratings may therefore be affected by personal biases on what constitutes acceptable and unacceptable turfgrass, their individual eyesight, and other factors which vary from person to person and even measurement to measurement (Keskin et al., 2003; Nutter et al., 1993). The 1 to 9 scale used also lacks the ability to describe small differences in turfgrass visual quality, either underrepresenting them by rating different qualities of turf equally, or overrepresenting them by rating these areas consecutive numbers when a smaller difference is merited.

Another shortcoming of this method is the time requirement by a trained rater. It can be time consuming to rate large areas of turfgrass, and brevity comes at direct expense of the spatial resolution of measurements. It also requires the use of a specially trained individual, who may not be available at the times and frequencies that quality measurements are desired, therefore this method is also likely to lead to low temporal resolution of data collection. Researchers hoping to collect data on turfgrass visual quality may be therefore limited when using this method, and homeowners and other turfgrass managers may not have access to this method of assessing visual quality at all.

Since the 70s, the spectral reflectance of plants measured through camera imagery has been used as an indication of plant health. Plant stress induces physiological changes in plant tissue which changes the reflectance of visible and invisible light, which can be used to detect and quantify stress (Kim et al., 2011). Reflectance in the visible red light band is strongly associated with chlorophyll concentration, with lower reflectance being related to an increased absorption by chlorophyll and therefore higher chlorophyll concentration and higher plant visual quality (Trenholm et al., 1999). Because light reflectance in this band is visually apparent, changes are more strongly related to visual assessments than changes in invisible light bands (Bremer et al., 2011b). For example, visible red light reflectance has been shown to strongly correlate with visual assessments of turfgrass disease severity (Nutter et al., 1993).

Beyond quantifying visual plant qualities, spectral radiometry is also indicative of invisible plant physiological changes related to stress. Near infrared light may also be detected by cameras, and its reflectance by plant tissue is related to the degree of light scattering within tissue. This scattering may be affected by several qualities, such as cellular damage induced by disease or water stress which create discontinuities leading to increased light scattering and reflectance (Bremer et al., 2011b; Trenholm et al., 1999). Near infrared (NIR) reflectance may therefore be used to detect physiological changes in plants resulting from stress which have not yet manifested visibly, allowing for advanced detection of stress. Near infrared reflectance has been shown to correlate to plant water status (Peñuelas et al., 1993).

The combination of reflectance levels in multiple light bands have been used to more comprehensively estimate plant health than reflectance of a single band. The first and most common index used to assess plant health is the Normalized Difference Vegetation Index (NDVI), which compares the reflectance by plant tissue of red and near infrared light. NDVI has

commonly been used as an objective and reproducible method to assess turfgrass visual quality, being able to evenly measure the full canopy area without the disadvantages of human bias (Bremer et al., 2011b). Strong correlation between NDVI and turf visual quality ratings has been demonstrated (Bremer et al., 2011b; Trenholm et al., 1999).

The most common methods of assessing crop health through NDVI involve the collection of aerial imagery by unmanned aerial vehicle (UAV) or satellite (Xiang & Tian, 2011). Like expert visual ratings, these methods are likely to come with limitations on temporal resolution- satellite imagery frequency is dependent on the orbit of the satellite and may only be in position once every few days or weeks, while drone imagery requires labor and favorable weather conditions which makes high frequency imagery challenging.

Stationary cameras overlooking an area of interest have been used as an alternative to UAV and satellite imagery in the generation of vegetation indices. In these systems, one or more cameras are mounted on a tall pole or nearby building and are controlled remotely or automatically to collect imagery at designated time intervals. Such designs offer advantages such as the elimination of labor time required to collect additional imagery and potentially infinite temporal resolution, which make these systems potentially valuable as continuous crop monitoring systems. Xiang and Tian (2011) developed a complete system for the automatic imagery acquisition, processing, and vegetation indices generation for monitoring corn research trials under different fertilization treatments. A tower mounted camera system with motorized control of camera position was also developed to generate NDVI imagery in a full 360 degree field of view surrounding the tower (Ahamed et al., 2012). Further improvements to imagery processing were made in orthorectification to eliminate the overrepresentation of nearer areas with higher pixel resolution when calculating the average NDVI value for a given area.

More easily than other methods of generating spectral radiometry, these systems have the potential to be integrated into other management programs for automatic crop health data collection, such as soil moisture and weather data collection, and used to trigger timely management decisions. These systems also have great potential for researchers in the generation of high temporal resolution crop health data. Considering NDVI's close correlation with visual turf quality ratings, pole mounted camera systems may provide an ideal solution to objectively and repeatably assessing turfgrass quality at high frequency.

However, turfgrass is dissimilar to other food crops with which pole mounted camera systems have previously utilized in some important respects. Most notably, turfgrasses are frequently mowed to maintain a regular canopy height, which tends to leave behind mowing 'stripes' in line with the mower direction. These stripes are visible to the human eye and create areas of darker and lighter appearing turfgrass which depend on the position of the viewer. Mowing stripes are not an indication of actual turf health or greenness despite their effect on the visual appearance of color, and therefore the effect of mowing patterns on vegetation indices must be investigated before NDVI captured from a tower mounted position can reliably be used to assess turfgrass quality.

The effect of varying levels of deficit irrigation on the visual quality of drought tolerant bermudagrass and the efficacy of using pole mounted camera systems acquired NDVI to assess turfgrass visual quality will be studied synergistically. First, this analysis will detail the development of a pole mounted camera system and software pipeline, including image acquisition and processing, in the measurement of turfgrass NDVI. The research will assess potential factors affecting NDVI derived from imagery with an acute angle of incidence, and a full model relating NDVI measured by the camera system to ground truthing data will be

developed. NDVI data generated through this method will ultimately be compared to ground truthing data of turfgrass visual quality in order to evaluate its efficacy in assessing turfgrass NDVI.

This research will also study the response of drought resistant bermudagrass visual quality to varying irrigation regimes, including levels of deficit irrigation. Turfgrass quality will be measured by the novel pole mounted camera system developed, as well as visual ratings and by other methods of NDVI measurement throughout a three month study period. Mean quality and under each treatment will be compared, as well as the ability of each irrigation treatment to consistently maintain acceptable quality and prevent water stress. The amount of time during which turfgrass under each treatment exhibits unacceptable quality will be compared in order to determine the minimum level of irrigation required to maintain acceptable turfgrass quality over an extended time. Through this analysis, we aim to give guidance to drought tolerant turfgrass owners on how much irrigation is required to meet their lawn goals, and to give confidence to those interested in water saving irrigation strategies.

Finally, three sensors used to measure information from turfgrass plots- soil moisture sensors, a handheld NDVI meter, and the novel camera system- will each be assessed in their ability to detect water stress in turfgrass during a drought period. Water stress will be quantified as the water stress coefficient, and the relationship between the water stress coefficient and sensor data will be evaluated. Empirical models using sensor data to predict the water stress coefficient will be developed and assessed. The sensitivity of each sensor to early water stress will also be evaluated.

**CHAPTER TWO: AN AUTOMATED ASSESSMENT OF TURFGRASS VISUAL  
QUALITY USING A POLE MOUNTED CAMERA SYSTEM**

## Abstract

NDVI and other vegetation indices are used to measure turfgrass health and quality. However, typical imagery collection methods suffer from high labor input requirements, low temporal resolution, or both. A stationary mounted camera system was constructed as an alternative imagery collection method, and an algorithm was developed to independently measure the NDVI of twenty-four bermudagrass turfgrass plots from non-orthographic imagery. Solar position and turfgrass mowing direction were both determined to have a significant effect on NDVI. The measured NDVI of turfgrass plots increased alongside an increase in solar azimuth ( $R^2 = 0.87$ ), while mowing away from the vantage point of the camera was associated with a slight increase in NDVI ( $p = 0.006$ ). The NDVI of turfgrass plots calculated from the developed model explained a majority of observed variance of that measured by ground-truthing data collected by handheld NDVI meter ( $R^2 = 0.71$ ).

## Introduction

Remote sensing has become a popular technique in the assessment of crop health, stress, and growth status (E. Fitz Rodríguez & C. Y. Choi, 2002). Visual assessment by a trained person in accordance with a standard rubric have long been the most accepted method of judging and comparing turfgrass visual quality. The National Turfgrass Evaluation Program (NTEP) rates turfgrass on a scale from 1 to 9 based on a combination of the color, uniformity, texture, and presence and degree of stress (Morris & Shearman, 1998). Remote sensing, and specifically the use of vegetation indices, have been shown to correlate strongly with expert assessments of turfgrass visual quality of the same turfgrass cultivar, although the relationship between NDVI and visual quality rating of one cultivar may not be similar to that of a different cultivar or species (Bremer et al., 2011b, 2011a; Trenholm et al., 1999). Remote sensing offers key

advantages over expert assessment, including freedom from human bias as an objective measurement (Bremer et al., 2011b).

The most common methods of collecting imagery for the calculation of vegetation indices have been by unmanned aerial vehicle (UAV) and satellite (Xiang & Tian, 2011). However, each of these methods are limited in key areas. First, achieving high temporal resolution is challenging or impossible by these methods. Satellites may only be in position to capture new imagery of a field once every two to sixteen days, and poor weather conditions during these windows of opportunity may even further reduce temporal resolution of data (Xiang & Tian, 2011). The capture of imagery by UAV requires the availability of a licensed UAV pilot each time imagery is to be collected, and thus a high temporal resolution of data may be impractical or uneconomical.

The use of a permanently mounted camera system has been proposed to make use of the advantages of remote sensing of crop health while being able to achieve very high spatial resolution at little to no marginal expenditure of labor. Ahamed et al. (2012) developed an automated camera system and processing algorithm capable of capturing imagery of plots of energy crops multiple times throughout the day. Xiang and Tian (2011) similarly developed a camera system which captured daily imagery of corn fields.

This experiment will develop and evaluate the performance of a mounted camera system and accompanying image processing algorithm in the assessment of visual quality of plots of bermudagrass. NDVI measurements using a sensor measuring turf NDVI under a controlled light source will be used as a measure of the true turf NDVI. Because NDVI and visual quality assessments of turfgrass have already been shown to correlate strongly for a wide variety of

turfgrass species, the significance of NDVI measured by our system as a predictor for turfgrass visual quality will be measured by its relationship to the true NDVI measured by this sensor.

First, a method of accurately identifying pixels of turfgrass within each plot in an image must be developed, as well as the ability to identify the identity of each plot across multiple photos. This will be accomplished using a low-cost system without the use of geographical position sensors or other sensors to provide information about the angle and position of the camera. The system will also be installed on a low-cost, easy to install pole. Because of this, a much smaller angle of incidence will be used than in Ahamed et al. (2011) or Xian and Tian (2011). A novel method of image processing will be developed to meet these challenges.

Next, turfgrass is subject to intense management like mowing, which has been shown to affect turfgrass NDVI (Lee et al., 2011). Mowing also bends grass blades in a uniform direction depending upon the direction of movement of the mower, affecting the reflection of light and creating darker and lighter mowing ‘stripes’ (Mellor, 2001). The appearance of these stripes depends upon the vantage point, where mowing toward the vantage point creates darker stripes and mowing away from the vantage point creates lighter stripes. The effect of mowing on NDVI derived from imagery captured at an acute angle, rather than orthographic imagery, must be determined.

Finally, it must be established whether the NDVI determined from imagery captured at an acute angle of incidence may be used to accurately measure the NDVI of turfgrass. The true NDVI of turfgrass plots will be determined by measurements taken by a Fieldscout TCM 500 NDVI meter (Spectrum Technologies, Inc, Aurora, IL). A model relating the NDVI of TifTuf plots using our method to the NDVI measured by TCM 500 measurements will be developed.

The accuracy of our camera system will be evaluated by comparing the NDVI of plots measured through imagery to the true NDVI of these same plots measured by the TCM 500 sensor.

## Materials and Methods

### **Site Description and Camera Installation**

A field evaluation site was developed at North Carolina State Turfgrass Field Lab in Raleigh, North Carolina. The growing site used for evaluation consisted of a 33 m by 33 m area of TifTuf bermudagrass (*Cynodon dactylon* x *C. transvaalensis*) divided into twenty-four 4.6 m by 4.6 m plots, with 0.9 m separating each plot on all sides. A red latex paint containing the growth regulator trinexapac-ethyl was sprayed to outline each plot.

The stationary aerial imaging system was installed on a small hill to the southeast of the research site. A 12.7 cm diameter hole was augered to a depth of 1.2 m. A 1.2 m long stainless steel pipe with an outside diameter of 11.4 cm and a wall thickness of 0.3 cm was installed in the hole as a sleeve for the mounting pole. The hole was filled back in until the sleeve rose to about 7 cm above the ground surface, and clay was tightly packed on the outside of the sleeve to fix it in place.

A 5.2 m long aluminum pole with an outside diameter of 10.3 cm was used as the mounting pole. A pulley system was installed on the mounting pole so that the camera system could be easily accessed for maintenance. Two pulley rollers were installed on one side of the mounting pole, one approximately 1.5 m from the bottom and the other approximately 8 cm from the top. An 8 gauge steel wire rope was wrapped tightly around the pulley rollers, and the two loose ends connected using JB Weld SteelStik epoxy putty. Next, a sliding sleeve was manufactured using a 30 gauge galvanized steel metal duct pipe with a 12.7 cm diameter and 60 cm length. High density foam weatherproofing strips with 2.54 cm width and 2.54 cm tall were

fixed to the inside of the duct pipe. The height of the foam strips were trimmed by approximately 0.6 cm, to such a point that when the sliding sleeve was fit around the mounting pole, the foam strips applied enough friction to firmly hold the sleeve in place while still allowing the sleeve to move vertically if strong force was applied. Then, the inner loop of the metal wire was fixed to the outside of the sliding sleeve with the epoxy putty, so that the sliding sleeve could be moved from near the top of the pole to approximately 1.5 m above the ground by the pulley system.

The mounting pole was next inserted into the buried sleeve. More high-density foam strips with a height of 0.6 cm were wrapped around the outside of the mounting pole 1 m from the bottom so that when inserted into the sleeve, movement within the sleeve was greatly reduced. Next, a 3/8" hole was drilled straight through both sleeve and mounting pole 4 cm below the top of the sleeve. A 15 cm long, 3/8" bolt was inserted all the way through both pipes and secured with a spring washer and nut to further fix the mounting pole in place and prevent twisting in place.

A bungee lock was installed on the pole to fix the sliding sleeve at the top of the mounting pole. With the pulley set with the sleeve at its highest position, a small loop was created in the wire rope at eye level with extra wire rope, an 8-gauge diameter wire rope thimble, and two wire rope clamps. A second hole was drilled through the mounting pole and ground sleeve near ground level, and a 20 cm long eye bolt was inserted. Then, a 91 cm bungee cable with carabiners on both ends was stretched and hooked to the loop on the wire rope on one end and the eye bolt on the other, such that tension applied by the bungee cable pulled the wire rope to force the sliding sleeve upwards. To move the sliding sleeve down for maintenance, one end of the bungee cable was unhooked to release tension. The full pole mounted camera system is shown in **Figure 2.1**.



Figure 2.1: Pole Mounted camera system installed at the field site

The camera and control system was developed to fit inside a weatherproof plastic box which could be affixed to the sliding sleeve. An IP67 ABS box measuring 285x195x130 mm was selected to house the electronics. A Raspberry Pi 4 (Raspberry Pi Foundation, Cambridge, England) was inserted into a case with mounting hole and attached to an inner mounting plate along the back wall of the box.

A ventilation system was next added. Two 44.45 mm diameter holes were drilled in the bottom of the box using a hole saw, and waterproof PVC cement was used to affix two 75 mm long PVC pipes inside the holes, each with a nominal diameter of 31.75 mm. Pipes were inserted into the holes such that approximately 15 mm extended up inside the box, and the remaining lengths extended below and outside the box. Two 40 mm 5V USB powered cooling fans were

then affixed to the top of the PVC pipes inside the box using JB Weld, with one oriented to blow air downward and out of the box and the other blowing air upward into the box. The fans were plugged into two USB ports on the Raspberry Pi.

Next, the camera system was added. Cameras consisted of two EO-1312 NIR machine vision cameras (Edmund Optics, Barrington, NJ) and one USB color webcam using an IMX179 image sensor (Sony Corporation, Tokyo, Japan). One machine vision camera was equipped with a red bandpass filter (LP660-25.4, Midwest Optical Systems, Palatine, IL), while the other was equipped with a near infrared bandpass filter (LP780-25.4, Midwest Optical Systems, Palatine, IL). Three 38 mm holes were cut into the front of the box, two directly next to each other with a space of 13 mm in between, and the last hole placed directly in between the others, 13 mm below. The insides of the holes were lined with 6.35 mm height, high density weatherproofing strips. Then, the cameras were inserted through the holes such that their lenses stuck outside of the box while their larger bodies remained inside the box, and the high density foam applied enough compression to keep the cameras tightly in place. A small amount of silicone gel was applied to the camera bodies and the inner wall of the box to help them stay fixed in place. The two machine vision cameras were placed side by side in the top holes, and the webcam in the lower hole. The webcam was plugged into the third USB port of the Raspberry Pi, while the two machine vision cameras were plugged into a 1-male-to-2-female USB splitter, and the male end in turn plugged into the fourth USB port on the Raspberry Pi.

In order to supply power and internet access to the Raspberry Pi, a 48V to 5V and ethernet power over ethernet (POE) splitter was mounted inside the box, with its USB-C power cable and ethernet cable plugged into the Raspberry Pi. Then, a 25 m long ethernet cable was buried from a nearby control box to the mounting pole, and run up the pole and connected to the

POE splitter inside the box. A POE injector was added to the nearby control box, supplying 48V and internet connectivity to the ethernet cable. The camera system electronics installed within the weatherproof enclosure are shown in **Figure 2.2**.



Figure 2.2: Camera system electronics installation

### **Image Acquisition**

A 128 gigabyte micro SD card was installed with the Raspbian 10 (Buster) operating system, which is based on Debian Linux, and inserted into the Raspberry Pi. The Raspberry Pi was connected to power and Wi-Fi from a home location, booted up, and VNC Connect was installed on the Raspberry Pi. A new account was created for VNC Connect and logged into within the application. The Raspberry Pi system configuration settings were accessed and changed to allow VNC connections at all times. With this basic system installation and setup completed, the Raspberry Pi was installed in the field camera box, and connected to power and internet supplied from a nearby control box over a buried ethernet cable.

VNC Viewer for Windows was then installed on a separate home computer, and the same account information was used to log into the application. The Raspberry Pi server was selected,

which then allowed for full GUI control of the field installed Raspberry Pi from a home computer or any other computer logged in to VNC Connect with the same credentials.

While accessing the Raspberry Pi remotely, next software for camera control and imagery acquisition could be installed. The IDS uEye computer vision cameras were designed to be controlled with the IDS Software Suite (IDS Imaging Development Systems, Obersulm, Germany), which was installed on the Raspberry Pi from the IDS Imaging website. The ARM Linux-based software suite includes the IDS Camera Manager application, which allows for basic camera parameter control and viewing and saving camera imagery.

The IDS Camera Manager software was used for imagery acquisition. Through experimentation, it was discovered that the IDS software was incapable of setting auto parameters such as auto exposure for both cameras simultaneously. Because using auto exposure settings and recording the exposure used is essential for achieving high resolution imagery and later correcting for differences in exposure settings, this required each camera to be accessed sequentially using the IDS Camera Manager GUI software. To accelerate the process of collecting imagery, standard parameters were saved for both cameras to automatically use auto exposure, while all other camera parameters were kept at system defaults. This was done by opening the camera properties, selecting auto exposure, and then navigating to File > Save Parameter > Set Parameter. Then, from the IDS Camera Manager main menu, each camera was selected and the Additional Functions button accessed, and the “Camera open parameter” setting was changed to “Parameter set.”

Each time imagery was acquired, one still image from each camera was saved- one to represent the red band reflectance and the other to represent the NIR light reflectance. The IDS Camera Manager application was first opened, and then one camera was accessed. This opened a

new window displaying the current camera imagery. Once opened, the camera would begin to find the appropriate exposure level for the best imagery. This process usually took two to three seconds, after which the exposure would stabilize. If the auto exposure level did not stabilize within ten seconds, it was determined that the lighting conditions were too unstable for high quality imagery, and imagery acquisition was delayed until a later time. After stabilizing, a snapshot was saved to the Raspberry Pi's local storage. All image files were saved with a filename indicating the time and date the image was taken, which camera took the image, and the exposure time used in the image. After the first image was saved, the camera was closed, and the process was repeated with the second camera. The time between saving images from each camera was usually around 30 seconds.

Imagery was acquired on most days between the start of the experiment in mid-June to October. On days where rain was occurring or lighting conditions were poor, imagery was not taken. Technical difficulties also prevented image acquisition on some days throughout the research period. Because imagery had to be acquired through manual control of the Raspberry Pi system, images were not captured at exactly the same time each day. However, a window of 30 minutes before noon to 30 minutes after noon was set as a target for acquisition whenever possible. This time period was designated because it was hoped that it would reduce the chance of shadows and would result in the most consistent lighting conditions and sun position close to directly overhead throughout the study.

On some days, many image pairs were taken throughout the day. Images were captured between the hours of 9 AM and 5 PM at intervals of 30 minutes to an hour on average.

A Google Photos folder was created to back up and share images taken by the camera system. On a weekly basis, photos were uploaded to the cloud folder from the remotely controlled Raspberry Pi.

## **Image Processing**

Image processing software in the Python 3 programming language was written in order to automate the process of deriving NDVI values for each plot of turfgrass from a folder containing raw imagery. There were several key challenges to calculating NDVI of turfgrass in our experimental setup which made the automation of this process necessary. First, one of the significant benefits to a stationary mounted camera for imagery collection is the possibility for very high temporal resolution without the additional expenditure of labor for data collection. However, if each additional data point requires additional labor for image processing to derive NDVI from raw imagery, then the benefits of this method are diminished. Additionally, the field site used was comprised of 24 individual research plots, each within frame of a single image, which needed to be identified and processed separately. To add, red and NIR images were captured by separate cameras, meaning that for a single instance of data collection, a total of 48 areas of interest needed to be identified. Manually identifying zone areas alongside high frequency imagery collection would therefore be prohibitively labor intensive, and an automation process was developed.

Orthogonal aerial imagery collection, for example by drone, has been widely used in the industry for many years thanks to software platforms which perform the tasks of plot identification and deriving NDVI for each. However, key differences in imagery collected by UAV and pole mounted camera prevent the use of existing platforms for processing imagery

collected by this system. Existing UAV-based software packages use a combination of orthogonal imagery and GPS and drone position information to determine the geographic position of objects within the field of view of the camera. Areas of interest may therefore be defined by geospatial data. In the camera system used in this research, imagery is captured from an angle, and geospatial sensors and data are not used. Therefore, an alternative method of reliably identifying areas of interest within imagery was developed.

While the cameras' viewing angle and lack of additional spatial information presented challenges, the mounted camera system also had one major advantage which made area of interest identification possible using only the imagery data itself: a consistent camera position. With only minimal camera movement and repeat photography of the same scene, features within the scene could act as anchor points and substitute for geospatial data. This technique became the basis for the image processing algorithm developed, and the general workflow is summarized in **Figure 2.3**.

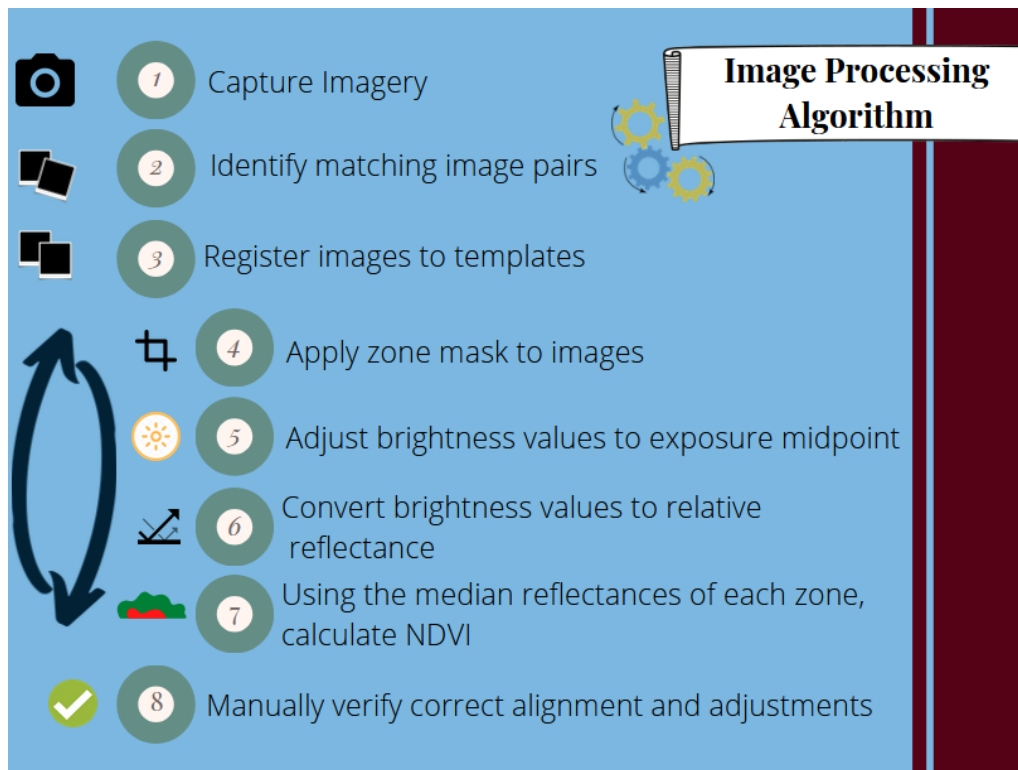


Figure 2.3: Flow chart of the image processing algorithm developed

The first step in the image processing algorithm is the image registration of all images. Although the cameras are fixed in position on the mounting pole, wind causing the pole to bend slightly affects the camera framing of the field. This prevents the ability to use fixed pixel coordinates for defining each zone area of interest across images taken by the same camera at different times, as even slight changes in position can cause zones furthest from the camera with the smallest resolution to be misidentified. Therefore, images were rectified so that the zone areas of interest are aligned across subsequent images.

Images from both cameras with good lighting conditions and minimal clouds were selected to be used as “template” images to which other images were aligned. It was found that some changes to the site within view of the cameras affected the ability of images taken before and after to be accurately aligned, so multiple template images were selected to best align images

taken throughout the entire research period. For each template image selected, the pixel coordinates of each zone were identified and saved into comma separated values (CSV) files.

Each unprocessed image is matched with the appropriate template image and file containing zone area coordinates based on the camera used and date of the image. To mitigate differences in lighting conditions from affecting the success of the image registration process, a copy of the unprocessed image is made and adjusted for the difference in exposure compared to the template image. The difference in exposure is calculated from the shutter speed and aperture, whereby exposure is calculated from **Equation 2.1**:

$$E = \log_2\left(\frac{F^2}{shutter}\right) \quad (2.1)$$

where E is the camera exposure, F is the F-stop, and shutter is the shutter speed in seconds (Jacobsen et al., 2000).

The brightness value of each pixel in the unprocessed image is then adjusted in order the approximate equivalent lighting conditions in both images. **Equation 2.2** describes the correction of pixel brightness values:

$$y = 1.05^{3*\Delta E}x + 22.9 * \Delta E \quad (2.2)$$

where y is the corrected brightness value of the pixel, x is the uncorrected, original brightness value of the pixel, and  $\Delta E$  is equal to the exposure value being corrected to subtracted from the original exposure value (Ritchie et al., 2008).

With image brightness of the image corrected to match the exposure of the template image, keypoints which identify the same feature in both images can be used to align the new image to the template image. Keypoints and descriptors are identified in both the exposure adjusted image and the template image using the ORB (oriented FAST and rotated BRIEF) feature detector function in the OpenCV 4.5.4.52 python package, as shown in **Figure 2.4** (Bradski, 2000).

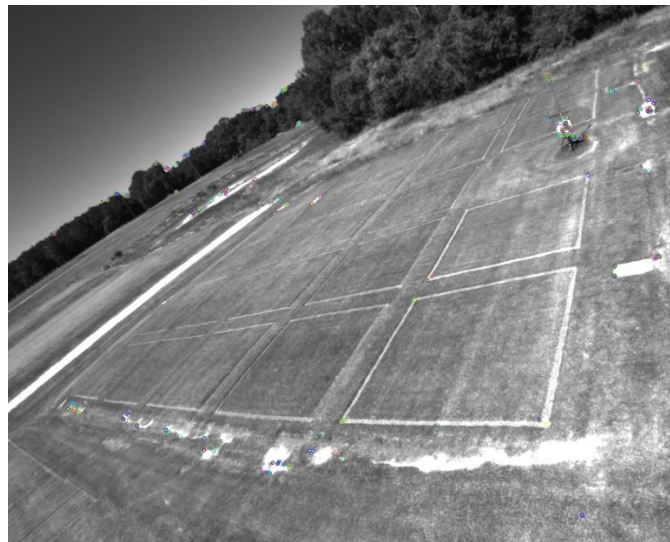


Figure 2.4: Camera imagery after colored circles were drawn around identified keypoints

Bruteforce hamming was next used to match identified keypoints across both images based on the similarity of the feature descriptors, and the top 20% nearest matches are saved. This process attempts to identify pairs of keypoints across both images which identify the same physical object or geographical feature, and identified potential matches are illustrated in **Figure 2.5**.

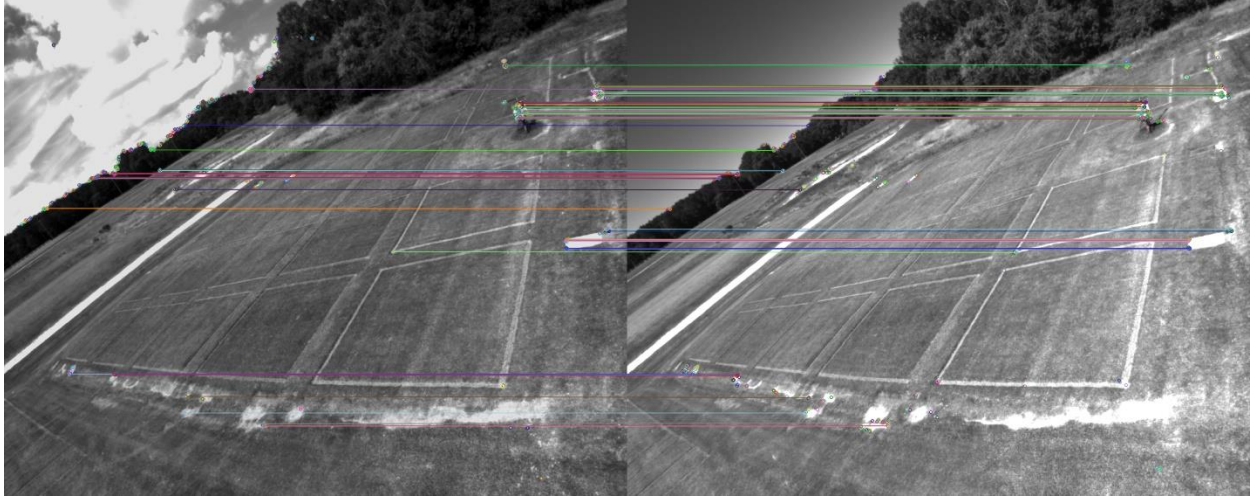


Figure 2.5: Matching keypoints between the template image (right) and the image to be registered (left)

These saved keypoints are then assessed using Random Sample Consensus homography to further eliminate inaccurate keypoint matches. A transformation of the original unprocessed image, without the brightness value correction, is then applied using the remaining keypoint matches. The shape of the original image is warped such the matching keypoints are overlaid, resulting in an image where zone areas of interest are overlaid with matching pixel index borders. The transformed images were then saved to a different folder, and the original images were saved to a different folder archiving all raw image files.

An additional step was taken to verify the correct alignment and identification of zone areas. For each registered image, the appropriate zone coordinate map file was used to define a polygon for each zone using the pixel coordinates of the four corners. An opaque blue fill was added to each polygon and overlaid on the registered image such that the zones as identified by the algorithm were clearly visible, and this image was then saved to another folder for a manual verification step of successful image processing completed after the algorithm was finished.

Once all images had been registered, the algorithm was next able to begin the process of generating NDVI averages for each zone in each set of images. Red and NIR image pairs are identified from the folder of all registered images by the filenames of the images, so that images taken at the same time and date and by opposite cameras are paired. Once a pair of images was identified, the appropriate zone coordinate map for each image is also identified.

Average NDVI for each zone was calculated by defining a polygon around each zone using the zone's coordinates, cropping the polygon area, and saving to a new image. Because the zone areas were irregular polygons, the polygons could not be directly cut out of the image and saved. Instead, the zone areas were cropped by the python algorithm by first using the zone coordinates to first draw a bounding rectangle, the smallest rectangle which could be drawn which also included all pixels included within the zone borders. Bounding rectangles were defined for both the red and NIR images and saved as new images. Next, two masks were created first by creating two new single dimensional images, one each of the same dimensions as the bounding rectangles, with brightness values all of zero. Next, for both masks, the corresponding zone coordinates were used to draw polygons on both masks, and filled with brightness values of 255. In doing this, the algorithm had created two new images where the zone areas were white and the extraneous background within the bounding rectangles were black. These images, or masks, were then used to isolate the zone areas from the background areas in the cropped boundary rectangle images while preserving the color information within the zones. This was achieved by using a bitwise operation algorithm- for both the rectangle cropped from the red image and NIR image, the brightness value of each pixel of the cropped image and mask were compared. For each pixel of equivalent index, if the brightness value in both images was higher than zero, the pixel value of the cropped image was saved. Otherwise, of

the pixel value of each image was 0, the pixel value was set to 0. The resultant images were saved, resulting in rectangular images where the brightness values within the zone areas of the original red and NIR values were retained, and the extraneous background area was black.

With the brightness data within the zone isolated from the rest of the red and NIR images, NDVI could be calculated. The first step in calculating the NDVI of the zone area was first to normalize the two images for differences in exposure values. For both cameras, an f-stop of f/4 was used. However, while the two images were taken from the same position and under the same lighting conditions, the different filters allowing through different light bandwidths mean that different amounts of light are allowed into the camera sensing element. It was found that the NIR bandpass filter allowed a significantly greater quantity of light through, such that if both images were set to the same shutter speed, either the NIR image would appear appropriately exposed while the red image would appear very dark due to underexposure, or the red image would appear appropriately exposed while the NIR image would appear significantly overexposed. While either image is either washed out or very dark, the dynamic range of the brightness values of pixels was greatly diminished (Ritchie et al., 2008). Therefore, in order to achieve the highest resolution of brightness values in both images, the shutter speed was set to the camera software's "Auto Exposure" setting for all images taken. However, the different shutter speeds allowing in light to the camera sensing element for different periods of time required a different post processing step to normalize for camera exposure. This is because NDVI is a comparison between the amount of light reflectance between two different light bands, so if light is measured for a greater amount of time for one light band than another, the difference in measuring times must be accounted for.

Then, the exposure used in each image was calculated using **Equation 2.1**. The difference in exposure was calculated by subtracting the exposure of the red image from the exposure of the NIR image.

Next, a simulated exposure value was determined to use in the adjustment of both images. In correcting for exposure, first the average brightness values in each image were calculated. Two arrays were first created to store brightness values for each image. For both images, the brightness value of each pixel was accessed. If the brightness value was higher than zero, it was added to the corresponded array. This excluded the black background outside the zone areas, leaving only a list of the brightness values of pixels within the zones. Then, the average of each array was calculated to determine the average brightness value of the zone area in each image. This was an essential step because image brightness values may occupy only a range of 0 to 255. The exposure adjustment involves raising the brightness values of all pixels in the image with a lower exposure and/or lowering the brightness values of all pixels in the image with the higher exposure. The pixel values of the lower exposure image may be adjusted to simulate the exposure of the higher exposure image, the pixel values of the higher exposure image may be adjusted to simulate the exposure of the lower exposure image, or the pixel values of both images may be adjusted to simulate an exposure value of somewhere between the two exposures used. Under certain lighting conditions or when the difference between exposures was very high, it was found that the exposure adjustment equation may result in brightness values lower than zero or higher than 255, which distorts the images. Therefore, the average brightness values of each image were calculated to determine which simulated exposure value should be used such that the transformation of the brightness values would not result in adjusted brightness values lower than zero or higher than 255.

It was found that the red band images were most often problematic when adjusting brightness values to an exposure point halfway to the two exposures used. Most commonly, when auto exposure settings were used, the cameras would adjust to exposure settings such that the average pixel value of turfgrass in the NIR image was near the middle of the brightness range, while the average brightness value of turfgrass in the red imagery was often lower than the middle of the range. A simple logic gate was found to be effective in greatly reducing the change of adjusted brightness values from extending beyond the range: if the average brightness value of the red image was less than or equal to 125, an exposure value halfway between the two exposures used was simulated for both images. If the red image had an average brightness value greater than 125, an exposure value equal to the lower exposure value plus 30% of the difference in exposure values was simulated.

Once the simulated exposure value was determined, brightness values of all pixels in both images were adjusted. The brightness value of every pixel was accessed, and **Equation 2.2** was again applied to change the brightness value to its adjusted value.

The adjusted brightness values in both images were then used to calculate an estimated relative reflectance for each pixel. Cameras save light information as a degree of brightness in a given color band, but NDVI is a comparison of light reflectance within the red and NIR light bands. Therefore, to relate pixel brightness to actual light reflectance detected by the camera, the brightness value of each pixel was accessed and **Equation 2.3** was applied to calculate the estimated reflectance for each image,

$$F(y) = -\frac{\ln\left(1 - \frac{y}{255}\right)}{3.39} \tag{2.3}$$

where  $F(y)$  is the equivalent reflectance of the pixel, and  $y$  is the brightness value of the pixel (Ritchie et al., 2008). Finally, the average and median reflectance values calculated from the zone areas in both images.

Finally, the median and average NDVI values were calculated for plots using **Equation 2.4**,

$$NDVI = \frac{NIR - RED}{NIR + RED} \quad (2.4)$$

where NIR was the average or median reflectance of pixels in the NIR image, and RED was the average or median reflectance of pixels in the red image.

With the average and median NDVI of the zone calculated, the time and date the images were taken, the zone number, the average number of pixels in the zone between both images, and the NDVI values were determined.

For diagnostic purposes and further analysis, a histogram was also created to display the brightness values of the turfgrass in the red and NIR images both before and after adjusting for exposure. These were used in the data cleaning and verification process to ensure a successful image alignment and exposure correction.

This process was used to analyze imagery captured by the camera system during a data collection period between September 2 and October 4, 2021. Images taken by the Raspberry Pi camera system were downloaded from the Google Photos folder and saved to the image processing environment's local storage. Images were first visually assessed to ensure that there were no obstructions, smudges, or other aberrations which would impair the usability of the images. Problematic images were discarded alongside their pairs, and the rest were moved to the

Unprocessed Imagery folder. Then, the image processing program was run, returning key values for each zone in each image pair in a CSV file.

### **Data Verification and Cleaning**

Several manual validation steps were taken to ensure the accuracy and success of the image processing program. First, the zone identification verification images generated by the program were checked. For each image the program processed, a new image was generated of the dimensionally transformed image, with translucent blue polygons overlaid marking the sections of the image identified as zones and used to generate NDVI values. Each one of these images were visually assessed to ensure that the image registration process has been successful and resulted in no distortion, and that the zone areas were all within the zone border lines. If the verification images indicated any problems, it was noted for additional steps to be taken.

The most common cause of image registration distortion and misidentification of zone areas was that the processed image was too dissimilar in background features from the designated template image. Occasionally a vehicle would be parked within view of the camera, or the camera box would shift position slightly, lighting conditions would be substantially different from those in the template image, or other differences in the image field would be present. In these cases, keypoints were sometimes mismatched, resulting in a distorted image. When this happened, the first step was to designate a different template image for that image. Permanent changes to the background or camera position required the creation of a new template image. An image affected by these changes and which also had clear skies and good lighting conditions was selected to be the new template. Zone pixel index borders were manually identified, and the image and zone coordinates were added to the Templates folder and zone

coordinates CSV file. Python code was modified to designate the new template for the appropriate set of images.

**Figure 2.6** illustrates examples of successful and unsuccessful image alignment and plot area identification. Areas highlighted in blue indicate pixels within zone borders, which were to be used in calculating the NDVI for each plot. The right image demonstrates an unsuccessful image registration where highlighted blue zone areas are not within painted zone borders, occasionally capturing turfgrass in the unirrigated middle sections. An image alignment like this would require follow-up, reprocessing the raw imagery using a new template file until zone areas were correctly placed within actual zone borders.

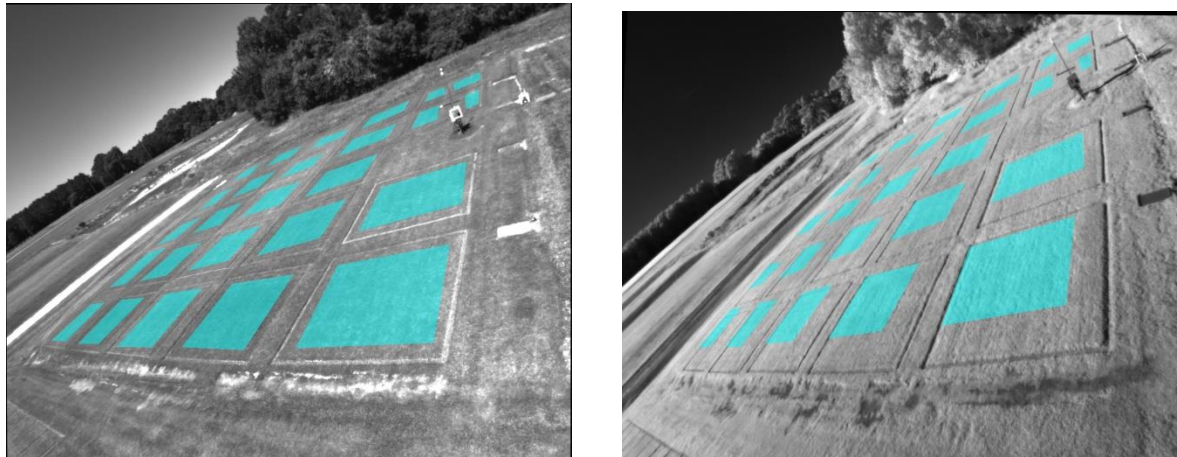


Figure 2.6: Two registered images with blue shading drawn over pixels within plot boundaries. The left image represents successful registration and plot area identification, while the right image represents registration resulting in misalignment of plot areas

In rare cases where designating a more similar image as the template image did not resolve the distortion, a new template image and zone coordinates was created using the problematic image itself. In the registration of nearly daily images for the months of June, July,

August, and September, a total of four templates for each camera were used. Roughly one new template image per month was found to produce consistent and successful image registration. Once this first verification step was taken and zone areas were confirmed to have been correctly identified, a second step to confirm the success of the color correction was taken. Brightness values of all pixels within zone areas were transformed based on exposure values to correct for the difference in exposure for image pairs, using **Equation 2.2**. For each image pair, a single histogram was generated displaying the brightness values for the untransformed red band image, untransformed NIR band image, transformed red band image, and transformed NIR band image. Each histogram was manually inspected to ensure that the mathematical transformation did not lead to brightness values outside of the 0 to 255 range.

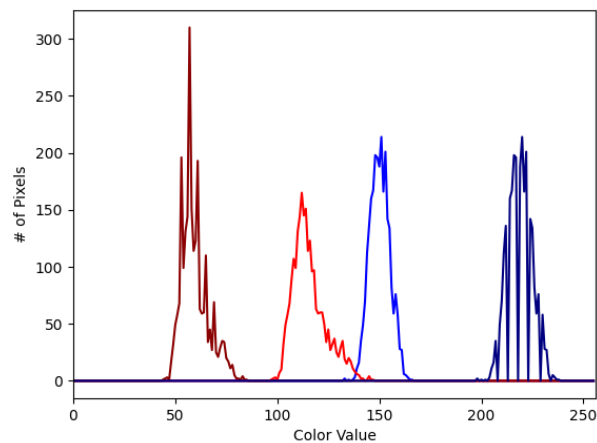


Figure 2.7: Histogram of the pixels within one plot from one red and one NIR image, before and after exposure correction.

**Figure 2.7** displays the histogram produced by a single zone in a single set of images. The lighter red and lighter blue lines represent the histograms of the section of the image cut from the raw red and NIR images, respectively. Both images were taken using an auto exposure time: the red image with an exposure time of 0.24 ms and the NIR with an exposure time of 1.80

ms. The darker red and blue lines represent the pixel brightness values of the red and NIR images after correcting for the difference in exposure.

### **Analysis and Modeling**

NDVI values calculated by the process detailed in the previous section were based entirely on imagery captured by the camera system. However, it was left to be investigated whether additional factors beyond the true turfgrass visual quality also affected the imagery-based NDVI values. Because the generation of NDVI from camera imagery with viewing angles less than 90 degrees have been significantly less studied compared to orthogonal imagery, especially with the subject of turfgrass, a variety of potential additional effects were investigated. Thought was given to the particularities of imagery captured from this angle and of turfgrass when identifying potential effects.

Time of day was investigated, as the moving position of the sun and subsequent direction of light reflectance from the earth's surface may have had a more significant effect on cameras with an acute angle compared to orthographic imagery.

Mowing direction was built into the experimental design as a blocking variable with all areas of each plot mowed in a uniform direction to enable investigation of its significance on camera-derived NDVI. The direction of mowing creates 'stripes' which appear darker and lighter depending on the position of the viewer, and therefore mow direction was investigated to determine whether this visual effect also affected NDVI. All plots were either mowed by the mower moving toward the North or toward the South, such that the entire turfgrass area within each plot was mowed by the mower moving in the same direction. The camera position was angled toward the Northwest, so plots mowed in the North direction were mowed in a direction moving away from the camera, and plots mowed in the South direction were mowed in a

direction toward the camera. There was, however, a roughly 45 degree difference in the angle of the camera position and North, so mowing directions were not perfectly toward or away from the camera.

Finally, resolution was also investigated for significance. A camera viewing angle of less than 90 degrees produces a vanishing point effect, where areas of the same size will appear smaller and will be captured in the imagery by smaller quantities of pixels. Simultaneously, the decreasing viewing angle of further away areas of turfgrass may have also had an effect. A smaller viewing angle diminishes the camera's penetration through the crop canopy. A camera looking straight down on a crop of corn would likely see areas of soil where the canopy is not closed, while a viewing angle of 20 degrees would only capture light reflected from the tops of the canopy. Though turfgrass was fully established with 100% coverage on all plots, the tops of grass canopy are also greener than the lower stalks. Thus, pixel resolution per plot was also investigated to measure the potential effects of light penetration to lower depths of the canopy as well as any possible reduction in measured NDVI accuracy with low pixel resolutions.

### **Solar Azimuth Correction**

Preliminary data analysis was conducted alongside data collection to identify other strategies for improving the algorithm. It was suspected that in addition to mowing direction, time of day may also have some effect on NDVI. It was reasoned that sun position or solar intensity may affect the amount of light received by the camera system differently in one light band than the other. Therefore, on selected days imagery was taken frequently throughout the day and compared to ground truth data collected on the same day. Ground truth data collected by handheld NDVI meter is unaffected by ambient lighting conditions, as data collection requires

the meter to be held tightly to the ground to block out light and will issue a warning when external light is detected. Therefore, NDVI meter data was used as the true value of turf NDVI regardless of the time of day it was collected.

On seven days between September 2 and October 3, camera imagery was collected multiple times between the hours of 9am and 5:30pm. Imagery was processed by the algorithm and the average NDVI per plot was recorded for every time and every date during this period. In order to identify any systematic bias introduced by the time of day that imagery was collected, NDVI values estimated at different times on the same days were compared. It was discovered from this data that the time of day did have a significant effect on the average NDVI, with the average NDVI estimated being higher between 4pm and 5pm than between 9am and 10am. The relationship between time of day was found to be strongly linearly correlated ( $R \geq 0.8$ ).

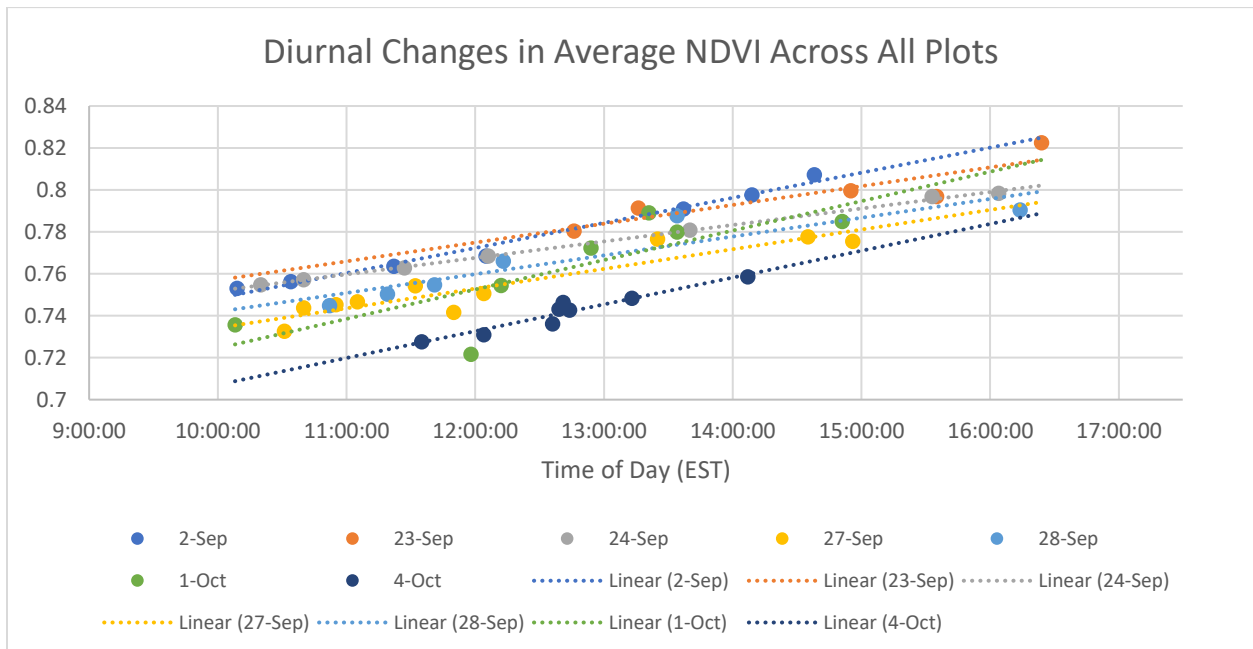


Figure 2.8: Diurnal changes in the average NDVI across all plots

This discovery prompted further investigation in order to identify the underlying mechanism by which time of day was biasing the average NDVI estimation. Due to the linear relationship shown by the data, it was assumed that irradiance was not the cause of this bias, as net irradiation is expected to peak around solar noon and decrease both earlier and later in the day. Therefore, solar position was next investigated. For each time of day imagery was collected, the solar azimuth was determined. On each date, the average NDVI across all plots was compared to the solar azimuth, as shown in **Figure 2.9**.

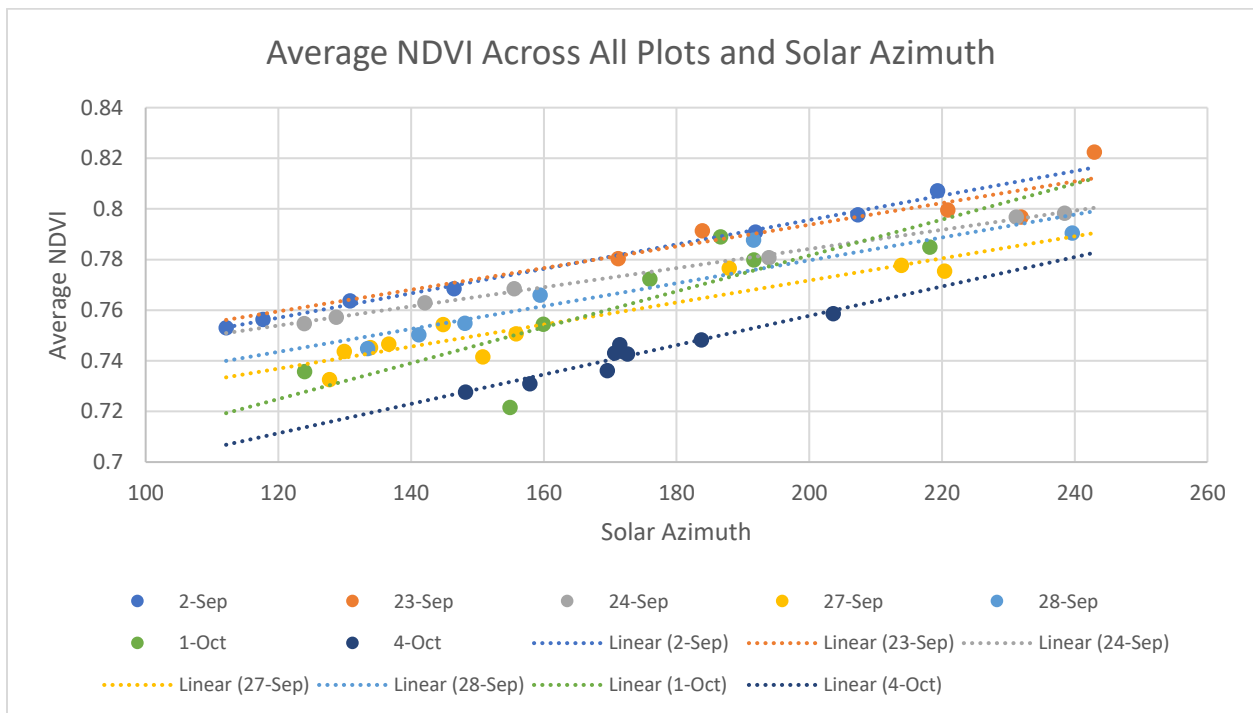


Figure 2.9: Linear regressions of the NDVI of turfgrass calculated from imagery taken at different solar positions

NDVI values are directly comparable only to other NDVI values measured on the same day, as changes in water conditions and accumulated stress did lead to changes in turfgrass

quality over time. However, daily trends indicated that the diurnal effect was consistent and strongly correlated with solar azimuth.

Solar azimuth was shown to have a strong relationship with average NDVI on all days, with an average  $R^2$  of 0.87, and correlation coefficients ranging from 0.82 to 0.99 across the seven days of data collection. Relative azimuth was also shown to have a strong but lesser correlation with average NDVI, with the correlation being weakest when the solar azimuth was nearest to the viewing angle. The absolute azimuth was therefore determined to be the superior predictor of the bias discovered at different times of day.

It was also determined that because of the very strong correlation between azimuth and NDVI within a single day and due to the consistency of the relationship, azimuth alone could be used to correct for this bias. Linear regression was performed for all date points on each day, and the results are shown in **Table 2.1**.

Table 2.1: Linear regressions of the average NDVI and solar azimuth

	2-Sep	23-Sep	24-Sep	27-Sep	28-Sep	1-Oct	4-Oct	Average
A	4.83E-4	4.28E-4	3.78E-4	4.35E-4	4.52E-4	7.09E-4	5.80E-4	4.95E-4
$R^2$	1.00	0.74	1.00	0.86	0.87	0.68	0.92	0.87
Data Points	7	5	8	10	6	8	8	7.43

A=slope

In **Table 2.1**, A represents the slope of the regression line, and ‘Data Points’ is the number of image pairs from which NDVI were calculated at varying points of the day. The average  $R^2$  across all seven days was 0.87, meaning solar azimuth explains a significant majority

of observed variation in the diurnal changes in NDVI measured within a single day. The average slope of the regression line was 0.000495. While the relationship between solar azimuth changes throughout the year, this relates to more than a 0.01 increase in NDVI per hour during the times of day that optimal imagery is captured. Therefore, when attempting to measure changes in turfgrass quality over time, it is essential that imagery used either be taken at the same solar azimuth or use an empirically determined correction factor to adjust for this diurnal effect.

These data were used to create a method for solar correction in the algorithm. For the sake of model simplicity and legibility, as well as due to the fact that the relationship between solar azimuth and diurnal changes in NDVI was so consistent and strongly correlated, a correction factor was determined separately from the rest of the modeling process. Solar azimuth was considered as a single effect with no interactions with other effects.

A solar azimuth of 180 degrees was used as the solar position to which all NDVI calculations would be corrected to. While the time of day and solar azimuth changes slightly throughout the year due to the axis of the sun, this azimuth corresponded to a time of approximately 1:30pm during the experimental period. The Pysolar 0.8 python package ([pysolar.org](http://pysolar.org)) was used to calculate the solar altitude and azimuth based on the geographical position of the camera and the time of day. Pysolar calculates solar position for use for solar radiation modelling, and is based in part on work published by the National Renewable Energy Laboratory (Reda & Andreas, 2004; Stafford, 2021). The latitude and longitude of the camera system were used alongside the time that imagery was captured to calculate the solar azimuth at the date and time of each image taken. Then, the difference between the azimuth at the time of the imagery and an azimuth of 180 degrees was calculated. Therefore, during the processing of imagery as described in the previous section, the NDVI calculated for each plot was next

adjusted according to this empirical correction factor. The uncorrected average NDVI for each plot was multiplied by 0.000495 times the difference between 180 and the instantaneous azimuth in order to arrive at the average NDVI of the plot of turfgrass normalized for solar position. Before proceeding to the next step of predictive modelling, all imagery was reprocessed by the algorithm with this additional solar correction factor applied after calculating NDVI, and the adjusted NDVI value was used in the modelling process.

However, further investigation should be completed to determine whether this relationship is unique to our experimental site design and how different camera positions and locations might be affected differently. A similar process should be conducted on pole mounted camera systems with different viewing angles and different geolocations to identify the appropriate correction factor of that site and to identify a more universal equation for correcting this bias. Additionally, because our camera was positioned toward Northwest at a viewing azimuth of 138 degrees, and because of our site's geolocation, the difference between the angle of incidence of sunlight and the camera viewing angle generally increased throughout the day. Sunlight was therefore reflected more directly toward the cameras later in the day, which may be a more universal metric than absolute solar azimuth. More research should be directed at investigating average changes in estimated NDVI by angled cameras in different positions due to solar position.

## **Model Development**

Imagery and ground truthing data were collected and analyzed to identify significant predictive variables and a complete model relating camera imagery to NDVI as measured by the handheld meter. The model was generated from data collected between September 2 and October

20, 2021. On ten days, imagery was captured from both cameras throughout the day. Ground truthing data was collected using the TCM 500 NDVI meter, taking nine measurements for each plot in a 3 x 3 grid pattern as described previously.

Additionally, preliminary analysis applied models developed early in the process to camera imagery collected during July and August. The resulting NDVI values of turfgrass plots were compared to TCM 500 measurements taken on the same days, and it was determined that models generated from data collected only in September and October performed poorly when compared to TCM 500 meter data of highly water stressed turfgrass in August. Due to frequent rains and cooler temperatures, little water stress occurred in September and October, and thus the range of NDVI values collected by TCM 500 was higher than those collected from unirrigated turfgrass in early August. Therefore, NDVI values of water stressed turfgrass plots collected by the TCM 500 sensor and from camera imagery collected in early August were included in the dataset. Data from fifteen plots collected during August were included in the model generation dataset, compared to data from 225 plots collected during September and October.

The true NDVI of each plot and each day was considered to be the average of all nine NDVI measurements taken by the meter (or all three measurements for data collected during August). To mitigate the effect that temporary poor lighting conditions might have on the accuracy of calculated NDVI (such as a cloud casting a slight shadow unevenly across the field), multiple image pairs were also collected throughout the day throughout September and October. Imagery was processed by the algorithm described in the **Image Processing** section, and processed images with overlaid zone identification polygons were inspected. Imagery with incorrectly identified zone areas and imagery with significant shadows or under overcast lighting conditions were thrown out. In nearly all cases, these two categories overlapped. Next, due to

findings described above, imagery captured earlier than 11 AM and later than 2 PM was discarded. From the remaining imagery, three image pairs per day were selected to be used in calculating the camera-based NDVI values on each day, except for September 7 and September 17, for which only two and one image pairs remained, respectively.

The median NDVI values for each plot in all remaining image pairs were obtained. This resulted in multiple NDVI values for each plot on each day, one for each image pair. For the sake of generating the model, the camera derived NDVI value for each plot on each day was assumed to be the average of all measurements taken per plot and per day. When determining the NDVI of plots from imagery, the solar azimuth correction method described in the **Solar Azimuth Correction** section was applied.

Alongside the meter and camera-based NDVI values, the following additional data points were also included and considered in the model generation: mowing direction (north or south), and resolution (pixels per square foot). A CSV file was created with a column for each considered variable, as well as the date and zone number for record keeping.

Data were then randomly assigned a designation as ‘Training’ or ‘Validation,’ with a 50% chance of being assigned either designation. Only the training data were included in the generation of the model, and the validation data were used to assess the performance of this model.

JMP software (SAS, Greensboro, NC) was used to perform statistical analysis of the data. A first order, full factorial design of model effects was analyzed. First, the fit of the model was assessed through analysis of variance (ANOVA) and linear regression of the actual values versus predicted values. ANOVA performed on the resulting initial model resulted in an F-statistic of 181.89, while linear regression determined the  $R^2$  of the data to be 0.769. From these tests, it was

confirmed that the model generated had significant predictive value, and further analysis was performed.

Next, residual analysis was performed to assess the distribution and bias present in the data. The residuals by predicted (Figure 2.10) plot indicated that variance within the model was centered around zero. The residual normal quantile (Figure 2.11) also indicated variance was reasonably normally distributed. Finally, the studentized residuals plot (Figure 2.12) showed that no significant outliers were present in the dataset.

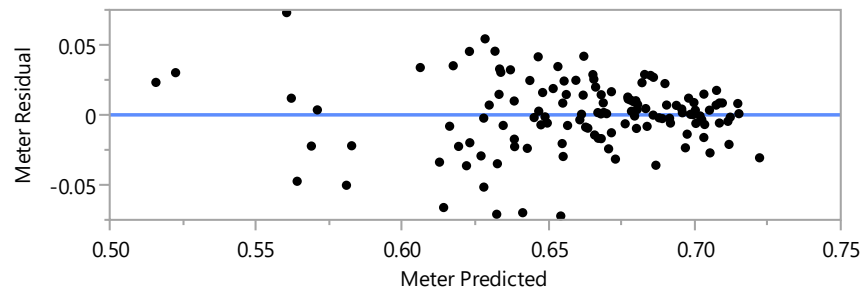


Figure 2.10: Residuals by predicted plot of the initial model

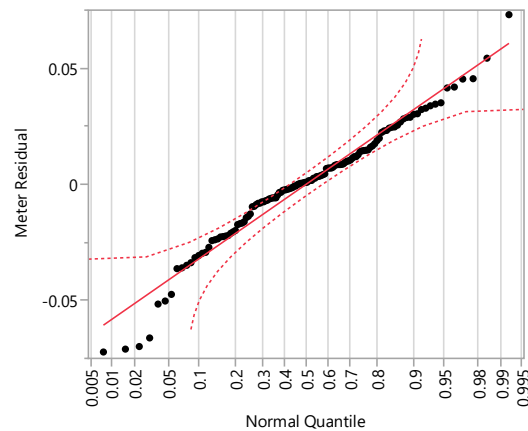


Figure 2.11: Normal quantile plot of the initial model

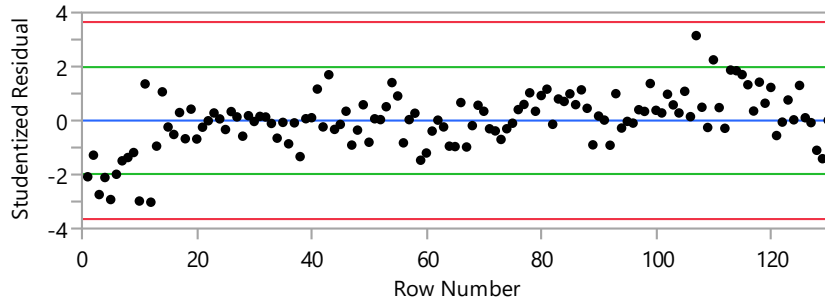


Figure 2.12: Studentized residuals plot of the initial model

The model thus confirmed as unbiased, the significance of all included individual effects were next assessed via partial tests. As a preliminary estimate of significant effects, a normal probability plot was generated and analyzed (**Figure 2.13**). As shown, all effects interactions are clustered closely along the plotted red line with a slope of 1, indicating low predictive value. Furthest away from this line are the first order effects, with the camera-based NDVI value shown to be highly active in the model, mowing direction being likely active, and resolution's value being uncertain at this stage of the analysis.

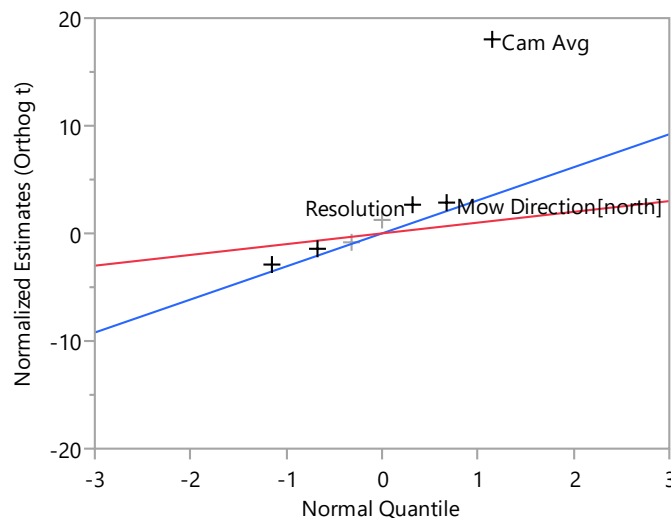


Figure 2.13: Normal plot of effects included in the initial model

Individual effects were further analyzed through ANOVA. The effects tests table in **Table 2.2** displays the F statistic and p-value for each individual effect. A 95% confidence level was used in the determination of effect significance. The p-value for both the camera NDVI and the second order of the camera NDVI both approached zero. The p-value of resolution also indicated significance. Mowing direction was determined to have a p-value of 0.06, indicating marginal significance, and all interactions had insignificant p-values well above 0.1.

Table 2.2: Partial effects tests of all initial model predictors and interactions

Effect	Sum of Squares	F-statistic	<i>p</i> -value
Cam Avg	0.1028	173.8	<0.0001
(Cam Avg) <sup>2</sup>	0.0058	9.9	0.0021
Mow Direction	0.0021	3.6	0.0614
Resolution	0.0047	7.9	0.0057
Mow * Cam Avg	0.0012	2.1	0.1500
Resolution * Cam Avg	0.0010	1.6	0.2041
Cam * Resolution	0.0009	1.6	0.2143

In combination with F-tests, parameter estimates were used to determine the significance of model effects (**Table 2.3**). While F-tests determined resolution to be statistically significant, the coefficient of this effect was determined to approach zero, indicating negligible importance. Therefore, for the sake of improving model legibility and simplicity, resolution was also removed from the model.

Table 2.3: Parameter estimates of all initial model predictors and interactions

Effect	Estimate	Standard Error	<i>p</i> -value
Intercept	0.1322	0.0409	0.0016
Cam Avg	0.6983	0.0530	<0.0001
(Cam Avg) <sup>2</sup>	-2.714	0.8633	0.0021
Mow Direction	0.0046	0.0024	0.0614
Resolution	1.16e-6	04.123e-7	0.0057
Mow * Cam Avg	-5.958e-7	4.113e-7	0.1500
Resolution * Cam Avg	-1.1e-5	8.677e-6	0.2041
Cam * Resolution	0.0812	0.0650	0.2143

Insignificant and unimportant model effects were then removed incrementally, starting with the highest *p*-values. After all effect interactions were removed, the *p*-values of remaining effects were recalculated for the revised model, and are shown in **Table 2.4**. As shown, with interactions removed, the significance of mowing direction as a predictor improved to meet the 95% confidence criterion.

Table 2.4: Partial effects test results of the first revised model

Effect	Sum of Squares	F-statistic	<i>p</i> -value
Cam Avg	0.1106	185.2	<0.0001
(Cam Avg) <sup>2</sup>	0.0053	8.9	0.0035
Mow Direction	0.0031	5.2	0.0239
Resolution	0.0042	7.0	0.0091

Due to its low importance as demonstrated by its estimate shown in **Table 2.3**, which approached zero, resolution was next removed from the model. F-tests were again performed on remaining effects and the intercept, and effects tests of the second revised model are shown in **Table 2.5**. The *p*-value of mowing direction again improved to a high degree of significance.

Table 2.5: Partial effects test results of the final model

Effect	Sum of Squares	F-statistic	<i>p</i> -value
Cam Avg	0.1069	170.8	<0.0001:
(Cam Avg) <sup>2</sup>	0.0060	9.7	0.0023
Mow Direction	0.0048	57.7	0.0063

Remaining effects were each statistically significant beyond 95% confidence, and were also important to the model. Therefore, each of these effects were included in the final model relating the NDVI calculated from imagery to ground-truthing measurements collected by the TCM 500. The resulting model is shown in **Equation 2.5**,

$$C_m = 0.13837 + 0.6975 * C_R + 0.0066 * D_m + -2.180 * (C_R - 0.7566)^2 \quad (2.5)$$

where  $C_m$  is the modelled NDVI of TifTuf turfgrass based on camera imagery,  $C_R$  is the raw NDVI value of TifTuf based on camera imagery, and  $D_m$  is the mowing direction where mowing North is coded as 1 and mowing South is coded as 0.

## Model Validation

This model was assessed using the validation dataset. The model was applied to the initial NDVI calculated by the algorithm from imagery. These NDVI values calculated from the model were compared to the NDVI values of the same plots as measured by the TCM 500 sensor. A scatterplot and linear regression of these data are shown in **Figure 2.14**.

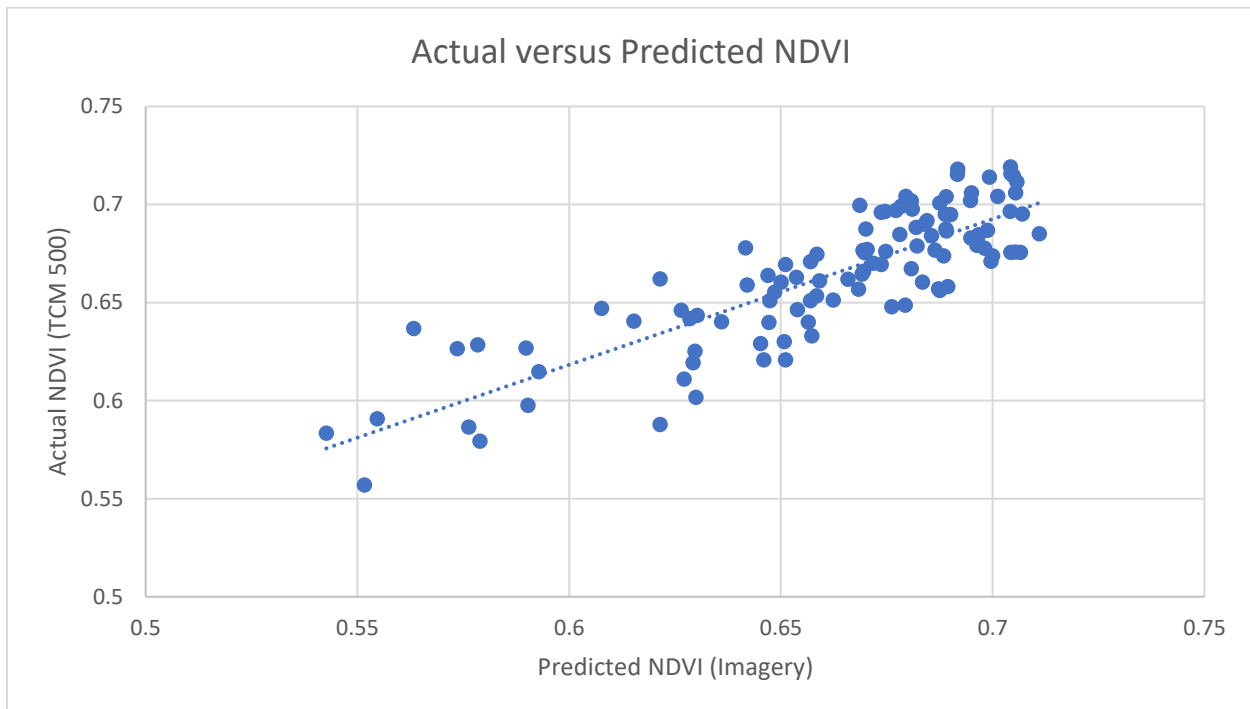


Figure 2. 14: Actual NDVI of plots measured by TCM 500 versus the predicted NDVI using imagery and the developed model

Linear regression determined there was a strong correlation between the predicted NDVI values and ground truthing ( $R=0.84$ ). The root mean squared error (RMSE) of the model was also calculated to be 0.0210. This RSME was equal to approximately 13% of the range of actual NDVI measurements.

Turfgrass visual quality was also rated by an expert throughout June until September, and these visual ratings were compared to TCM 500 measurements taken on the same day, as discussed in Chapter 3. The median NDVI values for each visual rating 4 – 8 were determined. Linear regression was performed on these data, and the difference in NDVI corresponding to one point on the NTEP scale was determined to be 0.0313. Using this same linear regression, the standard error of the model relates to an error of 0.67 on the 1 – 9 NTEP scale.

### **Discussion of Data Collection Methods**

During the modelling stage of the data analysis, it was discovered that certain improvements to data collection were important to accurate and repeatable results in both NDVI assessment methods. Measurements taken by the camera system and TCM 500 meter were taken of turfgrass plots beginning in June for an accompanying study evaluating the response in turfgrass quality to levels of deficit irrigation. It was intended that data collected throughout the entire growing season could be used to train the camera system, although data collected primarily in September and October were used in developing the model relating the two. Preliminary data analysis using data collected earlier in the season revealed a lower than desired correlation coefficient in models relating imagery-derived NDVI to TCM 500 measurements. In response, data collection methodology of both imagery and TCM 500 measurements were adjusted. Using data collected under these improved protocols, a model with a satisfactorily high correlation coefficient was achieved.

First, the average NDVI of turfgrass plots was at first calculated from three measurements from each plot. However, during data analysis it was found that from only three measurements, the standard deviation of measurements within a single plot and even the standard

error calculated from the three average NDVI values within a treatment were high. As described later, when calculating average NDVI from three measurements per plot, the standard error of average turfgrass quality of a single treatment was approximately twice as high as that of the other two methods. This was a primary reason why data collected during September and October were used to build the model relating camera-derived NDVI to meter NDVI, rather than using imagery and TCM 500 measurements taken throughout the entire growing season. Because of noise introduced in the TCM measured average NDVI by low spatial resolution, the correlation coefficient when including this data was diminished. Once discovered, spatial resolution of data collection by this method was increased in September to nine measurements taken per plot.

Similarly, information gained during data analysis also led to improvements in data collection by the camera system. During the first months of data collection, a single pair of images was collected per day of data collection. However, during data analysis, it was found that NDVI values of plots can vary throughout the day even after correcting for solar position. First, imagery taken far in time away from solar noon resulted in problems with the image registration step of the algorithm. As a general rule, imagery captured before 10 AM and after 4 PM often resulted in misaligned imagery and incorrect identification of zone areas, while imagery taken closer to noon on the same day could be registered properly. This was because imagery used as template images were captured closer to noon, and differences in lighting conditions very early or very late in the day were too great for the image registration algorithm. NDVI calculations from imagery captured in the early morning or evening were also occasionally substantially different than those calculated from imagery captured the same day but closer to solar noon, even when correcting for solar position. It is likely that this effect was created by dimmer lighting during these times, and potentially by dew in the morning. As a general rule, imagery captured

before 10 AM and after 5 PM EST often resulted in these problems. Therefore, the ideal window for capturing imagery was determined to be between 11 AM and 3PM EST during the summer. Imagery captured in this window could be most reliably registered and a linear relationship between solar azimuth could be applied to adequately adjust for diurnal changes in NDVI.

However, even during this window of data collection and after correction for solar azimuth, differences in NDVI calculated from imagery taken at different times were still present, particularly when looking at individual plots rather than the average of all plots. Relatedly, when modelling the relationship between camera-based NDVI and TCM 500 measurements using only a single pair of images to calculate the average NDVI of plots, only models with lower than desired correlation coefficients could be derived. Similar to the noise introduced by low spatial resolution of data collected by TCM 500 early in the experiment, it was suspected that low temporal resolution of imagery may have also resulted in noisy results. For example, a cloud shading part of the field while imagery was captured may have affected the NDVI values calculated for those shaded plots. A higher temporal resolution of data collection was therefore used to mitigate the effect of temporary partial shading of the research field by clouds or other obstructions. When collecting data during September and October for modelling, average plot NDVI values were calculated from an average of 4.5 image pairs per day. In combination with the increased data collection by the TCM 500, averaging daily NDVI measurements from multiple image pairs resulted in a model with a satisfactory correlation coefficient between camera-based and TCM 500 NDVI values.

Finally, major patterns also emerged in the manual verification of proper image registration described in **Data Verification and Cleaning** section. The large majority of image keypoints identified by the image registration algorithm were concentrated on two aspects of the

imagery: the treeline and a square metal sign installed in the center right of the field, as shown in **Figure 2.4**. As a result, by far the most common error of imagery misalignment occurred in turfgrass plots furthest away from these two features, to the Southwest of the field where far fewer keypoints were identified. Keypoints are identified where there are unique features in the image differentiating them from their surroundings, which the treeline and metal sign provided. In hindsight, the installation of additional marker signs positioned at all corners of the field would likely have provided additional potential keypoints, and therefore greatly reduced the occurrence of improper image alignment, as keypoints serve as ‘anchors’ in the translation of pixels during the image registration process.

## Conclusions

The use of nonorthographic imagery captured from a pole mounted camera was demonstrated to have significant value in measuring the NDVI and overall visual quality of TifTuf turfgrass plots. A novel method was developed to automatically measure the NDVI of multiple turfgrass plots using only two images, one using a red bandpass filter and the other using a NIR bandpass filter. This method is advantageous in that it does not require any additional position sensors and may be used effectively to identify and calculate the NDVI of multiple areas of interest using imagery taken from any angle of incidence. It also does not require the use of field installed color calibration panels or the manual adjustment of image framing to position markers. When using the image registration for image processing as in this paper, however, we do recommend the installation of some type of markers at the corners of the field, as these provide excellent ‘anchor points’ for the reliable alignment of images to the template image.

Additional factors affecting the measurement of NDVI of TifTuf plots from raw imagery were also identified, and correction factors were determined. Significant diurnal changes in uncorrected NDVI measurements were measured, and the solar azimuth was proposed as the causal factor. A method for developing a specific correction factor for a camera system with a fixed position was used and described. However, additional research is recommended measuring any diurnal changes in NDVI from imagery taken by cameras with different camera azimuths and angles of incidence in order to identify any universal correction equation or method.

Mowing direction was also discovered to have a significant, though small, effect on the measurement of NDVI of TifTuf bermudagrass from angled imagery. Mowing away from the vantage point of the camera, which created relatively lighter stripes of turfgrass, was associated with an increase in turfgrass NDVI ( $p = 0.006$ ). For the most accurate assessment of turfgrass visual quality and NDVI measurement, we recommend researchers take notice of and compensate for lighter and darker stripes determined by mowing direction. Other turfgrass cultivars or species may be affected differently by this effect, as well as by changes to the camera angle of incidence and the angle between the camera azimuth and the mowing direction. Therefore, the effect of mowing direction on NDVI should be measured using a similar process for each site independently.

A model was developed to determine the NDVI of TifTuf turfgrass plots from imagery which had a strong correlation with ground truthing data ( $R = 0.84$ ). We recommend the future use of pole mounted camera systems and the image processing techniques used in our algorithm for the assessment of turfgrass visual quality. These techniques resulted in an algorithm which measured turfgrass NDVI strong agreement with TCM 500 NDVI measurements, and offer the benefit of very high temporal resolution with little or no additional labor requirement.

**CHAPTER 3: RESPONSE OF TIFTUF BERMUDAGRASS TO IRRIGATION  
FREQUENCY AND DEFICIT IRRIGATION**

## Abstract

New, drought tolerant turfgrass cultivars have the potential to reduce water usage while maintaining desirable turfgrass aesthetics. Determining the dose response of turf visible quality to water saving irrigation strategies and the minimum level of deficit irrigation to maintain consistent acceptable quality are important to giving lawn owners the knowledge and confidence to use these water efficient strategies. The response of visual quality of TifTuf hybrid bermudagrass (*Cynodon dactylon* x *C. transvaalensis*) to varying levels of deficit irrigation and frequency was measured by visual assessment and two methods of measuring NDVI during 90 days of treatment. Soil was a fine textured Cecil sandy loam. Of all deficit irrigation treatments, only the mean visual quality of unirrigated turfgrass was significantly lower than the highest quality treatment (80% ET) as measured by all assessment methods. Overirrigation (120% ET) also resulted in significantly lower mean quality than the highest quality treatment as measured by camera-based NDVI. The total number of days turfgrass under each treatment exhibited unacceptable quality was also estimated. Unirrigated turfgrass experienced the highest number of days below acceptable quality (18-31 days). The handheld NDVI meter also measured 5 days of unacceptable quality in the 40% ET treatment. Unacceptable turfgrass quality was not measured in lesser degrees of deficit irrigation. Overirrigation resulted in an estimated 4 days of unacceptable quality measured by visual ratings and 23 days of unacceptable quality measured by handheld NDVI meter.

## Introduction

A significant source of municipal water use in America is turfgrass irrigation. In warm climates, turfgrass irrigation can constitute over 60% of total residential water use, often

stressing municipalities into placing restrictions on lawn irrigation to conserve water (Haley et al., 2007; Opitz et al., 1999; Ozan & Alsharif, 2013). Yet lawn owners also face social pressure to maintain consistently green lawns, and often irrigate excessively and ignore water restriction ordinances to avoid lowered quality caused by water stress (Henry, 1999; Ozan & Alsharif, 2013).

Turfgrass varieties with lower water requirements and attributes which allow them to maintain acceptable quality during droughts are therefore highly desirable, allowing the desires of lawn owners and municipal leaders to be met simultaneously (Jespersen et al., 2019). TifTuf (*Cynodon dactylon* x *C. transvaalensis*), a hybrid bermudagrass, is marketed for its drought tolerance and has demonstrated higher visual quality than other warm season turfgrass varieties, including other bermudagrasses (Jespersen et al., 2019).

For drought tolerant turfgrasses to translate into water savings, however, homeowners must have knowledge of and confidence in water saving irrigation strategies. One relevant metric to understanding how much irrigation is required to maintain attractive turfgrass is its minimum deficit irrigation level (MDIL), or the level of deficit irrigation which can be applied over time which still produces acceptable turf quality. In studies to determine the MDIL of a turfgrass variety, varying levels of deficit irrigation can be applied to plots and the visual quality of each treatment tracked over time. These studies are useful in that they can reveal the dose response of visual quality to irrigation and demonstrate the level of irrigation above which no appreciable gains in visual quality may be achieved. Such research may provide helpful management advice for a certain turfgrass cultivar for irrigation scheduling as well as convincing evidence for concerned homeowners hesitant to reduce their water use.

In this study, TifTuf will be subjected to varying levels of irrigation throughout a growing season, and the response of visual quality will be measured. The MDIL will be determined, as well as the water requirement for TifTuf and the potential water savings achievable by applying the MDIL.

## Materials and Methods

### **Site Description**

The research site was established at Lake Wheeler Road Turfgrass Research Center in Raleigh, North Carolina with twenty-four turfgrass research plots (4.57 m by 4.57 m), and 0.91 m of perimeters separating the plots. Soil at the site was a Cecil sandy loam, although previous soil sampling classified the soil as clay by texture (Ihab E Ghali et al., 2010). Popup sprinklers with multi-stream, adjustable spray pattern nozzles (53925, Toro Company, Bloomington, MN) were installed at all four corners of every plot, and each plot designated its own individually manageable irrigation zone. Each sprinkler nozzle was set to use a quarter circle spray pattern positioned such that the quarter circle was contained within the zone area. One Baseline 'bisensor' soil moisture sensor (BL5315B, HydroPoint, Petaluma, CA, USA) was installed at the center of each plot, buried 6.35 cm below the soil surface. Soil moisture was logged every hour to the nearest 0.1% volumetric water content (VWC). A Baseline BaseStation 3200 was installed as the irrigation controller. This controller allowed individual control of irrigation of each plot, including the programming of irrigation of multiple zones concurrently. Irrigation could be applied by runtime in minutes at a scheduled time or by soil moisture, whereby irrigation could be programmed to run for a designated time once a certain soil moisture depletion was reached

or could be programmed to irrigate until a certain soil moisture fill point was reached. Full control of the irrigation controller could be accessed remotely via [baselineapps.net/](http://baselineapps.net/).

Five underground control boxes were installed on the East side of the research area, one box for each row of plots going from East to West. Inside the control boxes were both solenoid and manual flow valves for laterals for each zone. Twenty-four flow meters (WM-NLC, Assured Automation, Roselle, NJ) were also installed in line with the lateral pipes. Flow meters had an accuracy of +/- 1.5%. Each of the flow meters was also equipped with a reed switch single pulse output (WM-C-SRS, Assured Automation, Roselle, NJ) which was positioned over a magnet on a spinning counter, resulting in a single pulse every 0.1 gallons pumped through the flow meter.

A control and data acquisition station was installed on the center East side of the research site. One CR1000X and one CR6 datalogger (Campbell Scientific, Logan, UT USA) were installed in a weatherproof enclosure.

A manual rain gage (All Weather Rain Gauge, Productive Alternatives, Fergus Falls, MN) was installed at the research site clear of any overhead obstructions. Following precipitation events, the depth of water measured by the rain gage was recorded and water was subsequently emptied.

## **Experimental Design**

The hybrid bermudagrass TifTuf was evaluated for visual quality under 8 different irrigation regimes. Six irrigation treatments were irrigated twice per week, with the depth applied being a fraction of potential evapotranspiration (ET) since the last irrigation event: 0% ET, 40% ET, 60% ET, 80% ET, 100% ET, and 120% ET. Two more treatments were irrigated at 100% ET, but varied in their irrigation frequency: 4 times per week, and 7 times per week. The ET

used to determine irrigation depths in this study was the potential ET, calculated by **Equation 3.1**,

$$ET = ET_0 * K_c \tag{3.4}$$

where  $ET_0$  was the reference evapotranspiration ( $ET_0$ ), and  $K_c$  was the monthly crop coefficient of TifTuf turfgrass.  $ET_0$  was estimated by the Penman-Monteith equation and weather data recorded by a weather station 1.2 km from the site. The monthly crop coefficient of TifTuf bermudagrass were previously determined experimentally at the research site (Pinnix & Miller, 2019b).

Turfgrass quality was assessed by visual ratings and two methods measuring the normalized difference vegetation index (NDVI) of turfgrass plots. Each week, all plots were given a rating between 1 and 9 according to NTEP standards, where 1 represents the poorest overall quality and 9 represents ideal quality (Morris & Shearman, 1998). A rating of 6 and above is commonly considered to be acceptable turfgrass quality. Turfgrass quality ratings consider all features of the grass, including color, density, disease, and uniformity, and ratings are generally comparable within a species but not across species.

Previous research has shown that mowing height has a affects turfgrass spectral reflectance and NDVI measurements (Sullivan et al., 2017). Scalping, which occurs when more than one third of the turfgrass root is removed, also produces areas of poor and uneven quality (Trappe et al., 2008). It was also suspected by researchers that the mowing direction, which produces “stripes” which appear darker and lighter based on the position of the viewer, may also similarly affect the NDVI measured by a camera system viewing the turfgrass from an angle (Mellor, 2001). Therefore, a mowing and management plan was devised to address these

concerns. First, a mower and mower blade configuration were selected to achieve the highest feasible mowing height to minimize scalping and the effects of mowing height on camera-based NDVI. A zero-turn mower (Z930M ZTrack, John Deere, Fuquay Verina, NC) with a blade height set to 6.35 cm was used until July 9. However, it was determined that the zero-turn mower, in combination with the uneven ground at the research site, led to unacceptable scalping. On July 13, mowing was changed to a reel mower (Reelmaster 3100-D, Toro Company, Bloomington, MN) set to a blade height of 5.2 cm, which was found thereafter to produce a significantly more even cut and quality of turfgrass.

Mowing frequency was also scheduled to minimize scalping. On most weeks throughout the study, turfgrass was mowed twice per week on Monday and Thursday except on those days where rain or schedule conflicts required mowing to be rescheduled for the next day. On some weeks in July and August, when turfgrass growth was at its highest, grass was mowed three times per week in order to prevent scalping and maintain a more even height of turfgrass. Finally, mowing direction was designated as a blocking variable in the experimental design. Mowing was performed such that for any given plot, the entire area was mowed with the mower moving in the same direction. Turf was mowed by the mower moving either North or South, blocked by row so that mowing passes could be made across entire rows. The full experimental design is shown in **Figure 3.1** below.

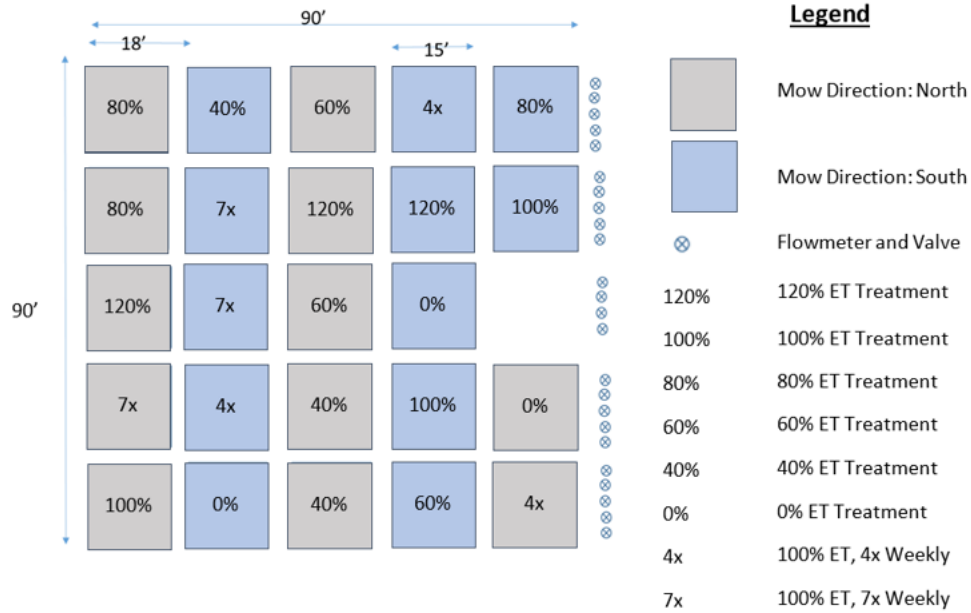


Figure 3.1: Experimental design and field site diagram

### Visual Quality Assessments

Visual quality was determined by three methods: expert turfgrass visual ratings, and two methods of NDVI measurements. Once per week, typically on Fridays, each plot was assessed by an expert and rated on a 1-9 scale according to the National Turfgrass Evaluation Program (NTEP) standards (Miller et al., 2021). Turfgrass quality was also measured using a Fieldscout TCM 500 NDVI turf color meter (Spectrum Technologies, Inc, Aurora, IL). The sensor measured NDVI using a controlled internal light source and a circular measurement area of 45 cm<sup>2</sup>. One to two times per week, three turf NDVI measurements were taken per plot using the meter. A random stepping pattern was created and used for all plots in a single day of measurements to prevent unconscious human bias from affecting the selection of sampling areas. Finally, a novel pole mounted camera system was used to capture imagery and measure the NDVI of all plots daily, the details of which are elaborated on in Chapter 2.

The visual quality of turfgrass for each treatment was measured separately by each method. The average visual quality of a treatment on a particular day was assumed to be the average value of all measurements taken by a single method on that day. For example, three measurements were taken per zone by the handheld NDVI meter once or twice per week. On a particular day, the average turf quality of the 100% ET treatment was assumed to be the average NDVI value of all nine NDVI measurements taken from the three zones receiving the 100% ET treatment.

### **Zone Application Rate**

Prior to beginning the experimental period, physical instrumentation at the site was carefully inspected and evaluated for the even and accurately measurable distribution of water to each zone. Both prior to and approximately monthly during the experiment, each sprinkler was inspected to ensure proper function and adjusted such that its distribution area was one quarter circle within the bounds of the zone. Replacements to nozzles and popups were made as necessary throughout the study.

Flow meters connected at the laterals of every zone were used to evaluate the flow rate of water being delivered to the sprinklers at each zone. Despite the fact that all sprinklers had built-in flow regulators to maintain even flow rates across sprinklers, it was suspected that imperfect manufacturing tolerances combined with significant variations in total friction head loss between zones in different positions may lead to significant differences in the rate of flow delivered to zones. Therefore, once the positioning and nozzle settings had been set, the flow rate of each zone was determined empirically as described below.

In order to simplify zone programming and to keep flow rates as consistent as possible, it was decided that during the experiment, each zone would be irrigated simultaneously with other zones of its same treatment, and no other zones. These three zones would start and stop at the same times with equivalent runtimes, and would be followed by the next set of three zones. Therefore, this same setup was used during the process of measuring average zone flow rate. For each treatment, the three zones belonging to the treatment were activated and allowed to run for 10 minutes. Flow meters measured water flow to each zone to the nearest 0.1 gallons, and recorded the total water moving through the flow meter per minute. Afterward, the average flow rate per minute for each zone was calculated using **Equation 3.2**,

$$Q = 6 * \frac{n}{10} \tag{3.5}$$

where  $Q$  was the volumetric flow rate in gallons per minute, and  $n$  was the number of pulses counted in the ten minute interval. This volumetric flow rate was converted to an average nominal application rate by converting to metric units and dividing by the surface area of the plot.

A catch can distribution uniformity evaluation was also performed to estimate the average distribution uniformity of all zones. Sixteen plastic wide mouth mason jar lids with a diameter of 8.9 cm and a depth of 1.9 cm were used as catch cans and placed in a 4 x 4 grid within one of the zones, such that there was a 0.575 m space between the zone border and cans nearest the border (one half spacing), and a 1.15 m spacing between one can and another (one full spacing). The zone valve was opened and allowed to run for 15 minutes, after which water was shut off again. Then, the water from each catch can was poured into a graduated cylinder

and the can number and amount of water recorded. Finally, **Equation 3.3**, Christiansen's Uniformity Coefficient, was used to calculate the application uniformity of the zone,

$$UC = 1 - \frac{(\sum_{i=1}^n |y_i - d|/n)}{d} \quad (3.6)$$

where  $y_i$  was the volume of water caught by each can ( $\text{cm}^3$ ),  $d$  was the average volume of water caught per can ( $\text{cm}^3$ ), and  $n$  was the number of cans (Christiansen, 1942). The application uniformity was determined to be 81.5%.

The actual application rate for each zone per minute was calculated by dividing the average flow rate of the zone by this distribution uniformity. These experimentally determined application rates for each zone were thereafter used when determining the necessary zone runtime required to apply a target depth of water during the experiment.

### **Irrigation Runtime Calculations**

The irrigation runtime for each zone was determined by the estimated evapotranspiration, effective rainfall, and effective zone application rate. First, the total evapotranspiration which had occurred since the last irrigation date was determined as the sum of daily evapotranspiration calculated by **Equation 3.1**.

Actual evapotranspiration was determined by multiplying the  $ET_0$  by a crop coefficient. Average monthly crop coefficients for TifTuf bermudagrass were previously determined at the Lake Wheeler Road research site (Pinnix & Miller, 2019a). The total  $ET_0$  was multiplied by the TifTuf crop coefficient for the corresponding month to calculate the estimated the potential ET.

The effective rainfall was calculated for every zone and for each day on which precipitation occurred. Due to the expected wide variations in soil moisture conditions across zones and the correspondingly varied capacities for infiltration and additional water storage capacity, a method of calculating effective rainfall which considered antecedent moisture conditions was selected. First, the antecedent soil moisture for every zone was gathered from the Baseline Manager webapp. The soil moisture data recorded by the sensor corresponding to each zone was accessed, and the volumetric water content prior to the start of rainfall was recorded. Next, the depth of precipitation recorded by the rain gage in inches was converted to millimeters. To calculate the estimated effective rainfall, **Equation 3.4** was used,

$$ER = f(D)(1.25 P_m^{0.824} - 2.93) * 10^{0.000955 * ET} \quad (3.7)$$

where ER was the effective rainfall in millimeters,  $f(D)$  was the antecedent soil moisture adjustment factor,  $P_m$  was the rainfall in millimeters, and ET was the average monthly evapotranspiration in millimeters (Huffman et al., 2011). The antecedent soil moisture adjustment factor was calculated by **Equation 3.5**,

$$f(D) = 0.53 + 0.0116 * D - 8.94 * 10^{-5} * D^2 + 2.32 * 10^{-7} * D^3 \quad (3.8)$$

where D was the soil water deficit within the root zone in millimeters (Huffman et al., 2011).

Finally, the soil water deficit in millimeters was calculated by **Equation 3.6**,

$$D = (FC - VWC) * 152.4 \quad (3.9)$$

where FC was the volumetric water content of the field capacity (%), VWC was the volumetric water content of the soil prior to the rainfall event (%), and 152.4 was the effective root depth of bermudagrass in millimeters (Huffman et al., 2011; Ross & Hardy, 1997). The field capacity of the soil was considered to be 33% volumetric water content, which was observed to be the average water content across turfgrass plots approximately 72 hours after heavy rainfalls observed in the winter of 2020 while turfgrass was dormant. If the soil water deficit was determined to be lower than the effective rainfall calculated by **Equation 3.4**, then the effective rainfall was considered to be equal to the soil water deficit.

The target effective application depth was calculated for every zone by **Equation 3.7**,

$$D_a = (ET_T - ER)/E_a \quad (3.10)$$

where  $ET_T$  was the total evapotranspiration having occurred since the last irrigation event (mm),  $ER$  was the effective rainfall (mm), and  $E_a$  was the application efficiency (%).

Finally, because irrigation zones were programmed by runtime, the necessary runtime for each zone was calculated by **Equation 3.8**,

$$T_R = D_a/R_a \quad (3.11)$$

where  $ET_T$  was the total evapotranspiration having occurred since the last irrigation event (mm),  $ER$  was the effective rainfall (mm), and  $E_a$  was the application efficiency (%).

Once the irrigation runtime for each zone had been calculated, the irrigation controller was reprogrammed to reflect the correct runtimes on every day irrigation was applied.

This process resulted in an irrigation runtime calculated for each zone, and due to differences in effective rainfall and flow rates across zones, even zones within the same treatment often resulted in small differences in target runtime. Because zone flow rates were affected by how many and which other zones were running simultaneously, and because average flow rates for each zone were measured while running alongside zones in the same treatment, it was important to ensure that zones always ran only alongside zones within the same treatment. Due to software limitations of the irrigation controller, this could only be accomplished by creating different programs for each treatment and adding all zones within the treatment to the same program. This required that all zones be irrigated with the same runtime during each application, despite slight differences in calculated target runtime. In order to determine which runtime to use for all three zones within each treatment, a random number generator was used to generate a number between 1 and 3. A number 1 generated would result in the runtime calculated for the lowest numbered zone to be used for the treatment, a number 2 would result in the runtime from the middle numbered zone selected, and a number 3 resulted in the runtime of the highest numbered zone selected. This was done to minimize systematic bias introduced by differences in flow rates resulting in zones within the same treatment, which otherwise may have resulted in some zones being consistently overirrigated or underirrigated even relative to their treatments.

The order in which treatments were irrigated was also randomized. Because only three plots out of twenty-one irrigated plots were watered at a time, completing a full irrigation often took several hours. Therefore, because irrigation always took place in the evening, it was possible that plots irrigated earlier in the day would experience a greater amount of evaporation, resulting in a lower effective irrigation depth. A priority setting could be used in the irrigation controller to designate the order in which programs were run when multiple programs were set to

run at the same start time. A list of numbers from 1 to 7 was given a random order using a random list generator for each irrigation event, and this was used to give each program its priority.

Because application depths on a single day could exceed 1.9 cm at application rates of approximately 2.54 cm per hour, and due to the fine textured soil at the site, irrigation events were also broken up to allow for soaking periods and to minimize potential runoff. This was accomplished by giving each program two start times two hours apart, and by setting the runtime for each event to half of the calculated target runtime per treatment. This meant that all seven programs would be run sequentially and apply half of their application depth, then wait until two hours had elapsed since the first program began running, and would then run all seven programs sequentially again to apply the second half of the full application. This allowed for over an hour of soaking time between the two half applications.

## Results and Discussion

### **Water Management**

Soil moisture, water applied by irrigation, and precipitation were measured throughout the experimental period. The cumulative water received in each treatment is compared to the cumulative evapotranspiration in **Figure 3.2**.

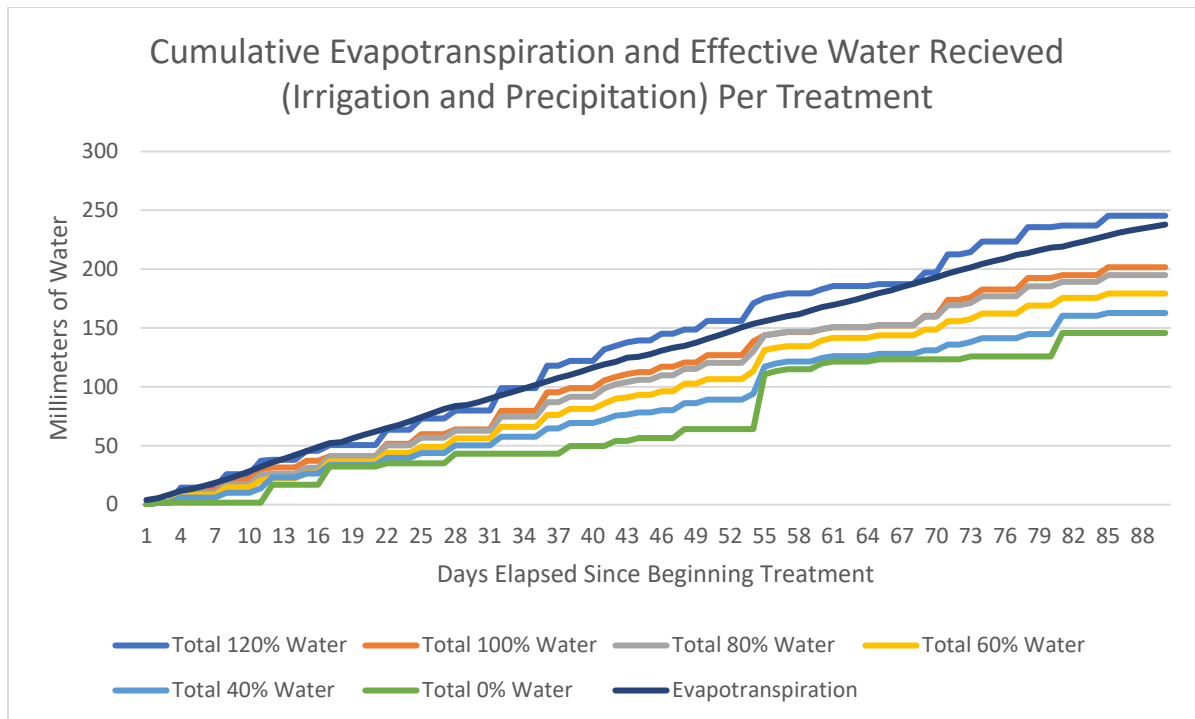


Figure 3.2: Cumulative potential evapotranspiration and water received by turfgrass plots in each treatment

Varying depths of water applied to different treatments resulted in an expected stratification in cumulative water applied. By the end of the experimental period, the proportion of total water received to cumulative potential evapotranspiration for the 120%, 100%, 80%, 60%, 40%, and 0% treatments retrospectively were: 103%, 85%, 82%, 75%, 68%, and 61%. The total proportion of water applied in each treatment to the 100% ET treatment, in the same order, were: 124%, 100%, 82%, 63%, 43%, and 0%.

The methodology and management used to calculate irrigation runtimes for different treatments throughout the season resulted in all treatments receiving quantities of irrigation nearly equivalent to their targets as described by each treatment designation. A wide and evenly stratified range of irrigation depths applied were achieved, as shown in **Table 3.1**.

Table 3.1: Average irrigation, effective rainfall, and soil moisture of treatments

Treatment	Total Water Received (mm)	Irrigation Applied (mm)	Effective Rainfall Received (mm)	Average VWC (%)
120%	245.4	197.8	47.6	30.4
100%	201.6	159.0	42.6	31.5
80%	195.0	130.8	64.1	29.7
60%	179.3	100.4	78.9	28.2
40%	162.8	68.3	94.5	28.7
0	145.8	0.0	145.8	24.2
7x	204.8	167.6	37.1	32.0
4x	202.0	164.3	37.6	31.3

While treatments designated for higher fractions of ET received proportionately higher quantities of irrigation throughout the season, typically lower soil moisture contents of lower fraction ET treatments received higher quantities of effective rainfall. This resulted in the differences in total water received between treatments being smaller than the differences in total irrigation applied. The proportions of total water received by each treatment to the 100% ET treatment, in the same order, were: 122%, 100%, 97%, 89%, 81%, and 72%. In other words, differences in irrigation depths applied across different treatments were partially mitigated by disproportionately benefiting from frequent rainfalls in the southeastern climate. Weather alone provided unirrigated turfgrass with 61% of its total water requirement throughout the study, as measured by potential ET.

The response of top soil moisture content to water applications and weather conditions is also important in assessing the efficacy of the irrigation management plan and the effects of differences in irrigation applied to plots, and is shown in **Figure 3.3**. Soil moisture as reported in this figure is the average soil moisture of the three plots in each treatment. Thunderstorms and technical challenges affected the ability to control irrigation and monitor soil moisture during some portions of the study. During a severe thunderstorm on August 14, some electronic equipment was damaged, resulting in the loss of network connectivity across the site.

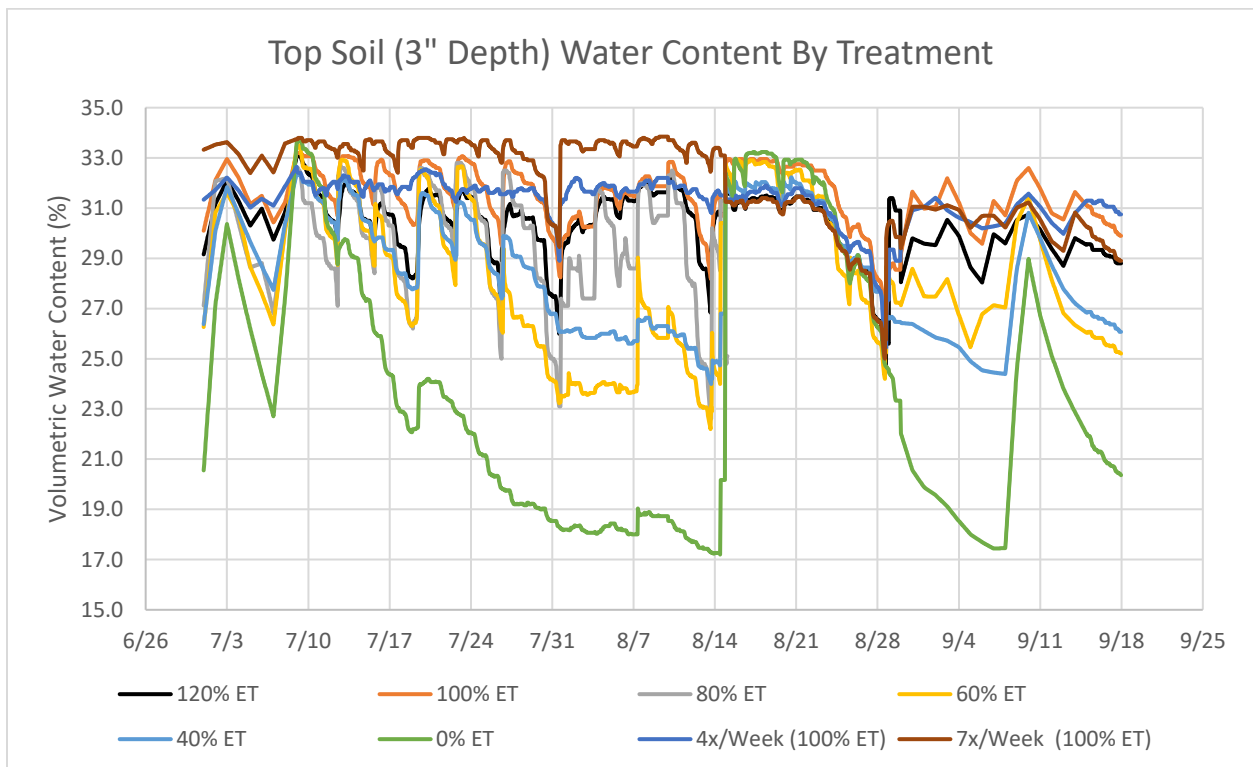


Figure 3.3: Average volumetric soil moisture of turfgrass plots in each treatment

A box plot of volumetric soil moisture data collected from plots under these irrigation treatments is shown in **Figure 3.4**. The distributions of soil moisture of treatments receiving 100% ET or greater are all similar, with lower quartiles above at least 29% and hinges above

26% VWC. Outliers within these treatments are attributed to the equipment damages which occurred on August 14, leading to a longer period between irrigation events until repairs could be made. The range of soil moisture levels experienced by treatments under deficit irrigation generally became wider as the deficit increased. The median soil moisture of the 80% ET treatment was only about 1% lower than the well-watered treatments, although the lower quartile indicates that soil moisture was below 29% greater than one quarter of the period. Soil moisture conditions experienced by the 60% ET and 40% ET treatments were similar, with medians approximately 2% lower than the 80% ET treatment and lower quartiles just over 26% VWC. The unirrigated treatment experienced soil moisture conditions significantly different from other treatments, with a median water content about 5% lower than the 40% ET treatment and a lower quartile of 19% VWC.

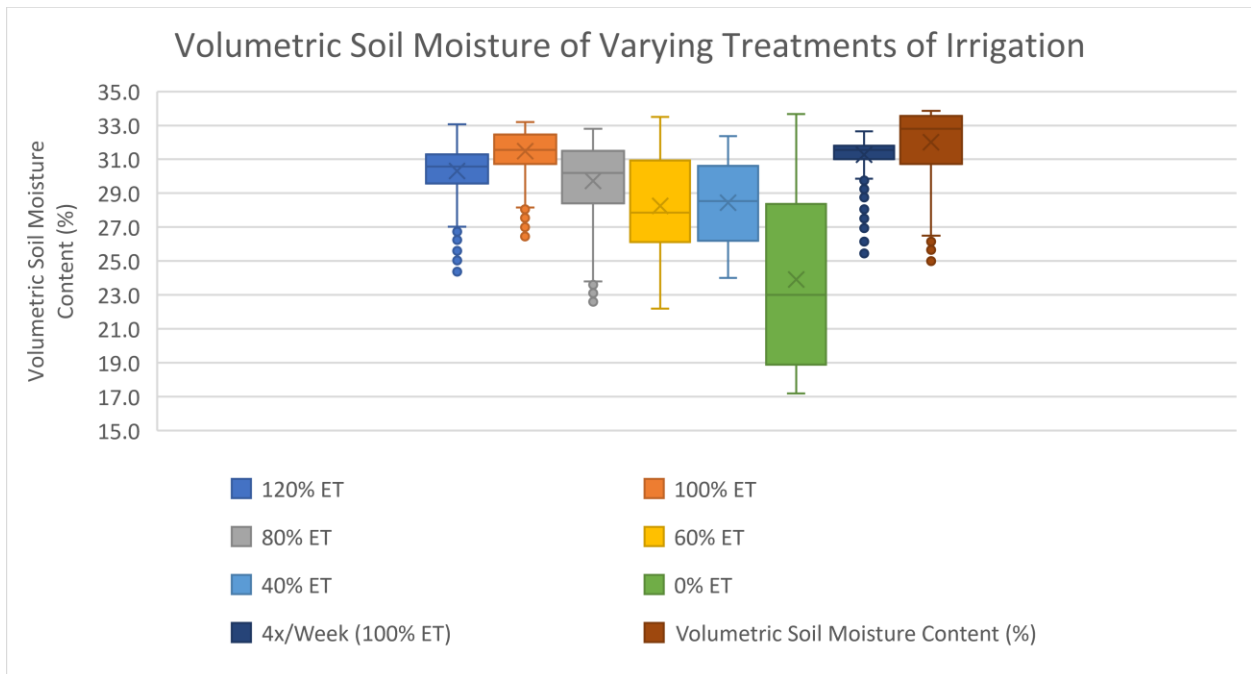


Figure 3.4: Box and whisker plot of soil moisture measurements throughout the experimental period

## **Site Management, Challenges, and Effect on Data**

Prior to the beginning of treatment, all plots were well watered with soil moisture-based irrigation scheduling which irrigated plots to field capacity when soil moisture was detected to drop below 28% VWC. The recommended basic fertilizer rate by North Carolina State University of one pound of nitrogen per 1000 square feet was also applied uniformly across the entire site on May 20 and on July 23 (Miller et al., 2021). At the time that treatments commenced on June 18, all treatments were rated above 7.

In the first month of the study, the quality of all plots dropped to below 7, including well watered plots. This decline is partially explained by two factors. First, it was expected that all plots would decline in quality somewhat over time as more time elapsed since fertilization. Nitrogen fertilizer resulted in a boost in visual quality and greenness, and some diminishing of the beneficial effects of fertilizer was expected.

The second factor which uniformly led to a decline in turf quality early in the study was scalping caused by poor mower management. At the start of the experiment, it was believed that the zero-turn Z930M mower was the ideal choice for mowing due to the highly adjustable mower blade height, which allowed the mower blade to be set at a height of 5.7 cm rather than at the 5.2 cm height possible by the other mower available. A higher mowing height can in some instances avoid scalping by lessening the chance that more than one third of the leaf is removed. However, it was discovered that this mower configuration caused substantial scalping during the first weeks. It is believed that the uneven ground at the site more significantly affected the small zero-turn mower's ability to maintain an even blade, leading to an uneven cut and many areas where the turf was cut too low. The excessively low cut areas were scalped, and created brown spots across the site. The scalping significantly affected turfgrass quality, and this explains the

decline in turfgrass quality during the first two weeks in July even in plots where no water stress was experienced.

In response, the mowing configuration was altered. Beginning on July 12, turf was mowed using a Reelmaster 3100-D reel mower. As a result, all treatments except 0% ET experienced a rebound in turf quality between July 9 and July 16, and all irrigated treatments had at least an average quality of 7 by July 30. This mower resulted in little to no scalping throughout the rest of the study, and previously scalped areas recovered over time such that they no longer significantly affected turf quality by July 30.

An approximately two week gap in camera measurements exists following the severe storm which occurred on August 14, due to equipment damage. The system was restored by August 30.

Additionally, a number of soil moisture sensors were also damaged by storms throughout the season. Three days after the commencement of the experiment, the soil moisture sensors in plots 1, 5, and 10 were damaged and stopped reporting following a storm on June 21. Replacing sensors would have required digging up areas of turf in the center of the plots nearly 50 cm long to recover the long blade sensors, and it was feared that this would negatively impact turf visual quality ratings and introduce challenges to accurately assessing turfgrass quality through the camera imagery analysis algorithm. Therefore, it was decided that soil moisture sensors would not be replaced during the study period, and that soil moisture for each treatment for estimating effective rainfall and use in results analysis would be estimated as an average of data from the remaining functioning soil moisture sensors within each treatment.

## Visual Ratings of Turf Quality

Turf quality was assessed by three separate methods throughout the experimental period. The first method of assessment was visual quality ratings performed by an expert at the Turfgrass Research Center. To determine the turf quality for each treatment each week, ratings for all three plots in each treatment were averaged for each day of assessment. The results of this method are given in **Figure 3.5**.

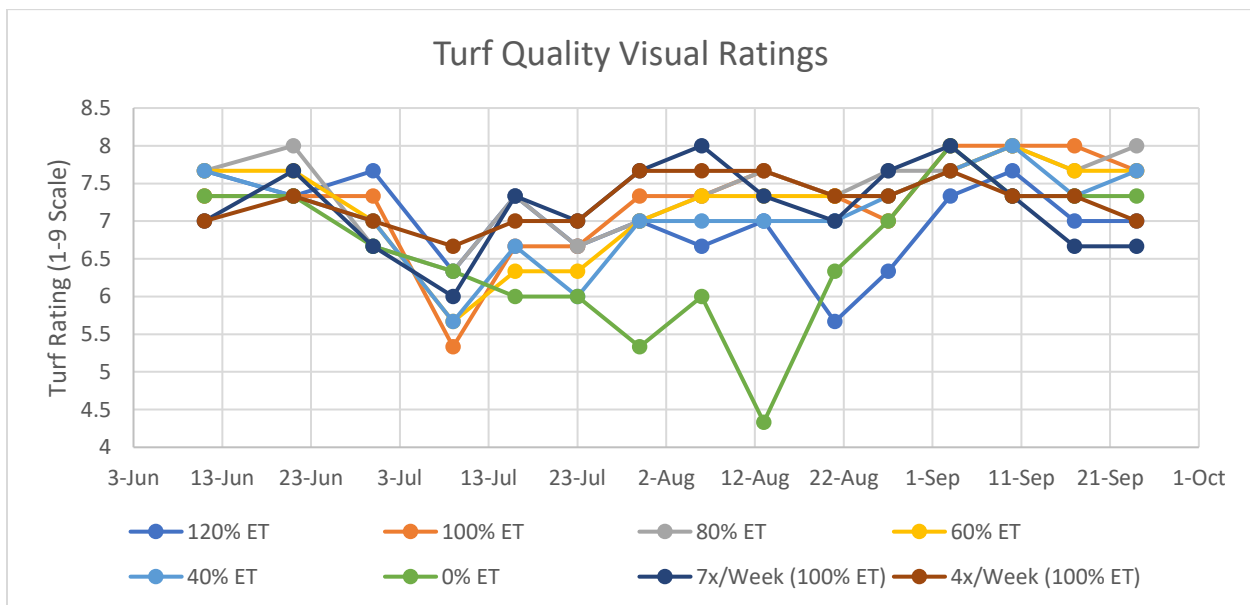


Figure 3.5: Average NTEP visual ratings of turfgrass of each treatment

## Relating NDVI Assessment Methods to Quality Ratings

The average NDVI of turfgrass taken from nine measurements by TCM 500 across three plots are shown in **Figure 3.6**. Additionally, the average NDVI of turfgrass under each treatment as measured by the camera system are shown in **Figure 3.7**, where the developed image processing algorithm described in Chapter 2 was used to calculate NDVI of plots from imagery captured throughout the season.

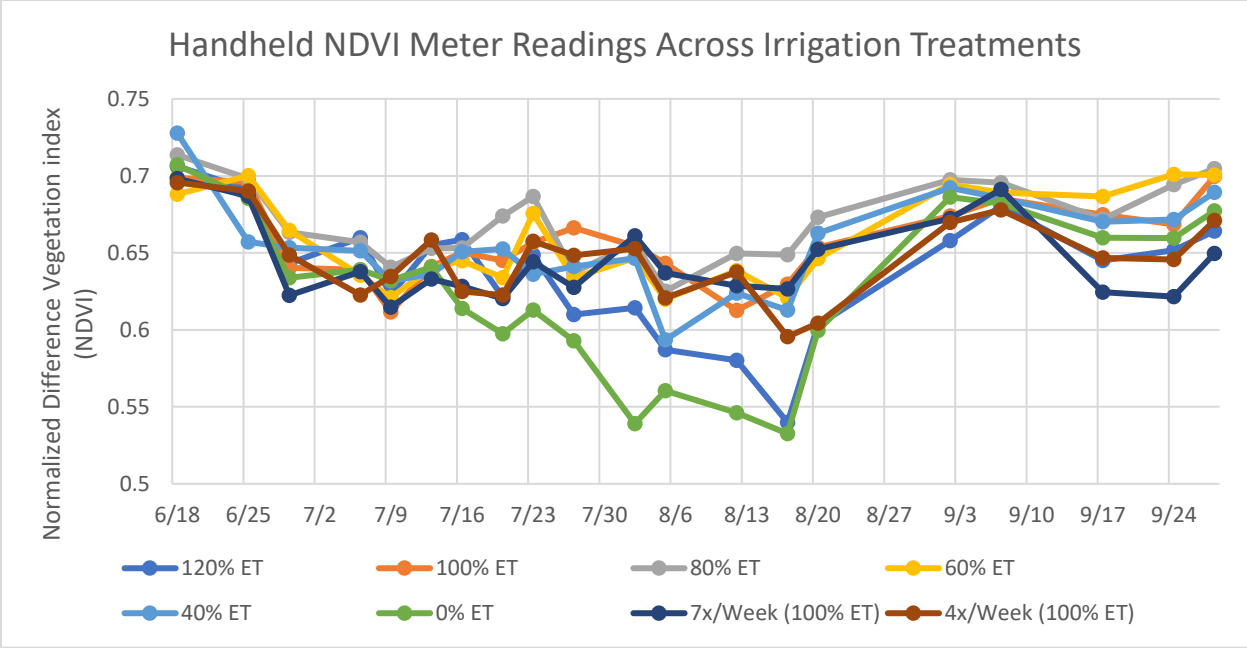


Figure 3.6: TCM 500 NDVI of turfgrass under irrigation treatments

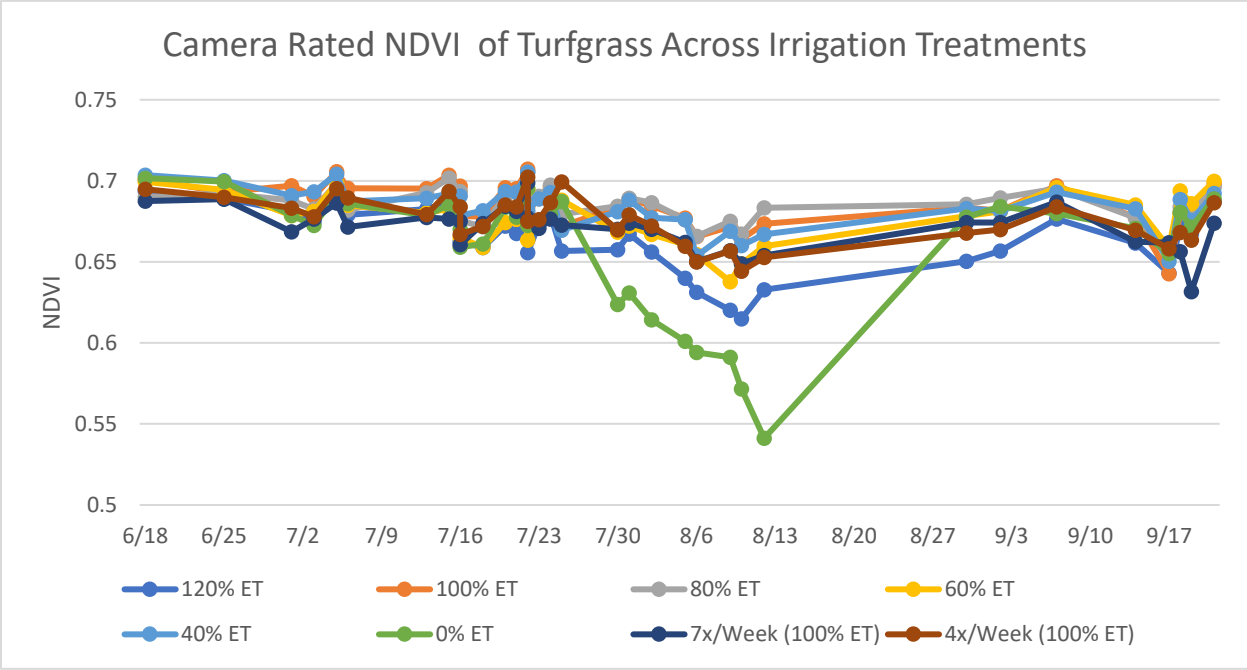


Figure 3.7: Camera-based NDVI of turfgrass under irrigation treatments

In order to make direct comparisons across all treatments and to best interpret the quality of turfgrass from NDVI values, a relationship between turfgrass visual ratings and NDVI determined by handheld meter was established. Previous research has shown that different models are necessary in relating NDVI to visual quality ratings for different turfgrass species and even cultivars of the same species (Bremer et al., 2011a). Therefore, a model was developed from experimental data collected during the study to relate the NDVI of TifTuf to NTEP visual quality ratings. On ten days throughout the study, visual ratings were performed within 24 hours that NDVI measurements were taken using the meter. Two of these days were excluded due to the presence of scalping which affected visual ratings. 192 measurements of plots from the remaining 8 days were used to relate ratings to NDVI. On these days, turfgrass ratings ranged from 8 to 4. Initially, turf rating and NDVI were plotted as a scatterplot as shown in **Figure 3.8**.

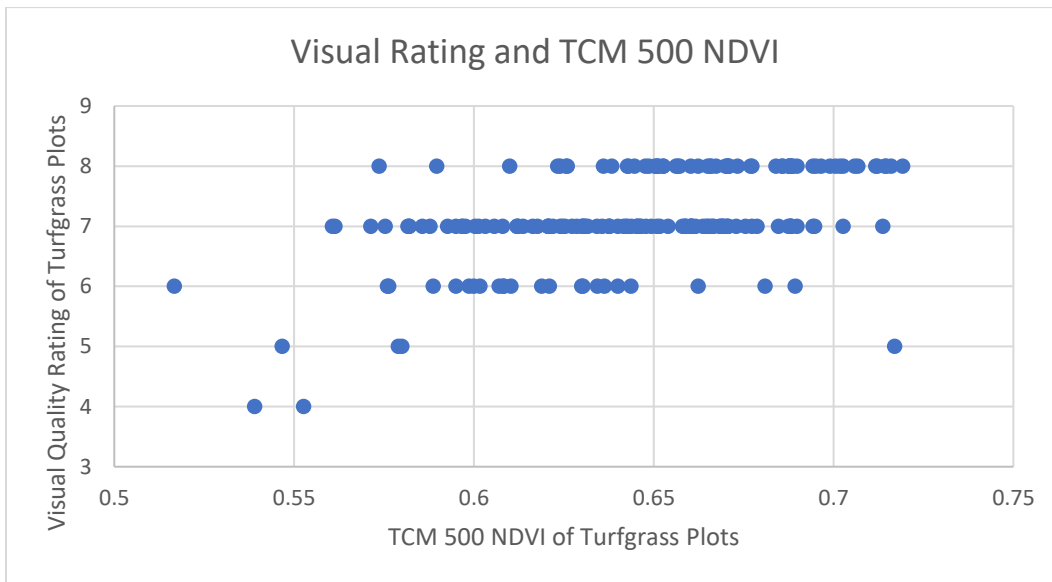


Figure 3.8: Visual quality and TCM 500 NDVI of turfgrass plots measured on the same day

The correlation between TCM 500 NDVI and visual quality ratings measured on the same day was found to be modest, with regression analysis revealing the correlation coefficient to be 0.52. Noise in this relationship may have been introduced by inherent shortcomings in both methods. First, visual quality ratings are subjective in nature and human error leads to imperfect consistency. Additionally, turfgrass quality is never perfectly even across a turfgrass area of 21 m<sup>2</sup> per plot, and TCM 500 measurements capture only a total sample area of 136 cm<sup>2</sup>, or 0.065% of the total surface area. Due to noise and sparse data collected at very low turfgrass ratings, this method also resulted in a regression equation which did not adequately extend throughout the full range of turfgrass quality.

In order to reduce the effect of noise and to derive an equation which adequately related visual rating to NDVI throughout the full range of turfgrass quality experienced, another method was used. For all plots of each quality rating 4 through 8, the distribution of TCM 500 NDVI values of plots given those ratings is shown in **Figure 3.9**. While **Figure 3.8** illustrates the relationship between quality ratings and NDVI was noisy, **Figure 3.9** illustrates a strong overall trend and correlation between the median NDVI of turfgrass plots at each quality rating. This relationship between quality rating and median NDVI is shown in **Figure 3.10**.

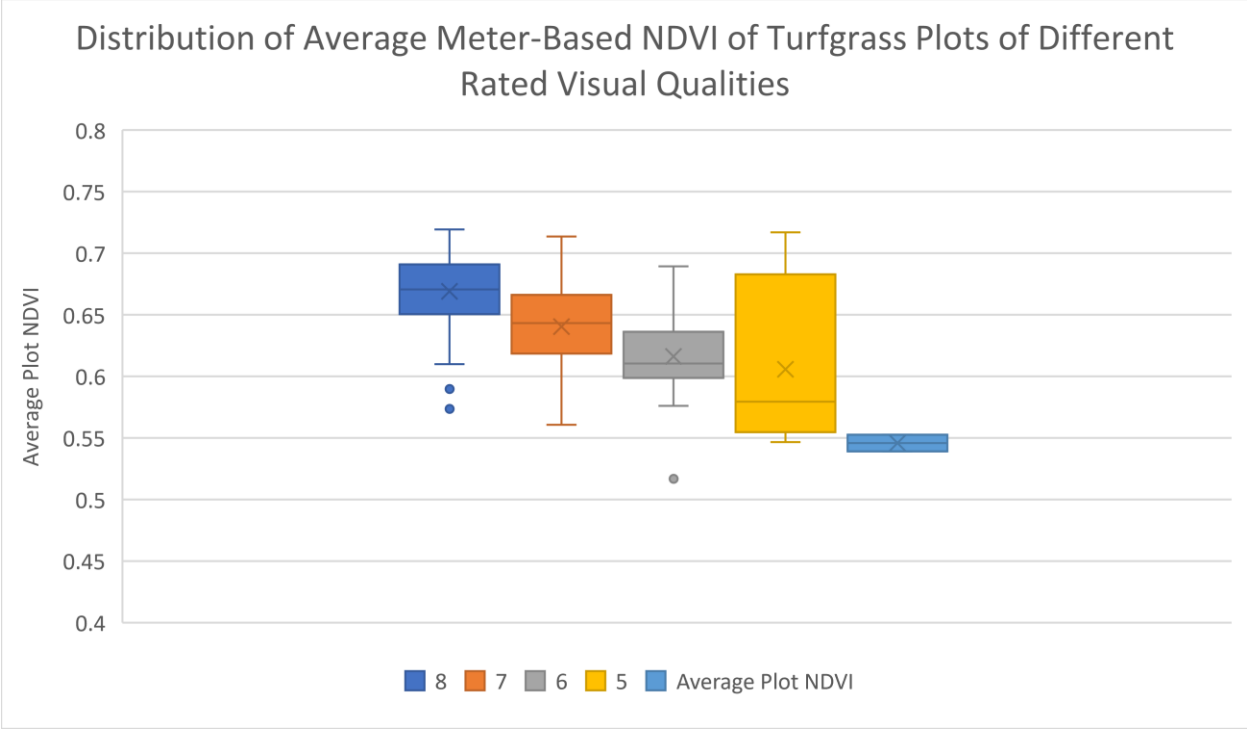


Figure 3.9: Distribution of TCM 500 NDVI measurements of turfgrass with varying rated visual qualities

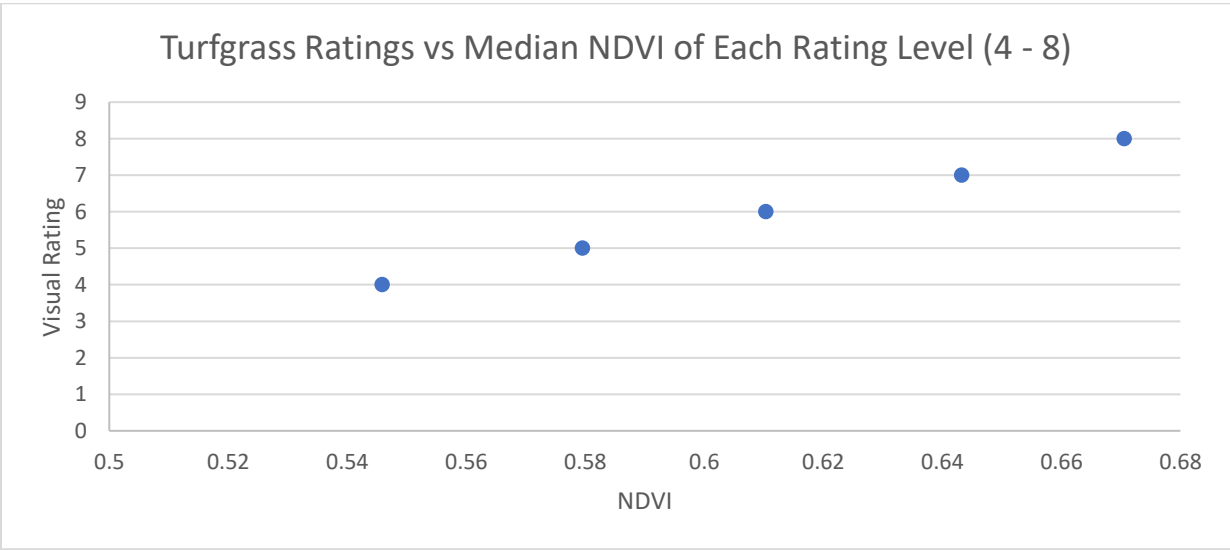


Figure 3.10: Median NDVI of turfgrass plots with visual quality rated between 4 and 8

The resulting regression between quality ratings and median NDVI shown in **Figure 3.10** was nearly perfectly correlated and linear ( $R = 0.99$ ). This regression equation (**Equation 3.9**) was therefore used to convert average NDVI values of plots to NTEP ratings. Also, because the model used to calculate camera-based NDVI from imagery was already derived from experimental data of meter-based NDVI as the response, this same equation was used to convert camera-based NDVI to ratings. The estimated visual quality rating of plots calculated from **Equation 3.9** was rounded to the nearest whole number.

$$VR = 31.896 * NDVI - 13.453 \quad (3.12)$$

Then, the ratings equivalent numbers of all three plots belonging to each treatment were averaged to determine the average turf quality of each irrigation treatment. Turfgrass quality per treatment measured by both NDVI methods as converted to NTEP equivalent ratings are shown in **Figure 3.11** and **Figure 3.12**.

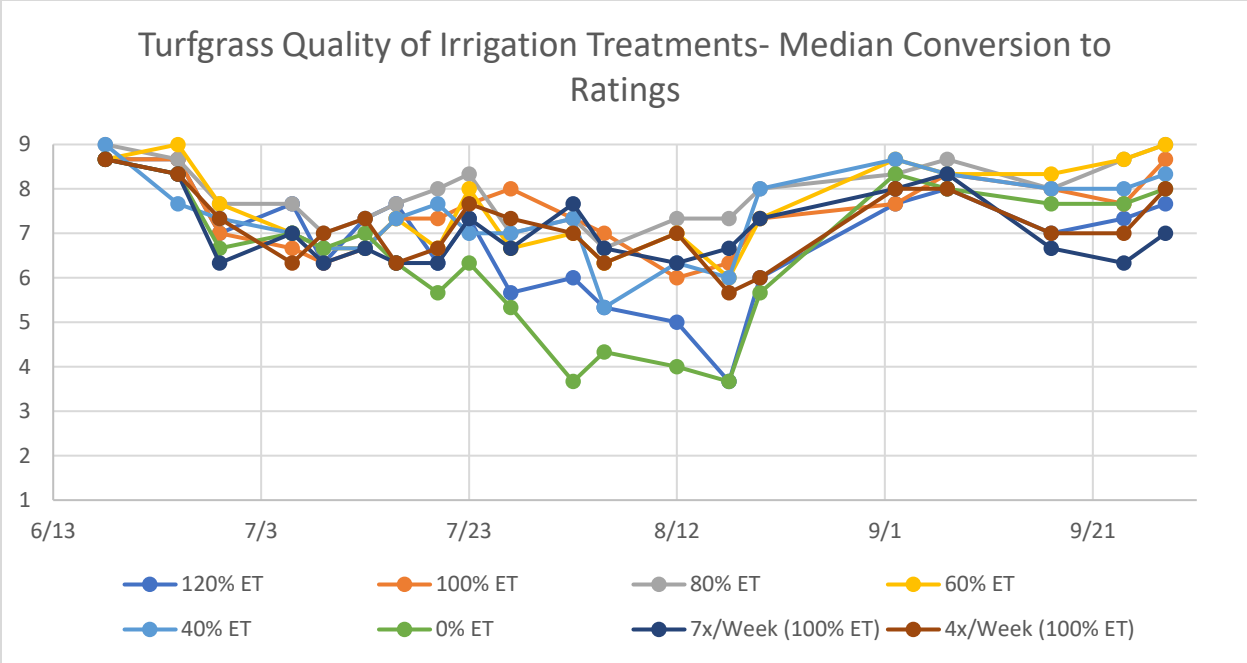


Figure 3.11: Estimated average turfgrass visual quality by TCM 500 NDVI measurements

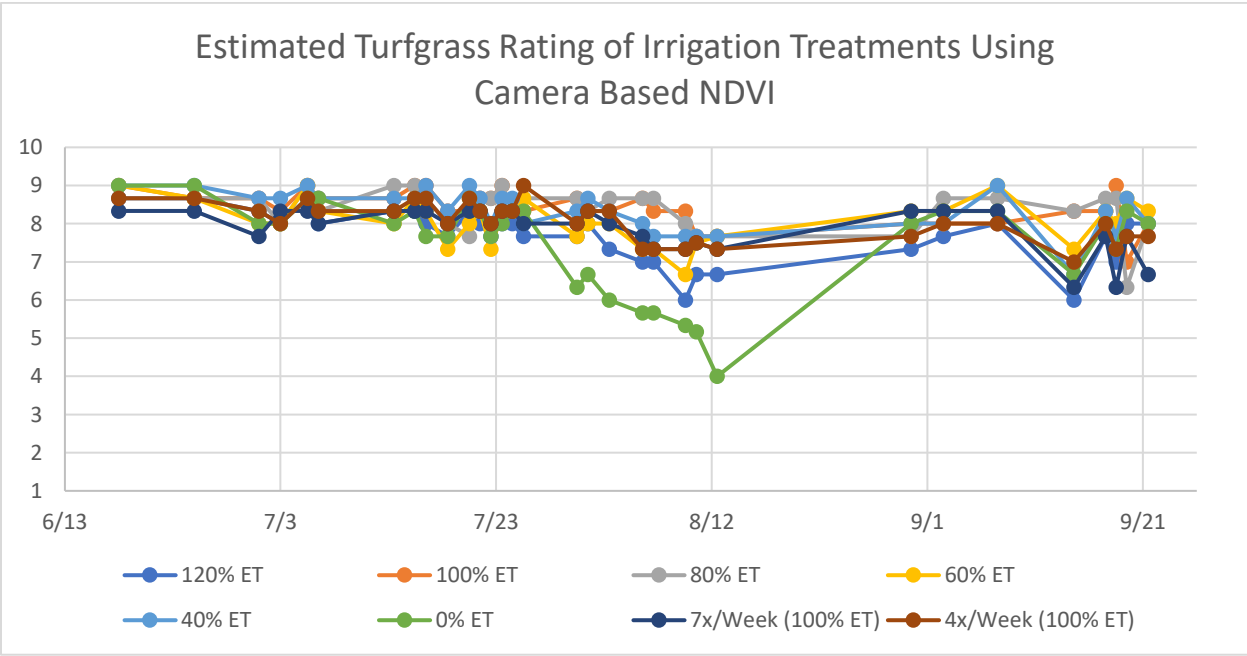


Figure 3.12: Estimated average visual turfgrass quality by camera-based NDVI measurements

### Significance of Turfgrass Quality Differences Between Irrigation Treatments

In assessing the performance of turfgrass visual quality under each irrigation regime, Tukey’s honest significant difference (HSD) tests were performed for each assessment method. Using a 95% confidence interval, a pairwise difference comparison table is shown in **Table 3.2** to illustrate significant differences in overall turfgrass quality measured under each method.

Table 3. 2: Least squared means (LSM) and pairwise difference comparison of turfgrass quality under varying irrigation treatments, as assessed by visual quality ratings, TCM 500 NDVI measurements, and imagery-based NDVI

Treatment	Visual Rating	TCM 500 NDVI	Camera NDVI
7x	7.2 (AB)	0.645 (AB)	0.671 (AB)
4x	7.3 (AB)	0.645 (AB)	0.676 (AB)
120%	7.0 (AB)	0.635 (AB)	0.663 (BC)
100%	7.3 (AB)	0.654 (AB)	0.686 (A)
80%	7.4 (A)	0.666 (A)	0.685 (A)
60%	7.2 (AB)	0.654 (A)	0.675 (AB)
40%	7.1 (AB)	0.651 (AB)	0.684 (A)
0%	6.6 (B)	0.620 (B)	0.656 (C)

By each assessment method, there was a large group of treatments between which no significant difference in mean quality could be established: 7x, 4x, 100% ET, 80% ET, 60% ET, and 40% ET. The worst performing treatment as measured by the least means squared estimate in all assessment methods was the unirrigated treatment, but which treatments could be established as significantly better performing than the unirrigated treatment depended upon the assessment method. Analysis of visual ratings determined only the 80% ET treatment- the best

performing treatment by least means squared estimate by all methods- to be significantly better performing than unirrigated turfgrass, as shown in **Figure 3.13**. Analysis of TCM 500 measurements determined both the 80% and 60% treatments to be significantly better performing than unirrigated turf, as shown in **Figure 3.14**. Finally, analysis of the camera-based system determined all treatments except the 120% ET treatment to be significantly better performing than unirrigated turf, and the 100% ET, 80% ET, and 40% ET treatments were each significantly higher performing than then 120% ET treatment, shown in **Figure 3.15**.

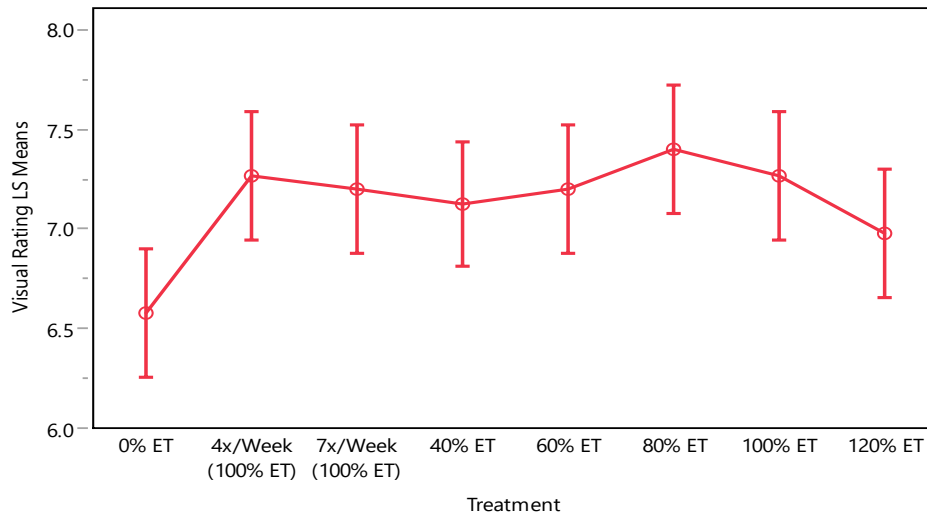


Figure 3.13: Least squared means and 95% confidence limits of visual quality of turfgrass treatments

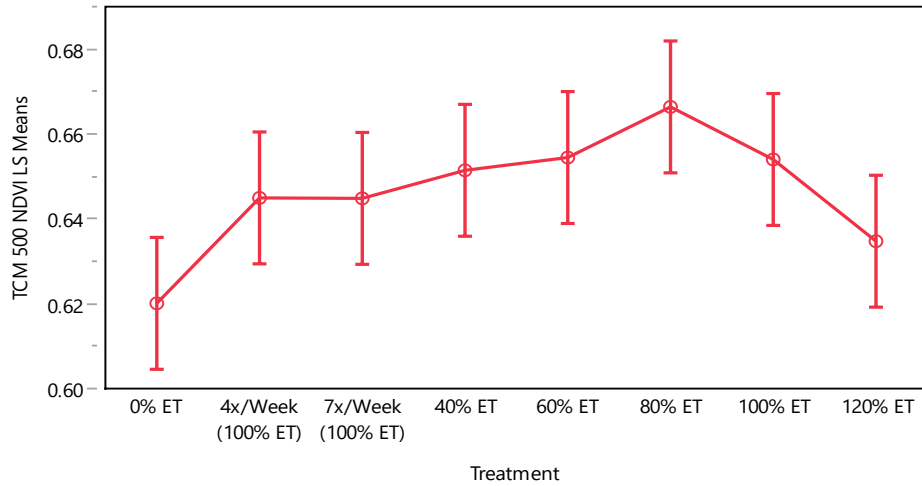


Figure 3.14: Least squared means and 95% confidence limits of TCM 500 NDVI of turfgrass treatments

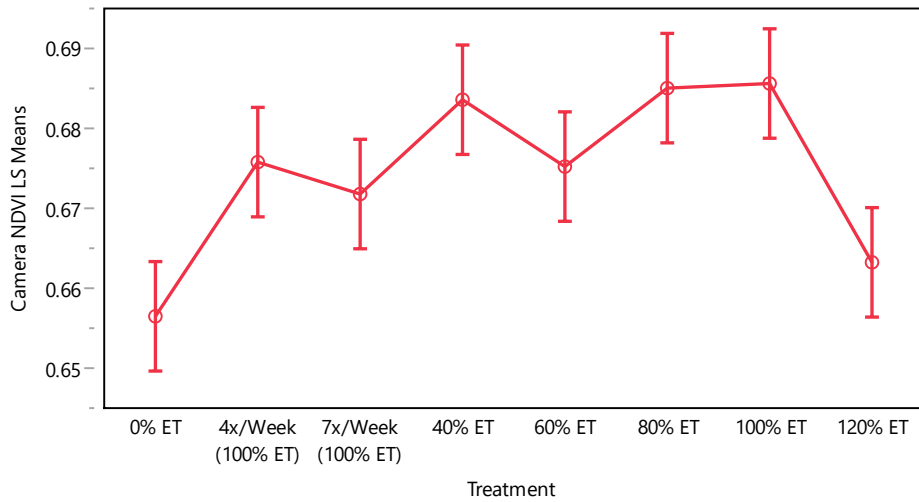


Figure 3.15: Least squared means and 95% confidence limits of imagery-based NDVI of turfgrass treatments

### Acceptability of Turfgrass Quality Within Treatments by Each Method

While establishing significant differences between treatments across the entire study period is important to demonstrate broader trends, additional analysis is important when considering the context of turfgrass quality. A higher average quality is one desirable trait for

turfgrass, but the avoidance of low visual quality is also an important one. Lawn owners and turfgrass managers are particularly sensitive to low visual quality turfgrass even for short periods, and social, financial, and even legal consequences may be risked if turfgrass quality falls below a given level (Henry, 1999). The ability for turfgrass and its management program to consistently maintain acceptable visual quality must therefore be assessed.

The performance of turfgrass in each treatment was assessed by estimating the total number of days of unacceptable quality experienced throughout the study. A rating of 6 was considered to be the minimum acceptable quality. **Equation 3.9** was used to convert the NDVI of each plot to an estimated NTEP quality rating. Average turfgrass quality for each treatment and each assessment method was calculated for each day that measurements were taken. Then, on all days where no measurements were taken, the estimated visual quality was calculated by linearly interpolating between the nearest two days when measurement did occur. The number of days with an estimated quality below a 6.0 rating were summed for each assessment method, and the results are given in **Table 3.3**.

Table 3.3: Estimated days of unacceptable turfgrass quality measured by three assessment methods during a 90 day period

Days Below Acceptable Quality (< 6)				
	Visual Rating	Visual (Scalping excluded)	TCM 500 Meter	Camera
120% ET	4	4	23	0
100% ET	6	0	0	0
80% ET	0	0	0	0
60% ET	6	0	0	0
40% ET	5	0	5	0
0% ET	26	26	31	18
7x/Week (100% ET)	0	0	0	0
4x/Week (100% ET)	0	0	4	0

As discussed above, it was suspected that scalping and turfgrass disease during the early part of the season led to a universal decline in turf quality as measured by visual inspection on July 9 despite well-watered soil moisture conditions in most treatments. Soil moisture in the 100% ET treatment was maintained near field capacity throughout the period when low turf quality was detected in this treatment, which provides evidence that low turf quality cannot be attributed to the irrigation treatment. However, because soil moisture in other treatments was not always maintained at field capacity, further evidence is required in order to discount the possibility of water stress in the deficit irrigation treatments during this period.

The fungal disease ‘dollar spot’ (*Clarireedia homoeocarpa*) was also detected on some plots during the month of July, which produces patches of brown turf and negatively affects turf visual quality. It is likely that disease and scalping each contributed to unacceptable turf quality

measured by visual ratings in the 100% ET, 60% ET, and 40% ET treatments, rather than water stress.

In addition to overall visual turf quality, each turfgrass plot was also rated for the prevalence of dollar spot in early July when the disease was detected. On July 9, all plots were rated between 7 and 9 (low or no disease presence) for dollar spot, except for plot #21 belonging to the 60% ET treatment, indicating an unacceptable level of disease. If this plot is excluded, then the average turf quality of this treatment rises to a 6, indicating acceptable quality. Thus, unacceptable quality of the 60% ET treatment on July 9 is attributed to disease rather than water stress. Finally, limited evidence explaining unacceptable quality measured in the 40% ET treatment from the TCM 500 data.

Therefore, visual rating measurements collected on July 9 were also excluded and the daily visual quality was estimated by interpolating between measurements taken on June 30 and July 16. The results of this analysis are shown by the Visual (Scalping Excluded) column in **Table 3.3**.

With measurements affected by scalping and dollar spot excluded, the agreement between assessment methods becomes clearer. The 100%, 80%, 60%, and 7x treatments maintained acceptable quality throughout the entire period as measured by all assessment methods. On one measurement day, the TCM 500 measured unacceptable quality in the 40% ET and 4x weekly treatments, leading to an estimated 5 and 4 days of unacceptable quality, respectively. Both visual ratings and the TCM 500 measured unacceptable quality in the 120% ET treatment, although the NDVI data estimated 23 days of unacceptable quality while visual ratings estimated only 4. Finally, all three methods estimated a significant number of days below acceptable turf quality in the 0% ET treatment. The camera-based method estimated the

unirrigated turf experienced 18 days of unacceptable turf quality, while the NDVI meter estimated nearly twice that at 31 of unacceptable quality, and visual ratings estimated a middle number of 26 days of unacceptable quality.

Box plots of all treatments measured by the three methods of assessment also illustrate how turf quality varied throughout the season under different irrigation regimes. Because of the aforementioned factors affecting turf visual ratings on July 9, this measurement was excluded from the below graph of visual ratings. Upper quartiles and hinges for all treatments and all methods are similar, as at the beginning of the season and after heavy rainfall when all plots were well watered, turf quality was comparable across all treatments. During periods near the beginning of the commencement of treatments or when precipitation equalized soil moisture conditions between plots, turfgrass quality was highly similar across all treatments. The significant difference between treatments is most pronounced at the lower quartiles and hinges, as periods of drought affected turf quality to greater degrees as deficit irrigation increased. In **Figure 3.16**, there is little difference in the distributions of turfgrass quality between all treatments receiving 100% or 80% ET irrigation, including those irrigated at higher frequencies. While the 80% irrigation performed about equally to the 100% ET treatment, lower hinges steadily decline with increasing deficit. While 60% and 40% ET treatments may not have resulted in unacceptable quality during this period, this suggests that turf quality was to a lesser degree negatively affected. The difference between the 0% and 40% ET treatment was dramatic, with a substantially lower median, lower quartile, and lower hinge in the unirrigated treatment. Finally, and somewhat surprisingly, the second worst performing treatment was the 120% ET turfgrass. Visual ratings estimated 4 total days of unacceptable turfgrass quality under this regime.

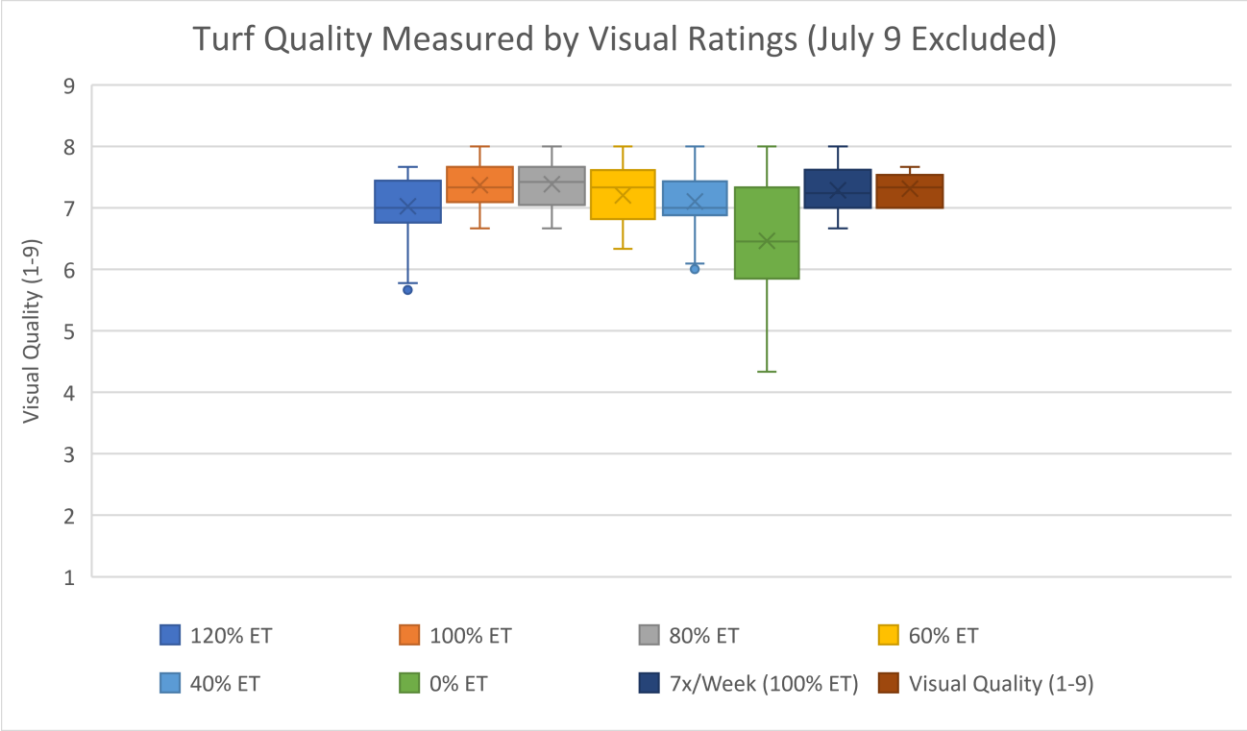


Figure 3.16: Daily estimated visual quality ratings of turfgrass treatments .

Both methods of NDVI assessment are largely in agreement with the visual assessment, with slight differences. The TCM 500 assessment agreed in the steady decline in the lower hinge as irrigation decreased below 80% ET. It also agreed that the unirrigated treatment performed poorly with a lower quartile below a 6 rating, and that the overirrigated treatment performed second worst as measured by lower quartile and hinge. However, the distribution of turf quality of 100% ET treatments was comparable to the 60% ET treatment, and the 80% ET treatment performed best.

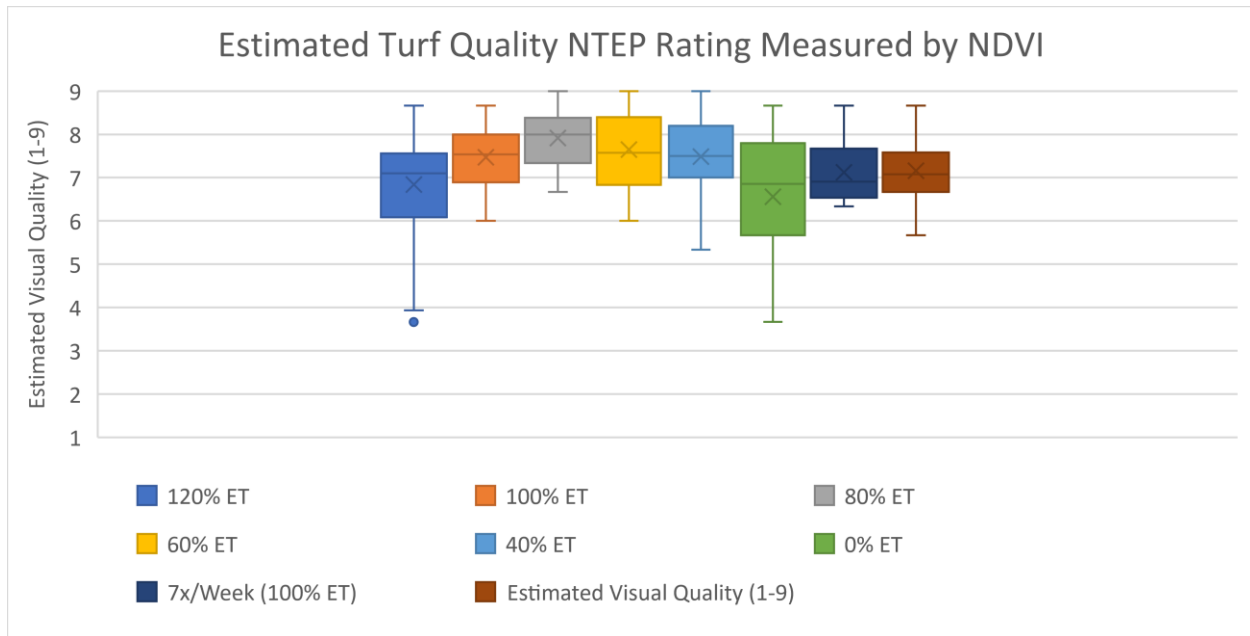


Figure 3.17: Daily estimated visual quality of turfgrass treatments

Box plots of turf quality as measured by the camera system were generally more compressed than other methods. However, similar to the visual ratings, upper hinges and quartiles are largely even across treatments. Also similar to the other methods, lower quartiles of the overirrigated and unirrigated treatments were substantially lower than those of the other treatments, which were similar. However, the camera-based method did not detect declining turf quality in the 60% and 40% ET treatments, the distributions of which were comparable to 100% ET treatments. This may be because, as shown in **Figure 3.18** and described in Chapter 2, the camera-based method did not accurately differentiate between turfgrass quality rated 7 and above.

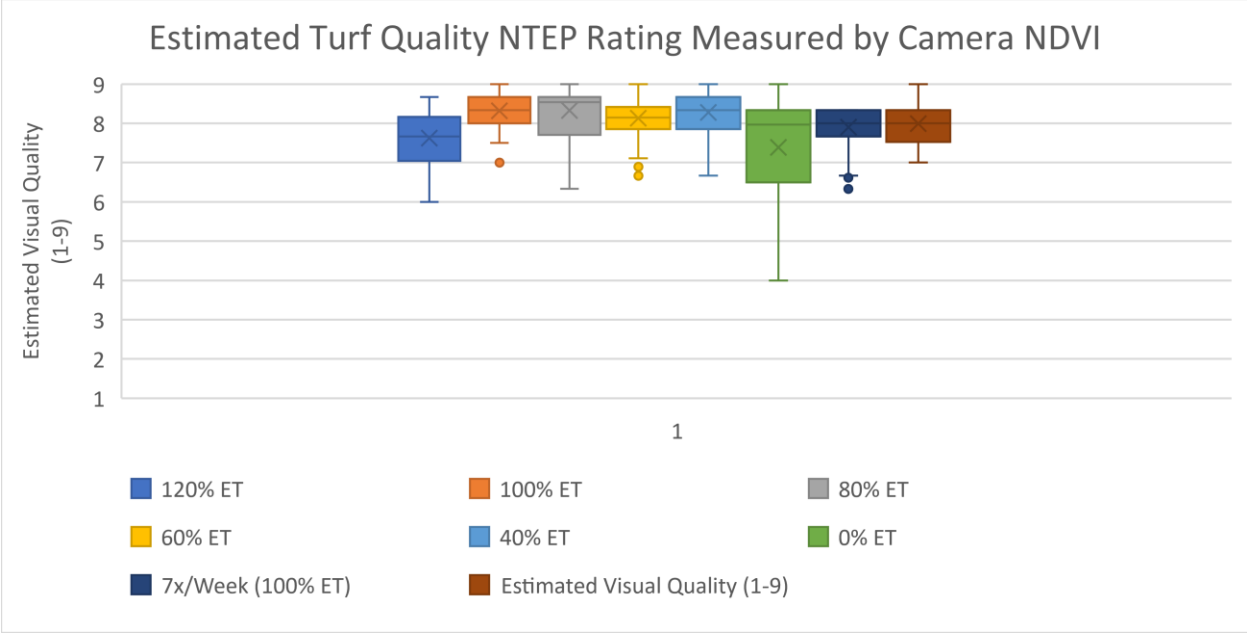


Figure 3.18: Daily estimated visual quality of turfgrass treatments by camera-based NDVI

**Unirrigated Turfgrass Quality**

The turf quality of the 0% ET treatment measured by three methods and the average soil moisture is shown in **Figure 3.19**. During this period, the average soil moisture began at approximately 23% VWC and declined to 17.2% VWC by the morning of August 14. Additionally, a soil moisture content below 19% was reached by July 30, after which soil moisture remained mostly constant throughout the next two weeks. Between July 23 and August 13, the difference between the Penman-Monteith estimated accumulated evapotranspiration and accumulated effective rainfall rose from a deficit of 2.78” to 4.25”. During the thirty-six days following July 8, 53 mm of precipitation was measured at the site, while the average July rainfall in Raleigh is 123 mm (Peacock & Bruneau, 2006). The decline in turf quality we therefore attribute to water stress due to a significant water deficit, leading turfgrass to experience conditions near the wilting point for approximately fourteen days.

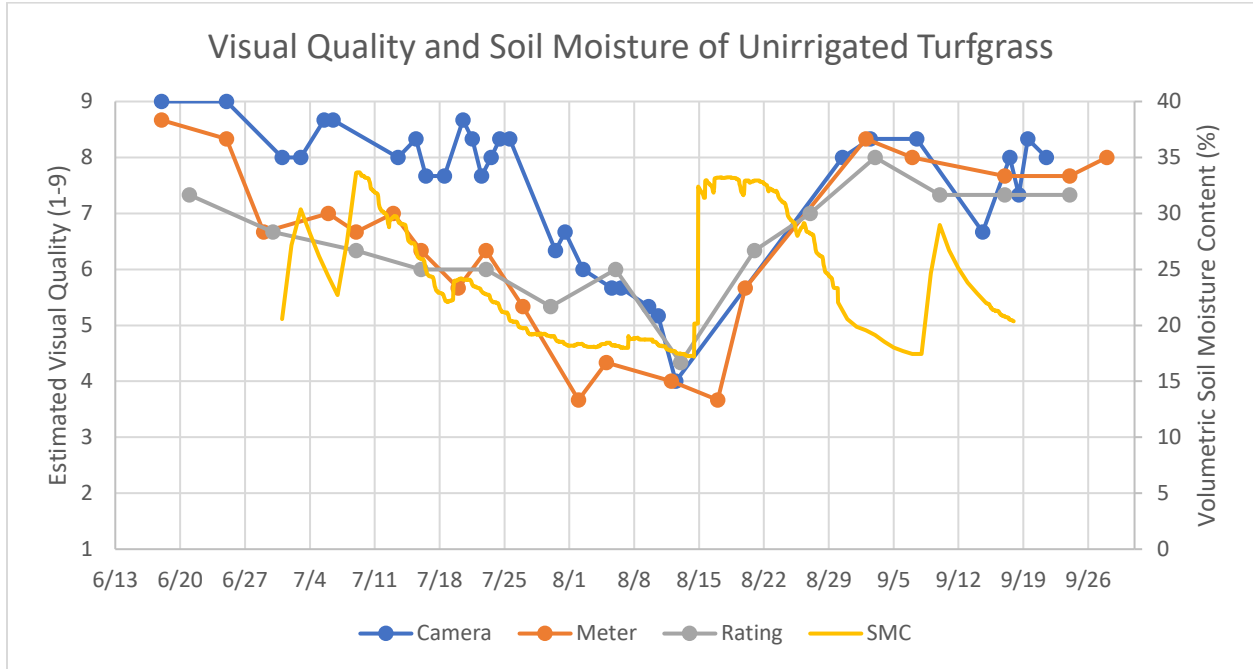


Figure 3.19: Estimated visual quality of unirrigated turfgrass by three assessment methods and soil moisture content over time

All days of unacceptable quality in the unirrigated treatment occurred during the drought period between July 16 and August 14, and differences in estimated number of days of poor quality between methods are mostly accounted by differences in quality during the first two weeks of this period. By August, all methods indicated unacceptable turf quality, but in July, the NDVI meter method first estimated unacceptable quality on July 19, followed by visual ratings on July 24 and by camera on August 3.

Similarly, there are differences between when each method first detected a notable and relatively steady decline in quality. While the camera method did not indicate unacceptable turfgrass quality until August 3, it also overestimated turfgrass quality relative to other methods prior to this period, and a significant decline in quality was detected before unacceptable quality.

On June 30, a significantly lower turfgrass quality was measured than on the previous measurement date of June 25. A measurement taken the next day was within the standard error, and subsequent measurements declined steadily until the drought period was over. However, in both other assessment methods, measured turf quality rebounded to an acceptable level after unacceptable quality was first detected. It was only on July 27 that the TCM 500 measured unacceptable turfgrass quality that did not rebound to acceptability until after the drought. Also, because of the low sampling frequency, no two sequential measurements of visual quality ever rated the unirrigated turfgrass below an average acceptable quality. Therefore, by this metric, both NDVI based assessment methods were similar in their ability to reliably detect the early effects of water stress in unirrigated turfgrass, and arguably did so before visual ratings.

### **Unirrigated Turfgrass Stress Recovery**

After this drought period, the site experienced a very rainy period beginning on August 14, when 7 precipitation events occurred within the next 11 days. A depth of 85 mm of rainfall was measured from a heavy storm on August 14 which brought the entire site above field capacity. From August 14 to August 24, subsequent precipitation events maintained soil moisture of the unirrigated treatments at or above field capacity. Throughout this period, effective rainfall was estimated to be 60.5 mm, significantly greater than the 26 mm of estimated evapotranspiration. During this well watered period, turf quality as measured by all three methods rebounded quickly. The first measurement taken after the August 14 storm was taken approximately 48 hours afterward by NDVI meter on August 17. Average estimated quality showed a further decline in quality since the previous measurement on August 12. These data suggest that turfgrass quality did not recover within 48 hours of relief from the drought period.

After six days of well watered conditions quality was assessed again by NDVI meter, and was measured to have recovered by 2 points to an average quality of 5.67. Visual ratings data indicate a similar recovery: seven days after the initial storm, average turf quality recovered by 2 points to a 6.33 rating.

Average soil moisture content of the unirrigated treatment dropped below 20% at one other point during the experimental period, between September 1 and September 8. During this period, average turf quality declined by 0.67 as measured by visual ratings and by 0.33 by NDVI meter, while remaining nearly steady as measured by the camera.

### **Overirrigated Turfgrass Quality**

By all methods of assessment, the overirrigated treatment was the second lowest performing in overall visual quality. Unlike low performance in the unirrigated treatment, water stress does not provide an obvious explanation for the decline in quality of overirrigated turfgrass, and thus alternative explanations must be explored.

Broadly, there is agreement in the general trend of quality over time between all assessment methods. Turf quality began high and remained steady for at least the first month before declining to its lowest point in mid-August, and finally recovered in late August and September. The TCM 500 and camera system measured a notable decline in turf quality by July 27 and August 2, respectively, while visual assessment measured this decline only by August 21.

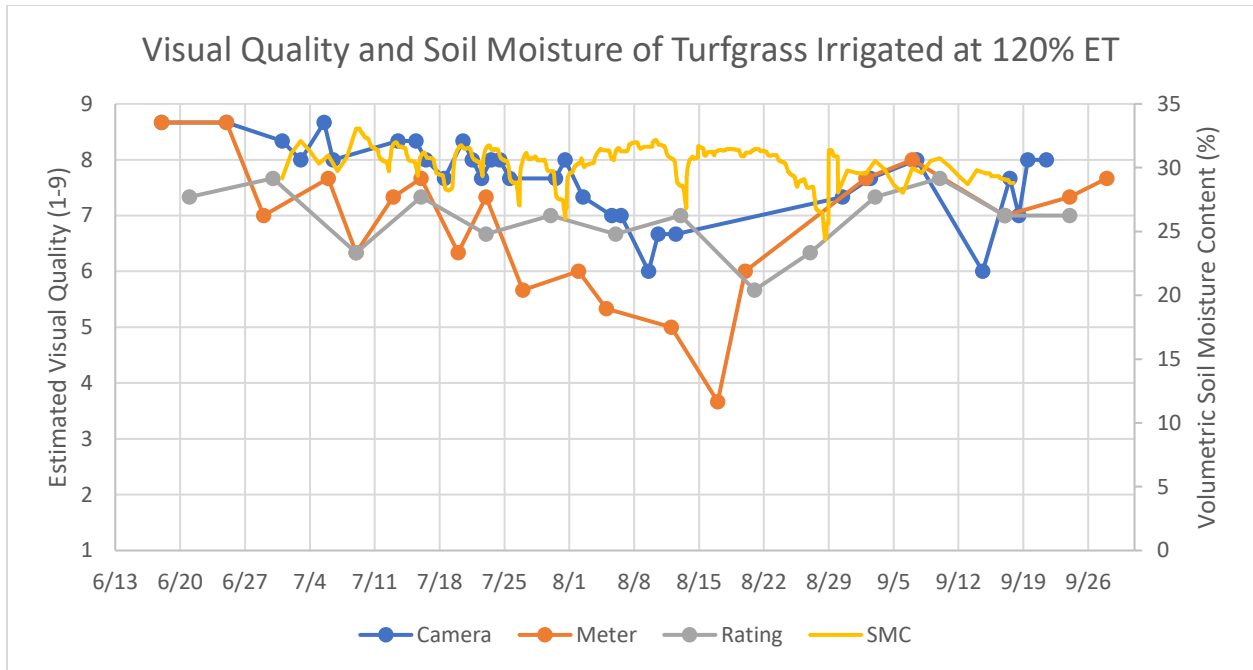


Figure 3.20: Estimated visual quality of overirrigated turfgrass by three assessment methods and soil moisture content over time

This trend is similar to the trend in quality of the unirrigated turfgrass, although soil moisture remained high through the point in time when each assessment method measured its lowest quality. However, the inverse cause of overly saturated soil remains a potential explanation for poor quality. Large areas of turf within two plots in this treatment, Plot 7 and Plot 8, were likely affected by excess moisture. Turf canopy in these plots was observed to be significantly less dense than other plots, and many smaller patches of straw colored turf were also observed within these areas, as shown in **Figure 3.21**. The straw color was caused by dollar spot scars. Prevalence of dollar spot is most common in warm, moist conditions. As could be expected, oversaturation of soil was more commonly observed during field visits in these intentionally overirrigated plots than in others. Zones 6 and 7, and to a lesser but still noteworthy extend Plot 8, also happen to sit in a slight depression and were observed to be occasionally

oversaturated after heavy rain. This effect was severe during the 2020 season, and was remedied to a significant extent by installing tile drainage along the entire East side of the site. However, significant oversaturation was observed in plots 6 and 7 on August 17 after three consecutive days of rainfall. Thus, the warm and frequently oversaturated soil caused by poor drainage and overirrigation likely contributed to the prevalence of dollar spot. Additionally, disease damage, oversaturation, and low root aeration likely also all contributed to the observed low canopy density.



Figure 3.21: Low density and dollar spot observed in overirrigated turfgrass in Plot 7 and Plot 8

These explanations also agree with the timing of the decline and recovery of turf quality within this treatment. Both NDVI assessment methods measured declining turf quality through the end of June and first weeks of July, when soil moisture was maintained above 30% VWC

throughout most of the period. Visual ratings also measured the lowest turf quality on August 21, after a week of frequent rainfall which maintained soil moisture above 30% VWC for approximately one week. In late August, it is likely that two factors led to an improvement in turf quality. First, technical difficulties led to a longer duration between irrigation events than usual, allowing soil moisture to decline between August 23 and August 28, when soil moisture reached its lowest point of the entire study at about 25% VWC. Additionally, fertilizer was applied to the site on August 23. Turf quality of nearly all plots improved after fertilizer was applied, and nitrogen fertilizer has also been shown to be an effective treatment for dollar spot (Williams et al., 1996). A respite from oversaturation, improved root aeration, and nitrogen fertilizer all likely contributed to the improved turf quality of the overirrigated turfgrass.

### **Comparison of Turfgrass Quality Assessment by Each Method**

In combination with this project to develop a process to measure the NDVI of turfgrass plots using imagery from a pole mounted camera system, a complementary study to evaluate the visual quality of turfgrass under different irrigation regimes took place. Various levels of deficit irrigation were applied to plots, and three different methods of turf quality assessment were used: expert visual ratings, measurements taken by a TCM 500 NDVI meter, and NDVI derived from the camera system and algorithm described in this chapter. As an additional method of evaluating the success of the imagery processing method developed, the quality of turfgrass as measured by the camera system can be compared to the quality measured by the additional two assessment methods throughout this experiment. By including this method of evaluation, the performance of the camera system may be compared over a three month experimental period over an occasionally highly dynamic range of turfgrass qualities.

In the companion study, plots were given a treatment of irrigation based on a certain fraction of actual evapotranspiration ranging from 120% to 0%. Each treatment was comprised of three replicates, and turf quality of a treatment was determined as the average turf quality of all replicates. In order to make direct comparisons across all three assessment methods, one of which did not use NDVI at all, a relationship between NDVI and NTEP visual ratings was established.

It should be noted, as discussed in Chapter 2, that data analysis led to improvements in data collection methods late during this period. Therefore, during most of this study, NDVI assessment methods may be more affected by sources of noise that later adjustments sought to address, namely low spatial resolution and uneven turf quality in the TCM 500 measurements and clouds and partial shading in the imagery based method. However, the fact that treatments in this study were evaluated as the aggregate of three plots similarly reduces the chance that random error and outliers significantly affecting the overall assessed turf quality of treatments.

The estimated turf visual quality rating and standard error (SE) of turfgrass under irrigation treatments by each assessment method were compared. Most treatments of turfgrass experienced relatively stable, acceptable visual quality over the course of the three month study period. The performance of one such treatment, well watered turfgrass irrigated at 100% ET replacement four times per week, is shown in **Figure 3.22**.

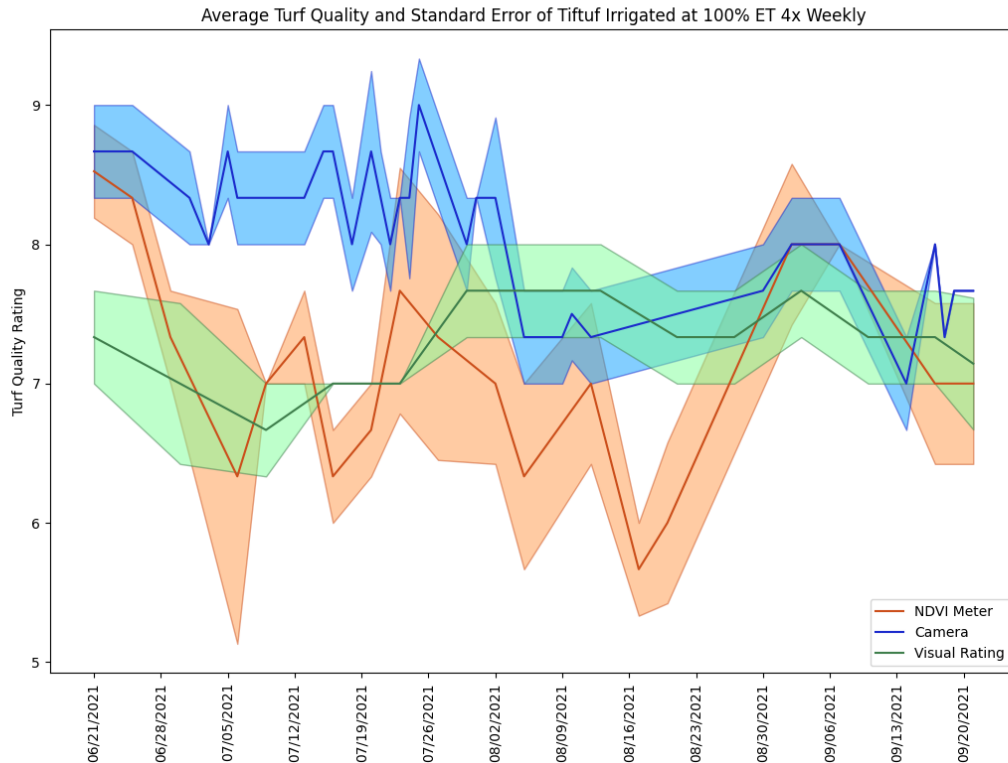


Figure 3.22: Visual quality and standard error of turfgrass plots irrigated at 100% ET four times weekly

If expert turfgrass visual ratings are considered to be the true quality, then the performance of the camera system and TCM 500 assessment methods can be compared. Throughout the study period, the standard error of the visual rating and estimated NTEP quality measured by the camera system intersected 51% of the time, while that of the visual ratings and the TCM 500 method intersected 47% of the time. By this metric, both NDVI methods performed similarly at predicting visual quality, with the camera system slightly outperforming meter measurements.

However, it should also be noted that the camera system did so with a significantly smaller standard error band of 0.3, compared to the average standard error band of 0.5 of the

TCM 500 method. The average standard error of the camera system was also equivalent to that of the visual ratings, also 0.3. This trend is present across all treatments, as shown in **Table 3.4**. On average, the standard error of estimated NTEP turf quality measured by the camera system closely matched that of the actual visual ratings, while standard error measured by the TCM 500 method was nearly twice as large.

Table 3.4: Average standard error of NTEP turfgrass quality ratings over a three month period across irrigation treatments by three assessment methods

Treatment	Camera SE	TCM 500 SE	Visual Rating SE
120% ET	0.22	0.56	0.24
100% ET	0.28	0.44	0.24
80% ET	0.29	0.28	0.24
60% ET	0.39	0.45	0.37
40% ET	0.30	0.49	0.28
0% ET	0.32	0.46	0.26
7x/Week (100% ET)	0.29	0.57	0.20
4x/Week (100% ET)	0.24	0.52	0.30
Total	0.29	0.47	0.27

When assessing the performance of the camera system in **Figure 3.22**, the chart may be broken up into two sections: the period before August 1, and the period after August 1. Before August 1, the error bands of visual quality as measured by the camera system and visual ratings

intersected only 2% of the time, with the camera system overestimating turf quality compared to visual ratings. After August 1, however, the error bands intersect 88% of the time. There is no apparent comparable trend in visual quality as measured by the TCM 500. This trend of the camera system accurately tracking visually assessed quality after August but overestimating turf quality early in the study is consistent across other treatments as well, as shown below.

Two potential explanations are offered. First, as detailed further in **Relating NDVI Assessment Methods to Quality Ratings**, the method of relating NDVI to estimated NTEP ratings was based on a limited dataset in which turf plots ranged in quality from 4-8. While the relationship between NDVI and quality rating was shown to be linear through this range, curvature may well be present outside of it. As turfgrass NDVI increases, the increase in visual rating may meet diminishing returns above a certain level. NDVI measured by the camera system was generally highest during the first weeks of the study, and using the linear relationship, turfgrass plots were often estimated to have a quality of 9 by the camera system early in the study. Should the suspected diminishing returns of NTEP visual ratings exist, this would partially explain the overestimation of visual ratings during this period.

Second, turfgrass quality during approximately the first month of the study period was affected by disease and a suboptimal mowing configuration, as discussed in detail in detail above. Due to the use of a mower poorly suited to the uneven ground of the research site, significant scalping was observed early in the study. This resulted in spots of straw colored turf where the mowing blade dipped too low and damaged the turf. The mowing configuration was adjusted after this was discovered, but scalping spots often persisted and affected turf quality until the end of June before they fully recovered during July. Similarly, some plots were affected by Dollar Spot fungus, a turfgrass disease which also produces spots of straw colored turf. Dollar

Spot presence was less widespread than scalping and appeared around the end of June. However, the disease contributed to lower turf visual quality ratings. It is possible that NDVI derived from the camera system was not affected by smaller spots of poor turf quality due to limitations in camera resolution and the small viewing angle at distant plots. Conversely, subjective visual ratings may give more weight to the unsightly blemishes than their relatively small surface area would otherwise be given, leading to steeper declines in turf quality than an objective measure of the average visual quality of the entire surface area of the plot.

The treatment which experienced the most dynamic range of quality was the unirrigated treatment. The average turfgrass quality rating and standard error bands measured by the three assessment methods are shown in **Figure 3.23**. Average quality of unirrigated turfgrass as measured by each assessment method began high, then dropped to an unacceptable level around the middle of the trial during a drought, and finally recovered to high quality following consistent rainfall and fertilization at the end of August. Throughout the study period, the standard error of the visual rating and estimated NTEP quality measured by the camera system intersected 41% of the time, while that of the visual ratings and the TCM 500 method intersected 39% of the time. Before and after the start of August, there was again a dramatic difference in the divide between turf quality as measured by visual ratings and the camera system. Before August 1, the camera system consistently overpredicted turf quality, while after August 1, the error bands of the two methods intersected 73% of the time.

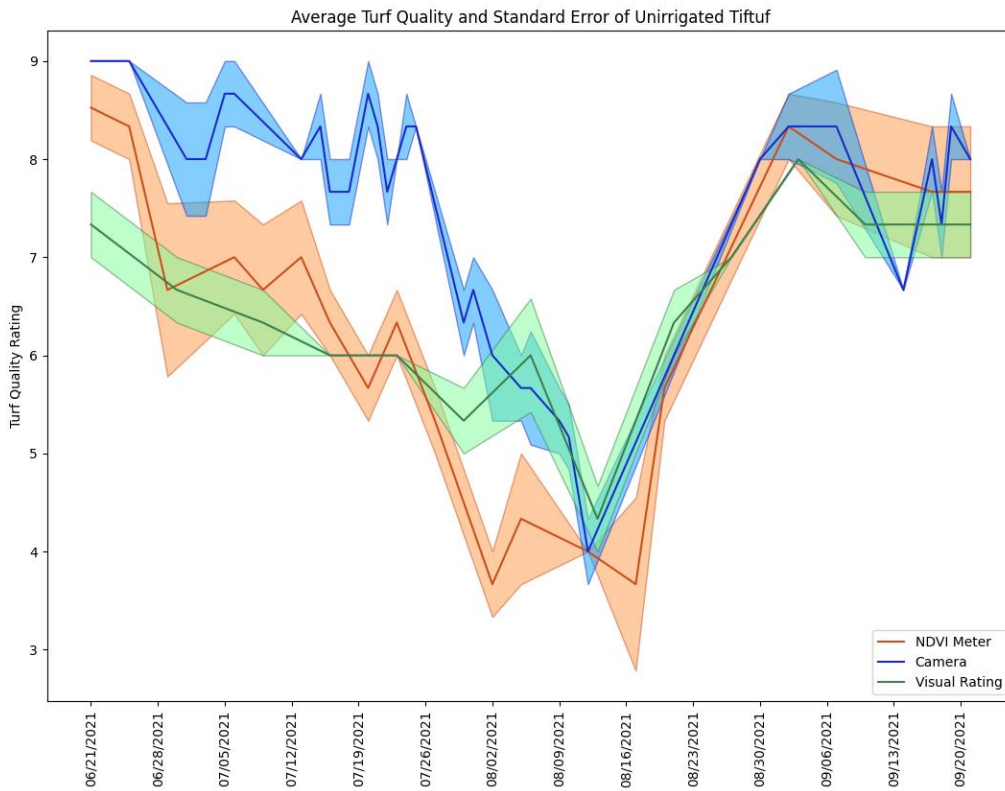


Figure 3.23: Visual quality and standard error of unirrigated turfgrass plots

**Figure 3.23** illustrates that the camera system developed was able to accurately measure turfgrass quality through a very dynamic period and across a wide range of turf quality. This is an essential ability of a system or method for assessing turfgrass quality, as the ability to distinguish between healthy and stressed turf and to identify declines in turfgrass quality are important to management decision making. These results provide evidence for the utility of the system developed.

## Conclusions

Results of this study have illustrated that knowledge of an appropriate irrigation plan is essential to maintaining good turfgrass visual quality. Inattentively applying water either far beyond or far short of plant needs can lead to an unhealthy and unappealing lawn. Determining how much water to apply to your lawn as a fraction of estimated evapotranspiration is an efficient strategy for adapting water application dynamically around plant water use, reducing the chance of water stress or wasteful use. Identifying the right fraction of ET to replenish is therefore key to the most efficient irrigation plan.

Findings in this study are the result of only one year of study and of one location. Research was conducted on a fine textured soil in the Southeast in Raleigh, North Carolina. As discussed, high precipitation characteristic of this region diminished the water deficit induced in all deficit irrigation treatments. While the 100% ET treatment received 160 mm more water over three months than the unirrigated turfgrass treatments, differences in effective rainfall resulted in the 100% ET treatments receiving a total of only 55.8 mm more water than unirrigated turfgrass from all sources over the period. The quality of turfgrass under deficit irrigation benefits disproportionately from higher precipitation, and therefore the visual quality of turfgrass achieved under deficit irrigation in this study should be considered in this context. These same methods should be carried out over consecutive years and under a range of weather conditions representative of the Central North Carolinian region in order to determine with confidence the MDIL. Additionally, research was conducted on a fine textured sandy loam soil. Soils of a dramatically different texture and available water holding capacity may produce different results, especially during a drought period.

Even a drought resistant variety of bermudagrass like TifTuf is likely to require irrigation during the hottest period of summer to fulfill lawn owners' goals. During this three month study, the MDIL, or the greatest level of deficit irrigation which was able to maintain consistently acceptable turfgrass, was 60% of ET. However, one week or less of unacceptable turfgrass quality during the harshest months is considered tolerable, then 40% replenishment of evapotranspiration is sufficient. Two out of the three assessment methods measured a brief decline in turf quality receiving 40% replenishment of ET during a hot three-week period of declining soil moisture, but only one method measured a decline below an acceptable level. However, further study over multiple seasons is required to determine with greater certainty whether a 40% replenishment of evapotranspiration, or even potentially an even smaller fraction, is sufficient to reliably maintain acceptable turfgrass quality under a broader range of representative weather conditions.

If a homeowner in the Southeast prioritizing water savings chose to irrigate at a rate of 40% of ET, we find that potential water savings could be 90.7 mm during a ninety-day summer period under similar weather conditions and soil types compared to a homeowner irrigating at a rate equal to ET, or approximately 30 mm per month. A homeowner prioritizing the highest quality turfgrass could still expect to save 28.2 mm of water by irrigating at 80% ET with no expected loss in visual quality compared to a homeowner irrigating a rate equal to ET under these conditions. This represents a water savings of 9.4 mm per month. Finally, a middle of the road approach, consistently maintaining acceptable turfgrass visual quality while achieving the highest possible water savings would expect to reduce water use by 58.6 mm over ninety days by irrigating at 60% of ET, saving an average of approximately 20 mm per month. However, these data are the result of experimentation from a single growing season, and thus subject to the bias

introduced by weather patterns experienced during the season. Repeat experimentation should be conducted over multiple years and more diverse weather conditions to corroborate these results.

In the rainy North Carolina climate, differences between treatments in effective rainfall helped to reduce water deficits induced by differences in irrigation depth applied. The 120% ET and 100% ET treatments received total effective rainfall depths within 5 mm of each other, as turfgrass under these treatments were typically near the field capacity. Turfgrass receiving deficit irrigation received progressively greater depths of total effective rainfall as the irrigation deficit increased, with the unirrigated turfgrass plots receiving on average more than 100 mm more effective rainfall than the 100% ET treatment during the three month period. Therefore, the consistently acceptable turfgrass quality experienced at significant irrigation deficits, such as the 40% ET treatment, likely benefited from a reduced need for irrigation due to high rainfall. Well-watered plots benefited least from rainfall due to consistently high soil moisture.

**CHAPTER 4: EARLY DETECTION OF TIFTUF TURFGRASS WATER STRESS BY  
SOIL MOISTURE AND NDVI MEASUREMENTS**

## Abstract

When soil water becomes less available to plant roots, the rate of crop transpiration is restricted. The ability to predict the degree of water stress from common agricultural sensors is valuable to maintaining optimal turfgrass quality with data driven management programs, especially if stress can be detected before visible turf quality is affected. The daily water stress coefficients of three unirrigated turfgrass plots during a drought period were compared to measurements by three sensors: soil moisture, a handheld NDVI meter, and NDVI determined by a pole mounted camera system. Of the three, soil moisture correlated most strongly with the water stress coefficient ( $R^2 = 0.87$ ), while the camera-based NDVI ( $R^2 = 0.63$ ) outperformed handheld NDVI measurements ( $R^2 = 0.53$ ). The sensitivity of sensors to early signs of stress were also determined through progressive partial regression to determine the no-effect ranges of each sensor data to the water stress coefficient. Again, soil moisture outperformed other sensors, with a significant response to water stress over its full range. The camera system's response to declining water stress became significant below a coefficient of 0.37, while the response of handheld meter measurements only became significant to water stress coefficients below 0.24. From limited data, the decline in visual quality ratings was determined to be significant below stress coefficients of 0.34.

## Introduction

Plant potential evapotranspiration under well-watered conditions can be mathematically estimated by two components: the potential evapotranspiration, which determined entirely by weather conditions, and the crop coefficient, which is an experimentally derived factor determined by the biology of a plant species or cultivar (R. Allen et al., 1998a). However, when

plants endure periods of drought and water stress, they will restrict evapotranspiration as a strategy of conserving water or out of necessity due to a lack of available water (R. Allen et al., 1998b). Under these conditions, an additional factor is necessary to estimate actual plant evapotranspiration which accounts for the degree to which the plant restricts evapotranspiration in response to lower availability of water. Rather than a single ratio, this correction factor must be determined by a formula related to soil water availability, as evapotranspiration will be increasingly restricted as the soil matric potential decreases (R. Allen et al., 1998b; Zhang et al., 2004). This may be given by **Equation 4.1**,

$$ET_c = K_s K_c ET_0 \quad (4.13)$$

where  $ET_c$  is the actual crop evapotranspiration under nonstandard conditions (mm),  $K_s$  is the water stress coefficient,  $K_c$  is the crop coefficient, and  $ET_0$  is the reference evapotranspiration (mm).

The water stress coefficient is also therefore a useful leading indicator of plant stress and quality decline, as well as an objective measure of plant water stress. Turfgrass quality is often rated by trained experts according to a standard method of assessment. However, these ratings are subjective and affected by the biases of the rater (Keskin et al., 2003). Visual quality ratings are also a lagging indicator of plant stress, and can only measure plant water stress after the inadequate water availability has already caused physiological damage to the turfgrass and resulted in a lower visual appeal. Detecting plant water stress before it results in a visible decline in quality would therefore be a more valuable method of measuring water stress than visual ratings, as this would allow management decisions to be informed to alleviate water stress before visual quality is affected. The use of multispectral imagery and vegetation indices have been

used to detect stress in plant tissue which is invisible to the human eye (Behmann et al., 2014; Rumpf et al., 2010). When assessing the accuracy and sensitivity of these methods at measuring plant water stress, using the water stress coefficient may be a useful point of comparison to ensure false positives are not being measured.

The conditions of greatest concern to turfgrass management decision makers are drought and dry conditions, when soil moisture content is in steady decline. The lack of sufficient precipitation and soil moisture requires a response from management by irrigating to prevent water stress from impacting turfgrass quality. There are therefore two questions that arise for managers: at what stress coefficient is visual quality negatively impacted, and which methods can be used to estimate the stress coefficient so that management decisions can be made to prevent water stress from reaching that degree?

Three methods of measuring turf quality were used in the assessment of turfgrass plots, described in Chapter 2 and Chapter 3. Turfgrass plots were maintained under eight different irrigation treatments, including four treatments of deficit irrigation, as described in Chapter 3. Assessing the sensitivity of these methods to water stress, especially in detecting early water stress prior to the degradation in visual quality, is an important point of comparison between these methods. Therefore, the water stress coefficient will be used as an absolute measure of water stress, and its relationship of turf visual quality measured by these three methods will be analyzed.

Additionally, data included in this analysis was representative of a consistent drought period. Both soil water potential and crop water stress coefficients are affected by hysteresis when drying soil is rewetted. The relationship between volumetric water content and soil water potential changes when soil is being wetted or dried, such that instantaneous volumetric water

content alone is insufficient to estimate the availability of water to plant roots (Royer & Vachaud, 1975). Additionally, as discussed in Chapter 3, when turfgrass was significantly affected by water stress and soil then rewetted, visual quality did not recover within forty-eight hours.

While rewetting events did occur due to precipitation during this study, data was carefully cleaned to reduce the impacts of rewetting and hysteresis on soil moisture, visual quality, and the water stress coefficient. As a result, conclusions from this analysis are representative only of turfgrass during a drought period. However, drought periods are of particular importance in guiding management responses.

The water stress coefficient is a measure of restricted water consumption due to a low soil water potential (Allen et al., 1998b). When water stressed, turfgrass undergoes physiological changes detectable by multispectral imagery before this stress manifests as lowered visual quality (Fenstermaker-Shaulis et al., 1997).

This study aims to evaluate and compare soil moisture and NDVI measurements in their ability to predict water stress in TifTuf turfgrass (*Cynodon dactylon* x *C. transvaalensis*) during a drought period. TifTuf is a drought tolerant variety of bermudagrass which has exhibited evidence of both drought tolerance and avoidance strategies (Katuwal et al., 2020). This study will also assess the sensitivity of these data to water stress to determine whether these methods are useful in the early detection of water stress before symptoms manifest visibly.

## Materials and Methods

Data collected from three unirrigated turfgrass plots between July 3 and August 13 were used in this analysis. The subject turfgrass was drought tolerant hybrid bermudagrass TifTuf, and

soil at the site was a fine textured Cecil sandy loam. During this period, the soil moisture content of turfgrass plots began near field capacity and declined near the permanent wilting point. Other than one rainstorm early during this period, the decline in soil moisture was relatively steady due to a high rate of evapotranspiration and little rain. During the thirty-six days following July 8, 53 mm of precipitation was measured at the site, while the average July rainfall in Raleigh is 123 mm (Peacock & Bruneau, 2006).

The water stress of turfgrass plots was measured by comparing actual water use to estimated crop water demand. First, the soil moisture of plots was determined each day at approximately 3 AM. Soil moisture in planted cropland changes most rapidly during the daylight hours when plants are transpiring, and least rapidly during the night. This creates a ‘stair step’ appearance in soil moisture over time graphs, where soil moisture descends quickly during daylight hours and flattens during the night. Therefore, 3 AM measurements were selected because this time was found to be during a range of time during which the rate of change of soil moisture was small, and could therefore be used to indicate the soil moisture between days.

Daily actual evapotranspiration in millimeters was calculated from soil moisture data by

**Equation 4.2:**

$$ET_a = 152.4 * \frac{(SMC_2 - SMC_1)}{100} \quad (4.14)$$

where  $ET_a$  represents the actual evapotranspiration (mm),  $SMC_1$  represents the volumetric moisture content at the start of the day (%), and  $SMC_2$  represents the soil moisture at 3 AM the following day (%). A 152.4 mm effective root depth of bermudagrass is used (Ross & Hardy, 1997).

To determine water stress, actual evapotranspiration was compared to Penman-Monteith estimated unrestricted evapotranspiration retrieved from a weather station 1.2 km from the site.

A daily stress coefficient was calculated from each plot using **Equation 4.3**:

$$K_s = \frac{ET_a}{ET_o * K_c} \quad (4.15)$$

where  $K_s$  is the crop stress coefficient,  $ET_o$  is the reference evapotranspiration (mm),  $ET_a$  represents the actual evapotranspiration (mm), and  $K_c$  is the crop coefficient. Monthly crop coefficients of TifTuf established by Pinnix (2018) were used.

Stress coefficients were calculated for three plots of unirrigated turfgrass between July 3 and August 14. During this period crop water demand far exceeded effective rainfall, such that initial soil moisture was at the field capacity and final soil moisture approached the permanent wilting point.

## Analysis and Results

### **Data Cleaning**

The scope of this analysis was to assess crop water stress during a consistent drawdown of soil moisture. Data from unirrigated turfgrass plots during a particularly hot and dry period of the summer were therefore selected to include in the analysis, during which soil moisture declined from the field capacity to near the permanent wilting point. Without the use of rainout shelters, however, precipitation contributing to soil moisture could not be prevented. Therefore, to simulate a perfect drying period with the data available, data from certain periods were excluded after precipitation events.

Precipitation frequently led to an observed rise in soil moisture, followed by a delayed rise in the water stress coefficient. Data were carefully assessed and cleaned such that these recovery periods were excluded and only data representative of drying soil moisture conditions were included.

First, when calculating daily stress coefficients, the days in which precipitation occurred were excluded. Water use could not accurately be measured from soil moisture data on days when water was added to the soil through precipitation and irrigation. Additionally, it was found that water use estimated from soil moisture on the day after precipitation was often similarly lower than expected, which can be due to water redistribution within the rootzone. After preliminary analysis, a precipitation depth of 5 mm was found to be general threshold above which water stress coefficients were significantly lower than expected the day after precipitation. This is likely because very small depths of rainfall were less likely to contribute to soil water storage below the root zone, and thus less likely to contribute to groundwater recharge in the days following. However, additional analysis, verification, and data cleaning were required in order to minimize the effects of hysteresis on the water stress coefficient.

The daily precipitation, average water stress coefficient, and average initial relative soil moisture depletion before cleaning are shown in **Figure 4.1**. When unmeasured water entered the root zone through these two means, the water stress coefficient as measured by water consumption was underestimated.

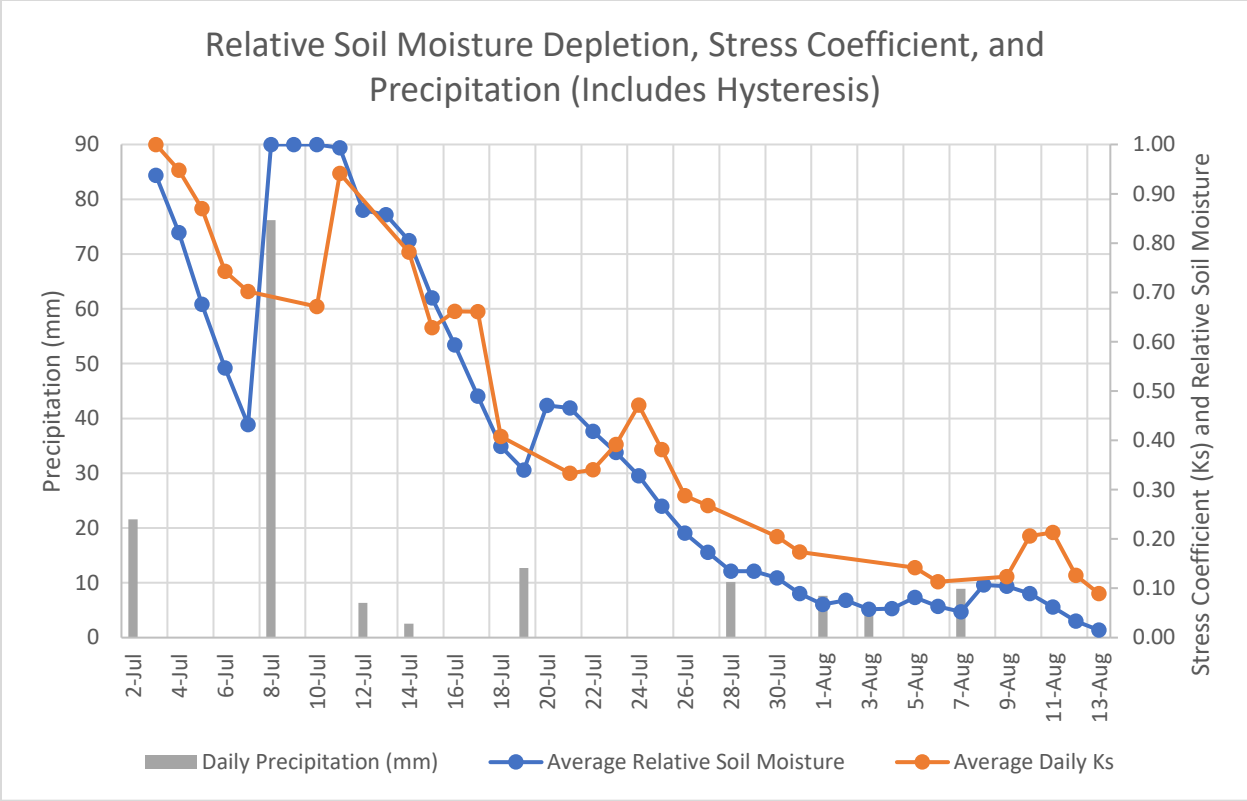


Figure 4.1: Original dataset of average water stress coefficients of three unirrigated turfgrass plots

First, the ability to accurately measure the water stress coefficient from soil moisture in the days following precipitation events was assessed. All but three precipitation events during the period analyzed were between 5 and 12 mm. On the day after rainfall of these depths occurred, it was found that the estimated water stress coefficient was consistently and dramatically smaller than the coefficients estimated on other days when soil moisture was similar. This consistent underestimation of the water stress coefficient shortly after rainfall was believed to have been caused by water movement from deeper in the soil profile into the root zone. For all precipitation events between 5 and 12 mm, excluded data from one day after rain eliminated this underestimation of water stress.

However, this rule of excluding all data collected one day after precipitation was determined to be inadequate for precipitation events outside the range of 5 to 12 mm. Following a 2.5 mm precipitation event on July 14, the estimated stress coefficients of Plot 11 and Plot 23 did not experience a dramatic underestimation indicative of groundwater contributions to the root zone. Thus, it was determined that the exclusion of these data was unnecessary. However, the stress coefficient estimated in Plot 15 dropped sharply for a single day on July 15 to 0.44 before rising to 0.52 the following day. Therefore, only data collected on July 15 from Plot 15 was excluded.

It was also determined that precipitation events exceeding 12 mm required a different ruleset for excluding data. First, a precipitation event with a depth of 76 mm occurred on July 8. Afterward, the pattern of dramatic underestimation of water stress occurred two full days after rainfall in all plots. Therefore, an additional day of data was excluded following this event. This same pattern was also observed following a 13 mm precipitation event on July 19, with one difference. While the water stress coefficients estimated from Plot 11 and Plot 23 rebounded to reasonable values by the third day following precipitation, those estimated in Plot 15 remained less than 50% of the stress coefficient measured directly before the rain for an additional day. Therefore, following the July 19 rainfall, two days of data were excluded from Plot 11 and Plot 23, and three days from Plot 15.

Next, rainfall was also observed to produce a delayed and brief increase in the water stress coefficient in some instances. Following precipitation events exceeding 12 mm, soil moisture recovered quickly while the elevation in water stress coefficient was delayed. This hysteresis led to some measurements of the water stress coefficient on July 10, July 11, and July 21 which had not yet recovered in response to an increase in soil moisture. When evaluating the

relationship to soil moisture to the water stress coefficient, this hysteresis could introduce noise, and is not representative of a continuous drying period. These data were therefore also excluded from later analysis by excluding data for two to three days following a precipitation event exceeding 12 mm.

Finally, the delayed and temporary elevation of the water stress coefficient following significant precipitation events was also a source of hysteresis in the data. Following a 13 mm rainfall on July 19, Plot 23 experienced a delayed and sharp recovery in water stress coefficient from 0.3 on July 18 to 0.63 on July 24, only to fall sharply back to 0.33 on July 27. Such a brief recovery in the water stress coefficient after turfgrass has already experienced water stress may not result in a recovery in turfgrass visual quality, and is also not representative of a continuous drying period. Therefore, data collected on July 24 and 25 from Plot 23 were excluded from further analysis. Similarly, following a rainfall event on July 14, the water stress coefficient rose slightly from 0.79 on July 15 to 0.84 on July 17 while the relative soil moisture declined from 73% to 51%. This delayed rise in the water stress coefficient following soil wetting was also determined to not be representative of a continuous drying event, and data from Plot 23 on these two dates were also excluded.

The results of these data cleaning steps are shown in **Figure 4.2**, where the average water stress coefficient is the result of the cleaned data across all three plots. The smoothing of the water stress coefficient line is the result of removing data affected by groundwater contributions to the root zone and the effects of hysteresis produced by precipitation.

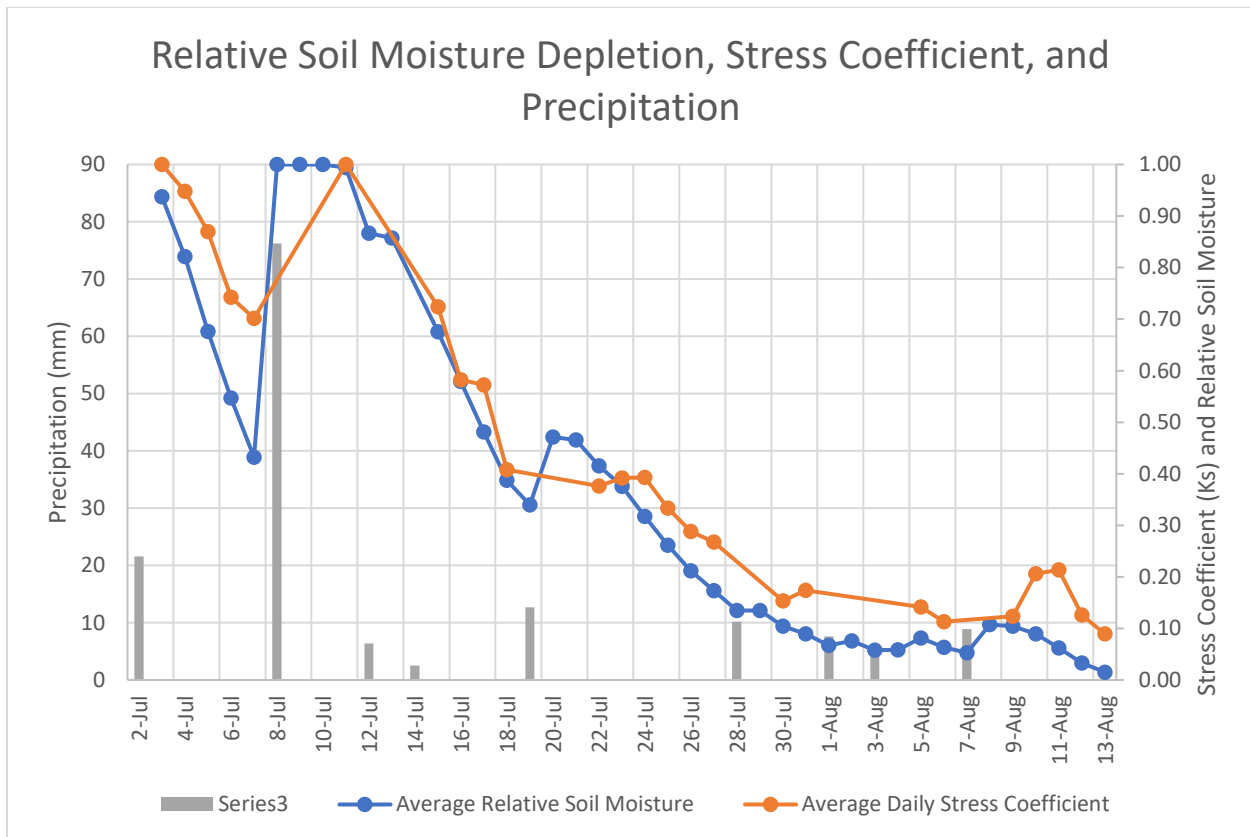


Figure 4.2: Cleaned dataset of average water stress coefficients of three unirrigated turfgrass plots

### Soil Moisture Deficit and Water Stress

Soil moisture of the three turfgrass plots during the period investigated is shown in **Figure 4.3**. During this period, precipitation resulted in an estimated 62 mm of effective rainfall, where effective rainfall was calculated in Chapter 3 by **Equation 4.4**. Most of this rainfall occurred in three events within the first week, on July 2, July 3, and July 8. Between July 9 and August 13, the soil moisture of all plots declines from field capacity to near the permanent wilting point, with only minor rewetting events from smaller rainstorms.

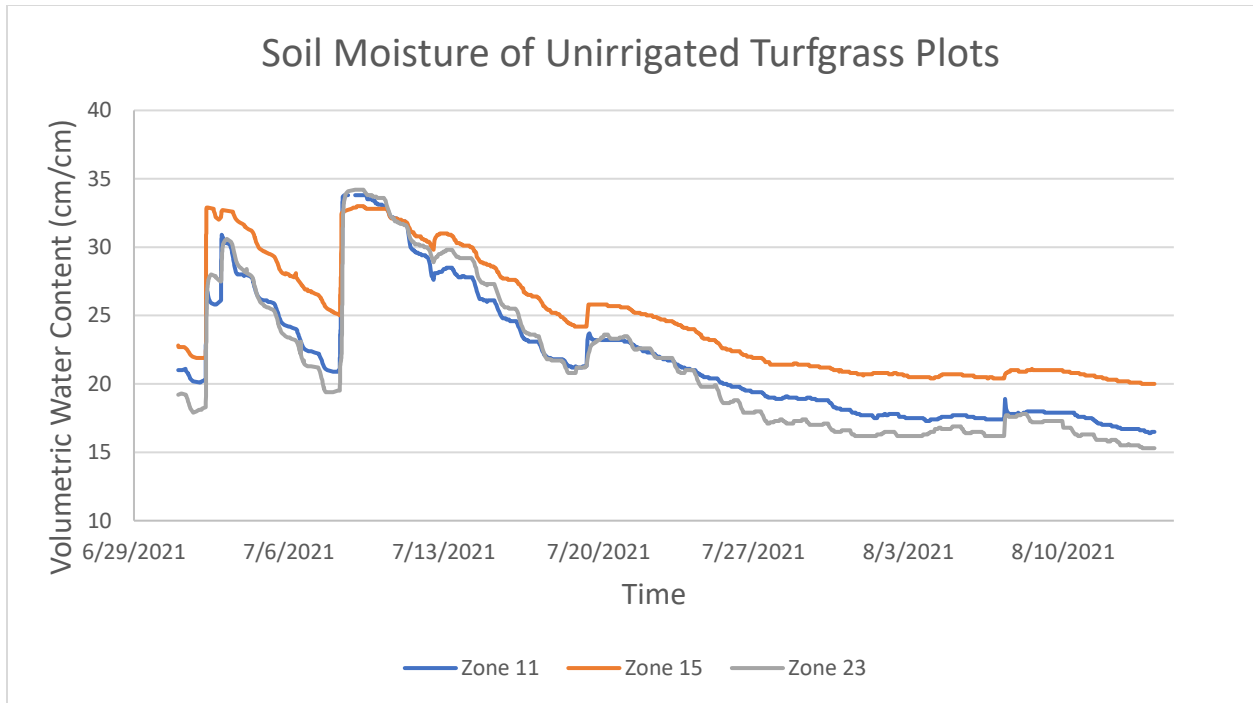


Figure 4.3: Volumetric water content of topsoil in three unirrigated turfgrass plots

Daily stress coefficients were compared to the initial soil moisture of plots as shown in **Figure 4.4**, and a linear regression was performed. Daily stress coefficients were strongly correlated with initial moisture content ( $R=0.83$ ).

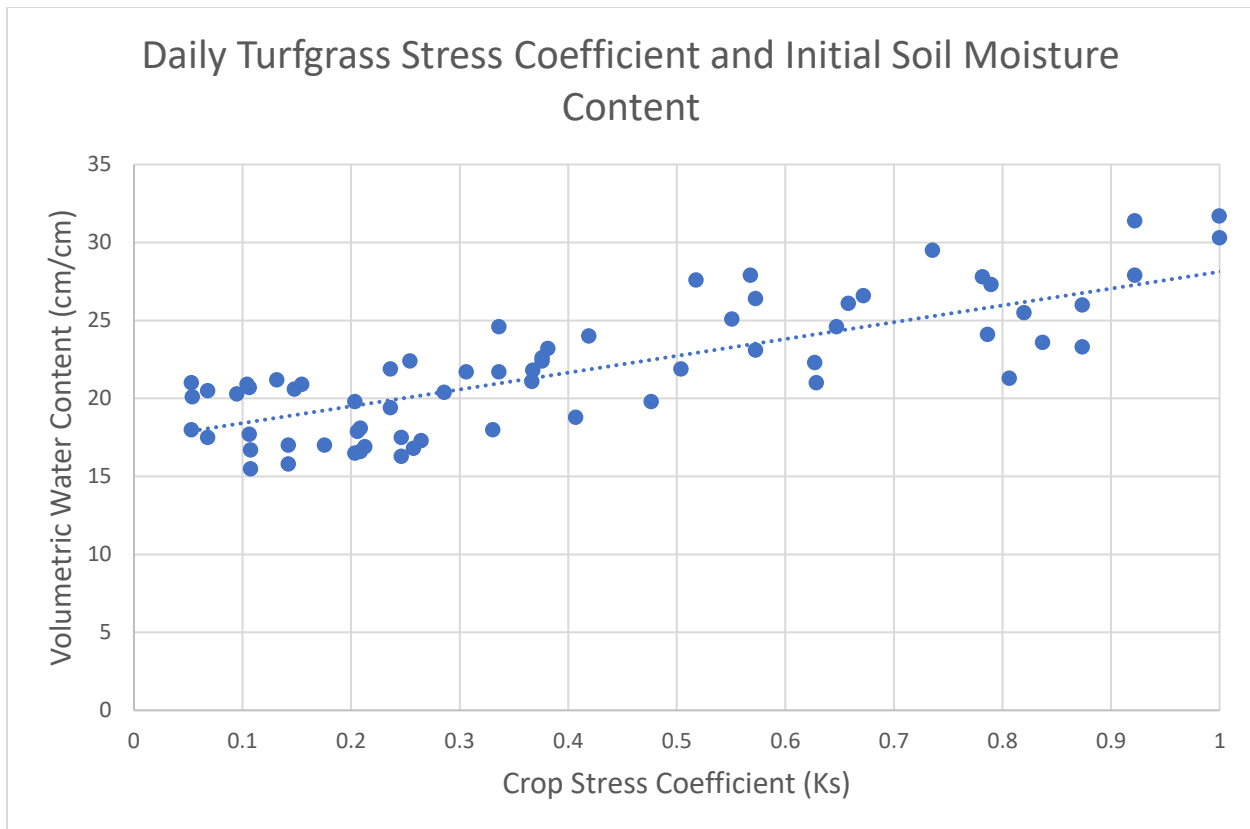


Figure 4.4: Daily turfgrass water stress coefficient and predawn soil volumetric water content

The same analysis was also performed using percent moisture deficit in place of volumetric water content. Water within different soils may be harder or easier for plant roots to extract while at the same VWC based on soil physical properties. One way to mitigate the effect of soil heterogeneity without the use of additional sensors is to consider the VWC within the bounds of plant available water, or the range between the field capacity and the permanent wilting point. In other words, to consider not the nominal VWC, but the percent depletion of total plant available water.

Additionally, the soil moisture of zone 15 remained higher than that of the other two zones throughout most of the period, despite being subject to the same environmental conditions and being physically about one meter away from zone 11. The soil moisture of all three plots

also remain level for several days, and the stress coefficient of zone 15 on the final day of the period was 0.05, while those of both other plots were 0.11. Stress coefficients between zone 15 and the other two plots were also highly correlated ( $R=0.93$ ). Therefore, we conclude that the soil moisture of zone 15, while on average 4% higher in VWC than that of the other two plots on the final day of the period, was similarly near the permanent wilting point. The lower stress coefficient suggests that zone 15 may have been even nearer the PWP than the other two plots, despite its higher VWC. This higher PWP may be caused by differences in soil texture between plots, or else a difference in calibration between soil moisture sensors. However, by comparing stress coefficient to soil moisture deficit rather than volumetric water content, the effect of the difference in texture or sensor calibration may be reduced.

Seventy-two hours after a 15 mm rainstorm on December 8 saturated all plots, and while turfgrass was dormant, the soil moisture of Zones 11, 15, and 23 were 32.5%, 32.2%, and 32.4%, respectively. These values were used as the field capacity, or 0% depletion. The stress coefficients on August 13 for these zones were, in the same order, 0.11, 0.05, and 0.11. The lowest observed soil moisture contents of these plots throughout the entire experimental period occurred on August 14, prior to precipitation which occurred on that day: 16.4% for zone 11, 20% for zone 15, and 15.2% for zone 23. These values of VWC were used as an estimate of the PWP, or 100% depletion. The resulting graph of the relationship between initial soil moisture depletion and daily stress coefficient is shown in **Figure 4.5**. Relating water stress coefficients to the percent soil moisture depletion improved the correlation coefficient to 0.93.

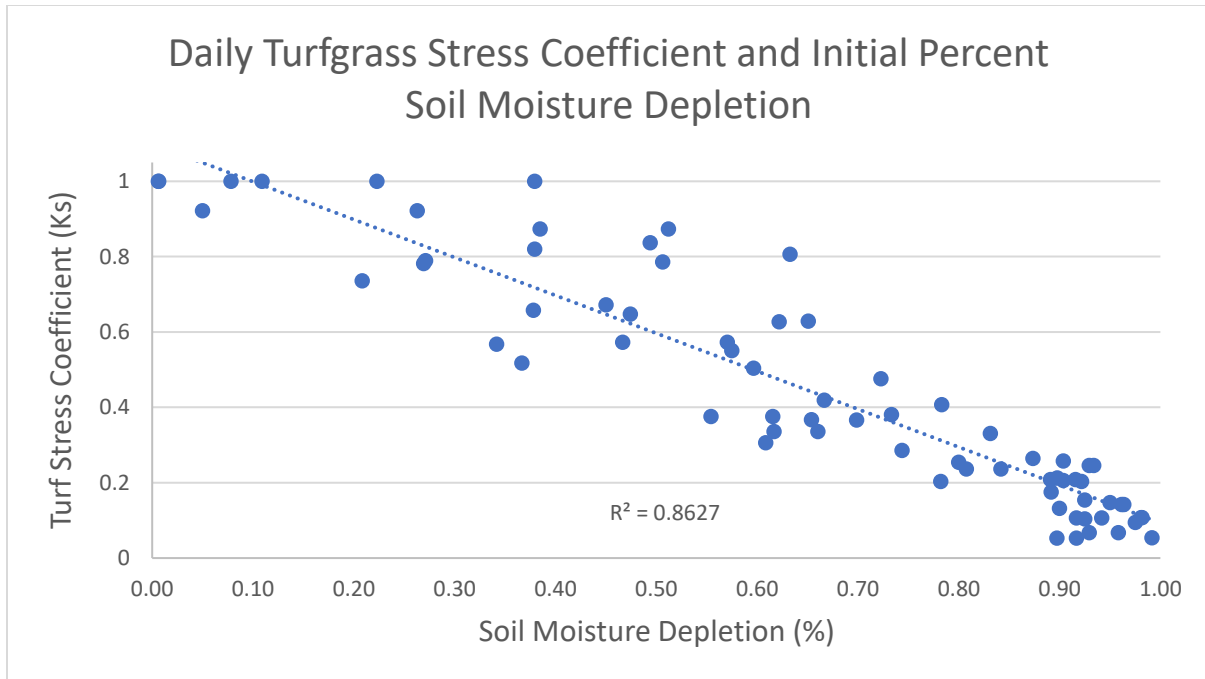


Figure 4.5: Daily turfgrass water stress coefficient and predawn soil moisture depletion

A second order polynomial regression model was considered using JMP, using the relative depletion as a predictor of water stress coefficient. First, diagnostic residual plots were assessed to determine the distribution of the data. The residual normal quantile plot, shown in **Figure 4.6**, indicated that the data were normally distributed. The studentized residuals plot (**Figure 4.7**) indicated that no outliers were present in the data. Finally, the residuals by predicted plot (**Figure 4.8**) indicated that error was centered around zero.

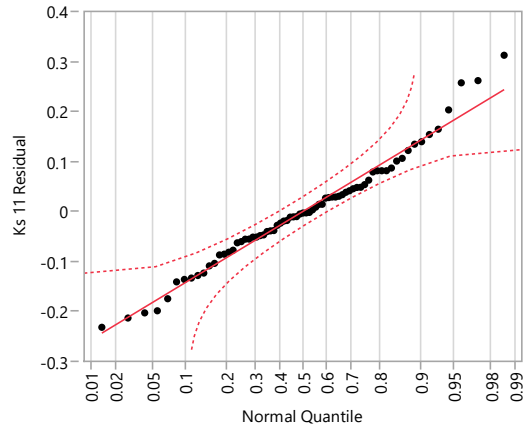


Figure 4.6: Normal quantile plot of second order linear model using soil moisture depletion as the predictor of water stress coefficient

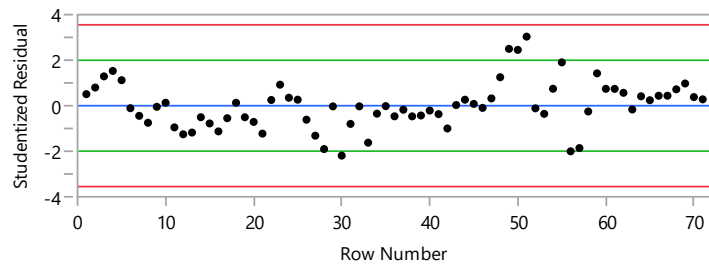


Figure 4.7: Studentized residuals plot of second order linear model using soil moisture depletion as the predictor of water stress coefficient

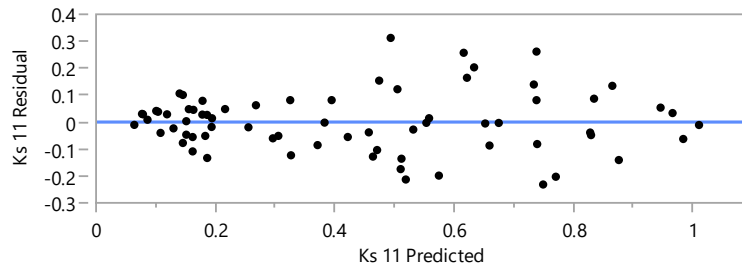


Figure 4.8: Residuals plot of second order linear model using soil moisture depletion as the predictor of water stress coefficient

However, residuals were higher within the data between a predicted water stress coefficient of 0.45 and 0.9. Two explanations are offered for the higher error in this model within this range. First, while data was cleaned with the intent of reducing the impact of hysteresis affecting soil moisture and the water stress coefficient, the data used in this model did experience rewetting. As shown in the uncleaned data in **Figure 4.1**, the water stress coefficient rebounded to a much greater degree while within the range of 0.4 to 0.9 than it did at lower stress coefficients when the turfgrass was more severely stressed. Therefore, error within this range is likely partially due to hysteresis that could not fully be eliminated from the dataset.

Second, F-tests were performed to determine the significance of depletion and the second order of depletion as predictive effects of the water stress coefficient. F-statistics of both effects were 349.2 and 4.7, relating to p-values of less than 0.0001 and 0.0332, respectively. Therefore, significance of a second order polynomial model was established. This model, given by **Equation 4.4**, indicates that as the stress coefficient rises, the value of soil moisture depletion as a predictor of water stress coefficient decreases slightly. This may also partially explain the higher error present in this model at higher predicted water stress coefficients. In the model given below,

$$K_s = 1.177 - 0.377 * (D - 0.656)^2 - 1.079 * D \quad (4.16)$$

D was the percent soil moisture depletion, and  $K_s$  was the water stress coefficient.

The actual by predicted water stress coefficient values are shown in **Figure 4.9**. The root mean square error of this model was 0.1107.

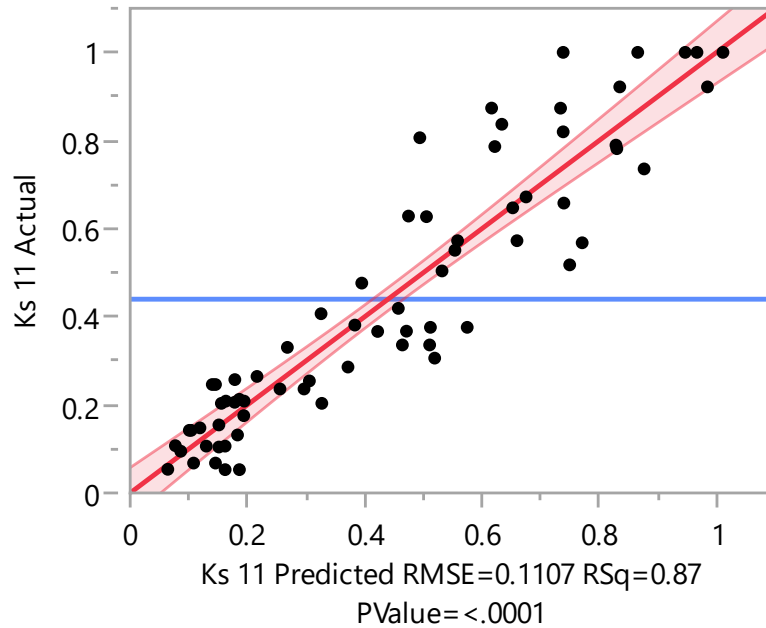


Figure 4.9: Actual by predicted plot of the final model using soil moisture depletion as the predictor of water stress coefficient (Equation 4)

### TCM 500 NDVI Sampling and Stress Coefficient

The average NDVI of turfgrass plots was also compared to the daily stress coefficient observed. Data were included where the stress coefficient could be determined from soil moisture data within twenty-four hours of TCM 500 measurements. A scatterplot of these data is shown in **Figure 4.10**.

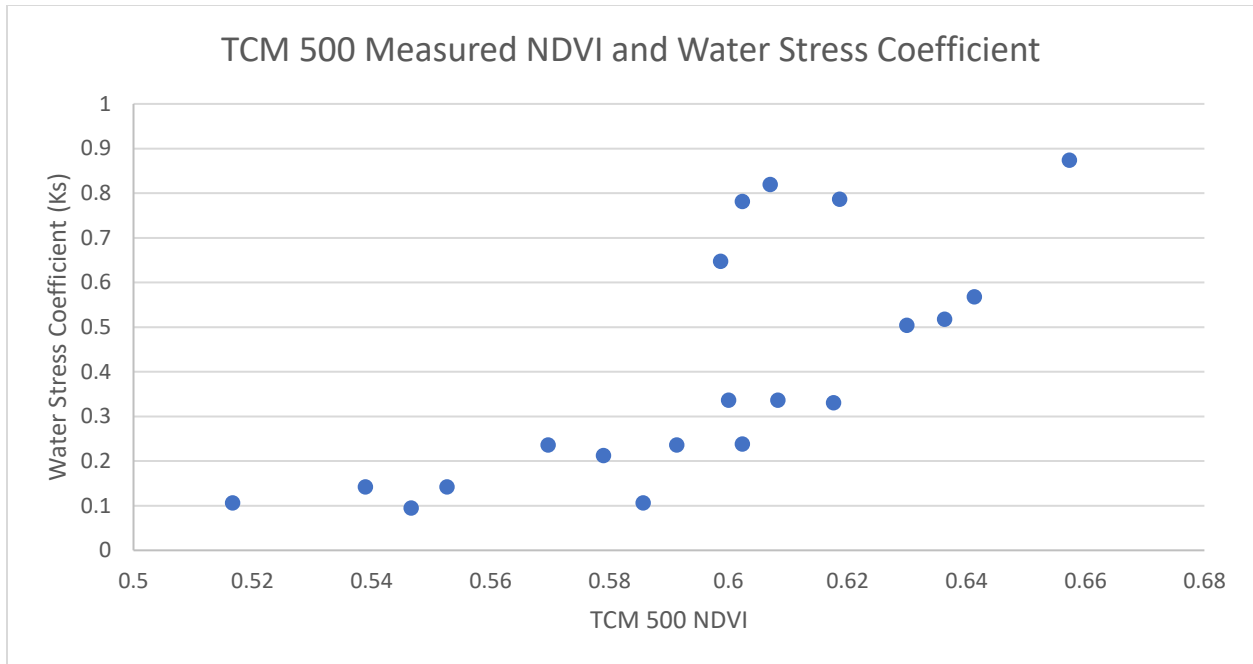


Figure 4.10: Daily water stress coefficient and TCM 500 NDVI of unirrigated turfgrass plots

The value and significance of TCM 500 sampling as a predictor of the turf water stress coefficient was assessed using JMP. Twenty total data points across the three turfgrass plots fit these criteria, ranging from July 6 to August 12. A second order polynomial model was analyzed with NDVI as a predictor of water stress coefficient.

First, residuals diagnostic plots were assessed to determine whether ANOVA and regression analysis could be used to assess the model. The normal quantile plot (**Figure 4.11**) indicated that the data was reasonably normally distributed. Studentized residuals (**Figure 4.12**) indicated that no outliers were present in the dataset. The residuals by predicted plot (**Figure 4.13**) indicated that error within the model was random and reasonably centered about zero.

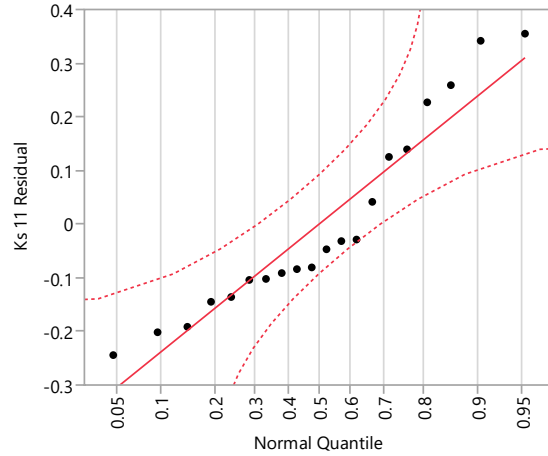


Figure 4.11: Normal quantile plot of second order linear model using TCM 500 NDVI as the predictor of water stress coefficient

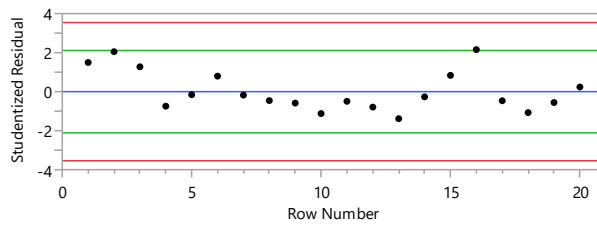


Figure 4.12: Studentized residuals plot of second order linear model using TCM 500 NDVI as the predictor of water stress coefficient

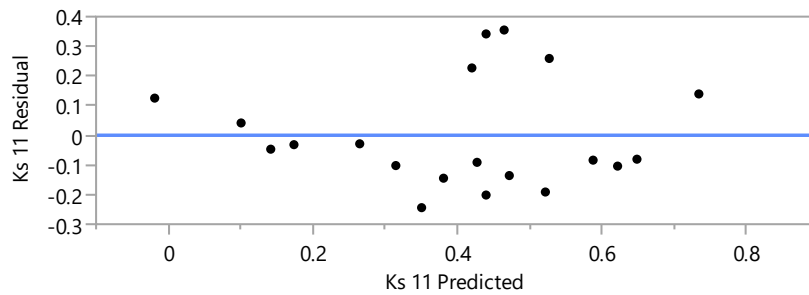


Figure 4.13: Residuals versus predicted plot of second order linear model using TCM 500 NDVI as the predictor of water stress coefficient

Next, partial F-tests were performed on each of the effects to determine their significance, and a 0.05 significance level was used as a threshold. The F-statistic of NDVI was determined to be 19.6, relating to a p-value of 0.0004, indicating significance. The second order of NDVI, however, was determined to have an F-statistic of 0.44 and a p-value of 0.52, indicating insignificance as a predictor of water stress coefficient. Therefore, in this partial test the null hypothesis could not be rejected. The second order of NDVI was removed as an effect in the model and a linear model was used in subsequent analysis.

A partial F-test was again performed using NDVI as the sole predictor of the stress coefficient. The F-statistic was determined to be 20.7, corresponding to a p-value of 0.0003 and indicating significance. A t-test was then performed on the intercept, finding the model intercept to have a t-statistic of -3.97 and a p-value of 0.0009. ANOVA was then performed on the whole model, and results are shown in **Table 4.1**. Overall, the model F-statistic was 20.7 and the p-value was 0.0003.

Table 4.1: ANOVA table of the final model using TCM 500 as the predictor of water stress coefficient

	Degrees Freedom	Sum of Squares	Mean Square
Model	1	0.714	0.714
Error	18	0.622	0.035

With the significance of the model established, linear regression analysis was performed on the dataset, as shown in **Figure 4.14**. The correlation coefficient of the linear model was 0.73, and the root mean square error (RMSE) was 0.1859.

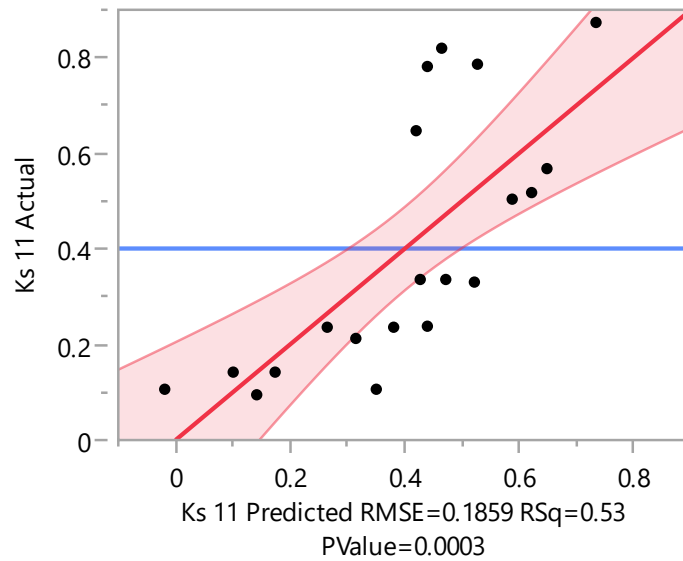


Figure 4.14: Actual by predicted plot of the final model using soil TCM 500 as the predictor of water stress coefficient (Equation 5)

Linear regression was used to determine the final model using TCM 500 measurements as a predictor of turf water stress coefficient, as shown in **Equation 4.5**,

$$K_s = -2.785 + 5.354 * NDVI \quad (4.17)$$

where  $K_s$  was the water stress coefficient and NDVI was the average TCM 500 NDVI of the plot.

### Imagery Based NDVI and Stress Coefficient

NDVI measurements derived from the imagery processing algorithm were also compared to daily stress coefficient values in order to determine the extent to which this turf assessment method may be useful in predicting turf stress. A scatterplot of the NDVI and stress coefficients of three unirrigated turfgrass plots are shown in **Figure 4.15**. Data representative of a continuous

drying event where the water stress coefficient could be determined from soil moisture data within twenty-four hours of camera imagery collection were included.

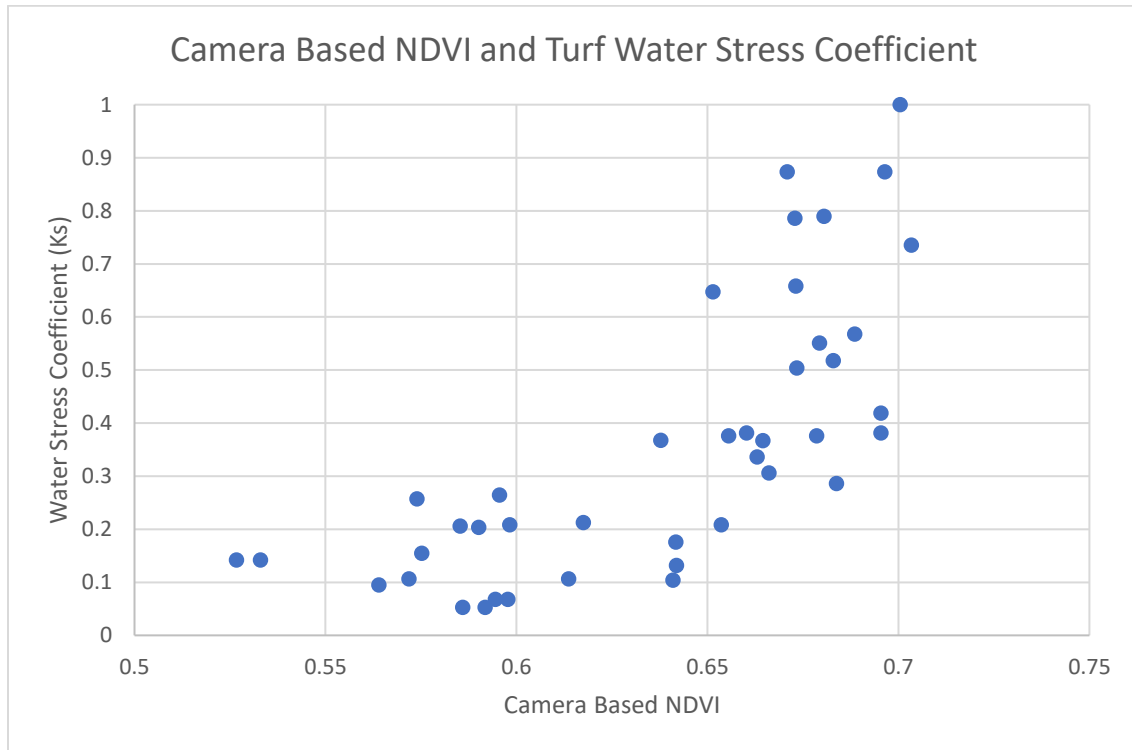


Figure 4.15: Daily water stress coefficient and camera-based NDVI of unirrigated turfgrass plots

Further analysis of a model using camera-based NDVI to predict turf stress coefficient was performed in JMP. F-tests performed on NDVI and the second order of NDVI as effects determined their F-statistics to be 64.3 and 9.4, respectively. These values related to p-values of less than 0.0001 and 0.004., respectively, indicating that both effects were highly significant and use of a second order polynomial model was justified.

Next, residuals diagnostic plots were assessed. Studentized residuals (**Figure 4.16**) indicated that no outliers were present in the dataset. The residuals by predicted plot (**Figure 4.17**) indicated that error within the model was random and reasonably centered about zero.

Finally, the normal quantile plot (**Figure 4.18**) indicated that the data was reasonably normally distributed. Therefore, ANOVA and regression analysis were used in the assessment of the model.

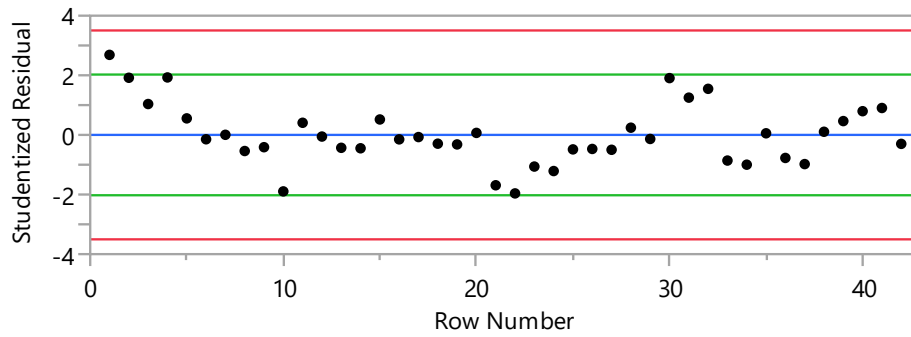


Figure 4.16: Studentized residuals plot of second order linear model using camera-based NDVI as the predictor of water stress coefficient

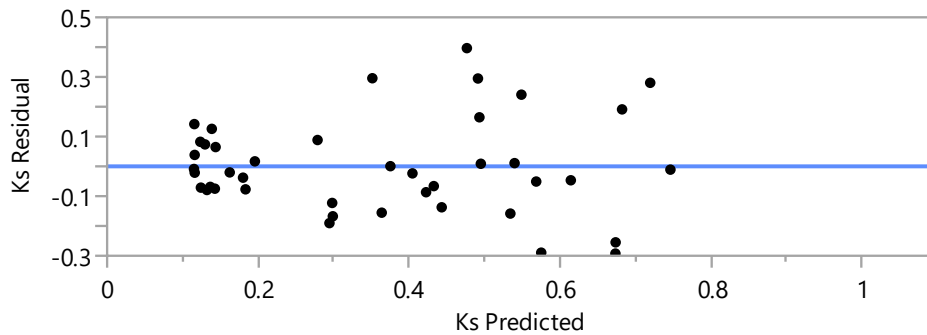


Figure 4.17: Residuals by predicted plot of second order linear model using camera-based NDVI as the predictor of water stress coefficient

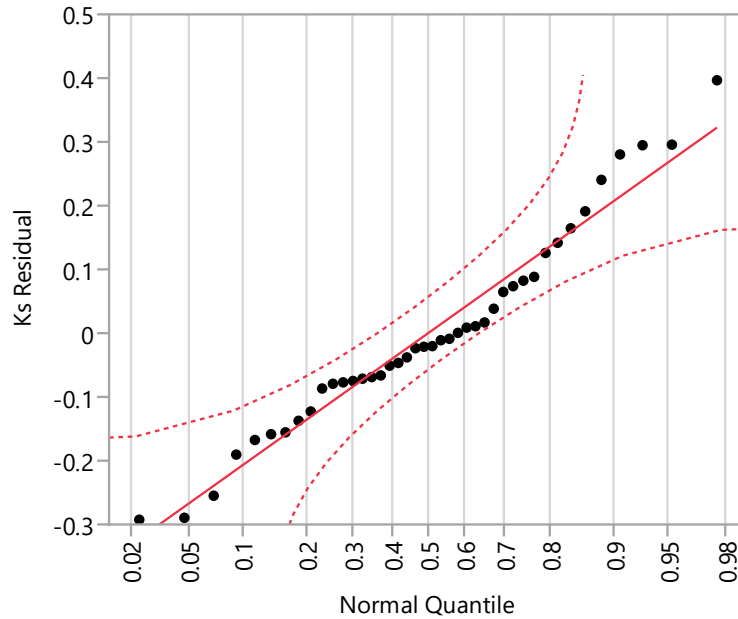


Figure 4.18: Normal quantile plot of second order linear model using camera-based NDVI as the predictor of water stress coefficient

Next, partial F-tests were used to determine the significance of model predictors. The first order of camera-based NDVI was determined to have an F-statistic of 64.3 and a corresponding p-value  $< 0.0001$ . The second order of camera-based NDVI was determined to have an F-statistic of 9.4 and a p-value of 0.004. Therefore, both predictors were determined to be significant using a confidence level of 0.05, and second order polynomial regression analysis was performed.

ANOVA was performed on the whole model, and results are shown in **Table 4.2**. The F-statistic of the model was determined to be 32.7 and the corresponding p-value to be  $< 0.0001$ . Therefore, the second order polynomial model was determined to be significant.

Table 4.2: ANOVA of the final model using camera-based NDVI as the predictor of water stress coefficient (Equation 6)

	Degrees Freedom	Sum of Squares	Mean Square
Model	2	1.714	0.857
Error	39	1.023	0.026

The actual by predicted plot using the second order polynomial model is shown in **Figure 4.19**. The root mean square error of this model was 0.162, and the  $R^2$  was 0.63.

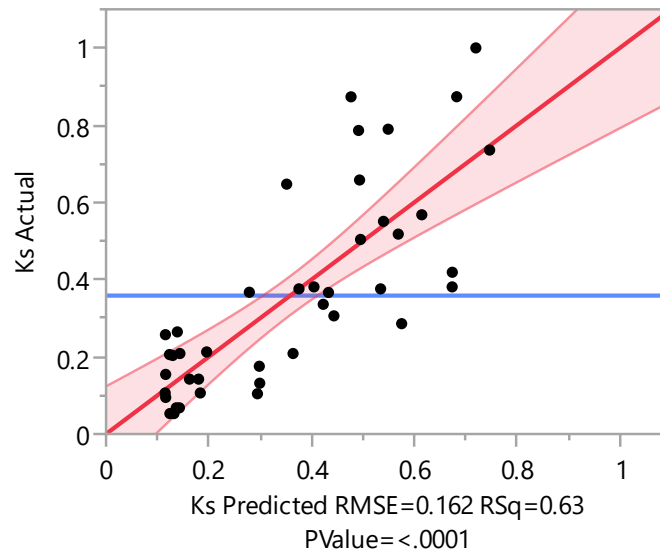


Figure 4.19: Actual by predicted plot of the final model using camera-based NDVI as a predictor for water stress coefficient (Equation 6)

Finally, parameter estimates were performed by linear regression analysis to determine the model equation for the second order polynomial model **Equation 4.6**,

$$K_s = -2.77 + 4.78 * NDVI + 35.33 * (NDVI - 0.637)^2 \quad (4.18)$$

where  $K_s$  is the predicted water stress coefficient and NDVI is the camera-based NDVI of the plot.

### Summary of Predictive Models

A summary of the fitness of all predictive models developed from field data is shown in

**Table 4.3.**

Table 4.3: Fitness of models using sensor data to predict the water stress coefficient of turfgrass

Sensor	R <sup>2</sup>	RMSE
Soil Moisture Depletion	0.87	0.111
TCM 500 NDVI	0.53	0.186
Camera NDVI	0.63	0.162

As measured by both R<sup>2</sup> and RMSE, soil moisture depletion was found to be the strongest predictor of the daily turfgrass water stress coefficient under constant drawdown conditions.

NDVI measured by both methods were also determined to be significant predictors of the water stress coefficient with greater than 95% confidence. Of the two, NDVI measured by the camera system resulted in a stronger predictive model.

### Early Detection of Water Stress

By developing predictive models of turfgrass water stress coefficient from empirical data, data collected from soil moisture sensors and NDVI measurements can be used to estimate the water stress coefficient across its full range. Each of these models developed from different

sensor data were evaluated by comparing the accuracy of their predictions by the  $R^2$  and RMSE of each model. However, another method of assessing each type of sensor data and its usefulness in predicting the water stress coefficient is by comparing their no-effect ranges. By determining the breaking point above which there is no significant response between the water stress coefficient and sensor data, the sensitivity of each turfgrass assessment method to water stress may be compared.

PartReg (waterlog.info) is a software program which iteratively performs progressive segmented regression on a dataset to identify the breaking point corresponding to the maximum possible no-effect (Oosterbaan, 2018). By using this statistical approach, the breaking point of water stress coefficient on which water stress results in a degradation in turfgrass visual quality was first determined.

Using the water stress coefficient as the predictor of turfgrass visual quality, partial linear regression was performed iteratively on an increasingly larger subset of the data, beginning with paired values where the water stress coefficient was 1.0. Partial regression is often used where the breaking point is set equal to the point which results in the lowest error. In some cases, these types of segmented equations fit data better than second order curved models, or else are useful in their simplicity. Basal crop coefficients of annual crops, such as corn, often use such segmented models. However, in this case, the breaking point was set not at the point which gives the resulting line the best fit, but rather at the lowest stress coefficient where the resulting regression coefficient was determined to be significantly different from a horizontal line, or zero. This type of segmented regression is useful when measuring the sensitivity of some response, such as the sensitivity of crops to salinity (Oosterbaan, 2018). 95% confidence intervals of the regression lines were calculated using the methodology described by Oosterbaan (Oosterbaan,

2017). **Figure 4.20** shows the resulting analysis, where a box encloses the 95% confidence interval of the breaking point.

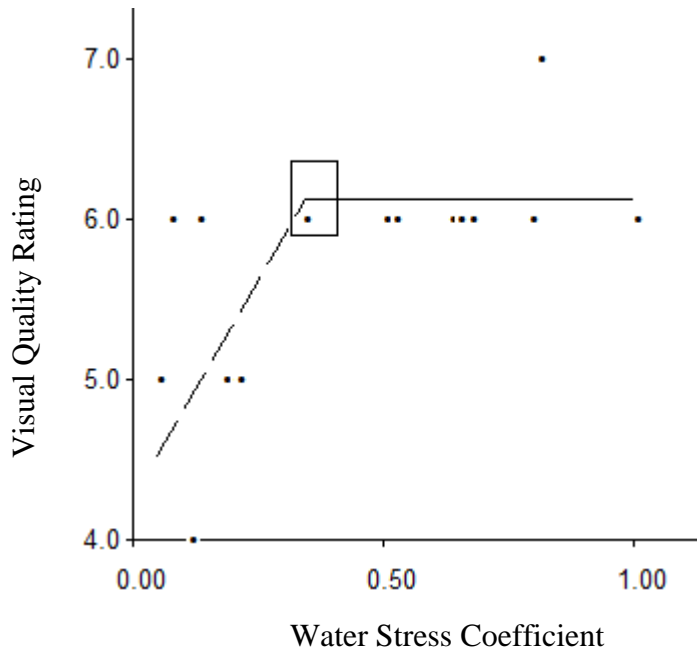


Figure 4.20: Breaking point defining the no-effect range between the water stress coefficient and visual quality ratings of turfgrass

The breaking point was determined to be a water stress coefficient of 0.34, with the bounds of the 95% confidence interval being 0.32 and 0.41. Using the predictive model using the percent soil moisture depletion to estimate the water stress coefficient (**Equation 4.4**), the water stress coefficient at which visual quality begins to degrade would be predicted at a soil moisture percent depletion of 77%.

Next, this same analysis was performed on the dataset of TCM 500 measurements and water stress coefficients used to develop a predictive model above. The results are shown in **Figure 4.21**.

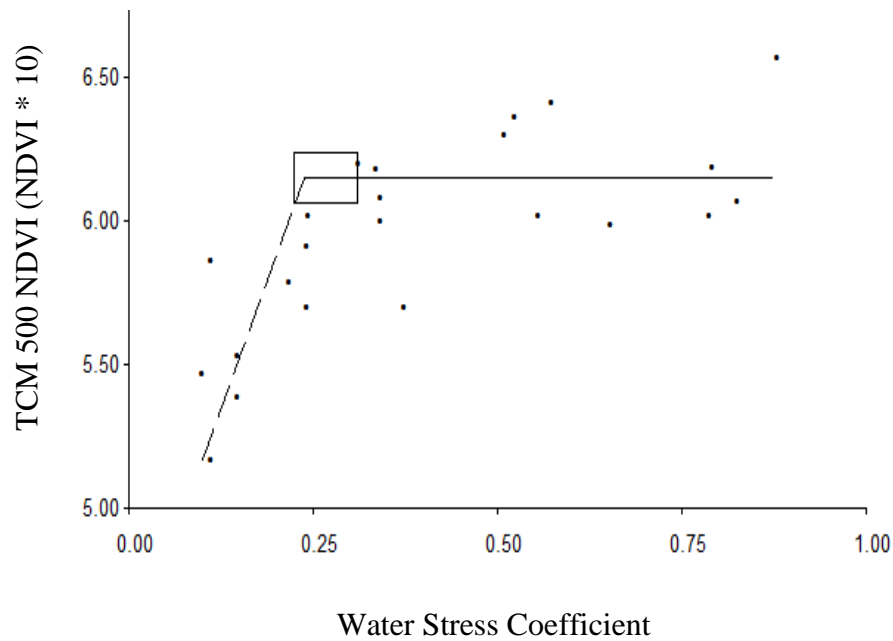


Figure 4.21: Breaking point defining the no-effect range between the water stress coefficient and TCM 500 measurements of NDVI of turfgrass

The resulting breaking point in the stress coefficient was 0.24, with 95% confidence interval bounds of 0.22 and 0.33.

Next, this analysis was performed using the dataset used to develop a predictive model of the stress coefficient using camera-based NDVI. Results are shown in **Figure 4.22**.

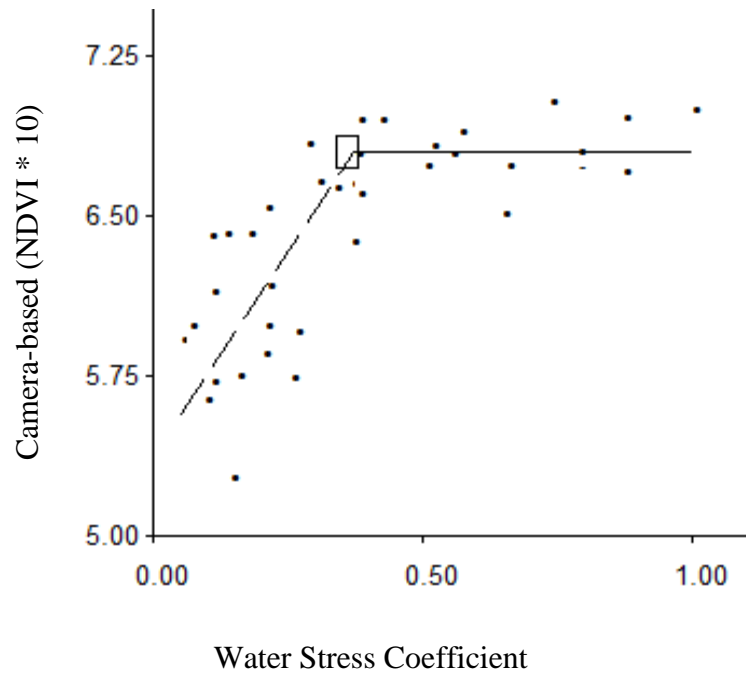


Figure 4.22: Breaking point defining the no-effect range between the water stress coefficient and pole mounted camera-based NDVI of turfgrass

The resulting breaking point in the stress coefficient was 0.37, with 95% confidence interval bounds of 0.34 and 0.38.

Finally, analysis was performed on the dataset used to develop a predictive model for the stress coefficient using soil moisture depletion as the predictor.

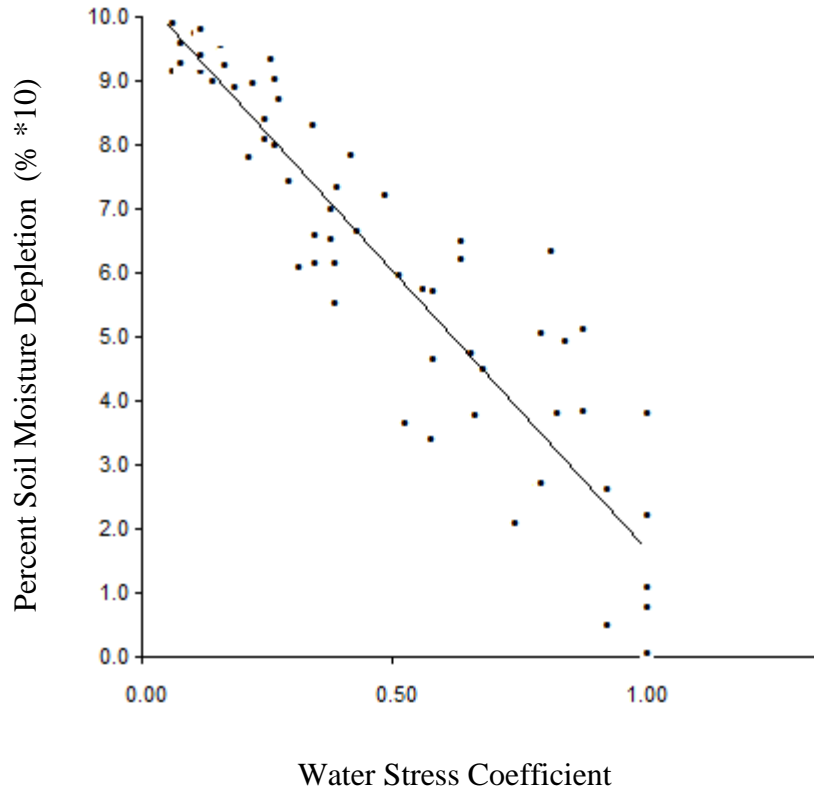


Figure 4.23: Attempt to identify a breaking point defining a no-effect range between the water stress coefficient and soil moisture depletion of turfgrass

As shown, the analysis performed found no breaking point within the data- the regression coefficient was significantly different from zero across the entire range of water stress coefficients.

### Summary of Water Stress Detection Sensitivity

A summary of the breaking points for each turfgrass measurement is shown in **Table 4.4**.

Table 4.4: Summary of breaking points defining no-effect areas of turfgrass sensors and water stress coefficient

Measurement	BP Lower (95% CI)	BP	BP Upper (95% CI)
Visual Quality	0.32	0.34	0.41
TCM 500 NDVI	0.22	0.24	0.33
Camera NDVI	0.34	0.37	0.38
Soil Moisture	-	-	-

The breaking point at which the water stress coefficient was determined to have a significant effect on turfgrass visual quality was 0.34. However, it should be noted that the dataset used was small due to the low temporal resolution of visual ratings performed (once per week), and only one turfgrass plot was rated where the water stress coefficient was between 0.5 and 0.25. Further study is suggested to more confidently establish the water stress coefficient at which the visual quality of turfgrass is affected.

It was determined that there was a significant effect between soil moisture depletion and the water stress coefficient throughout the entire range. Therefore, soil moisture was determined to be the sensor measurement most sensitive to water stress and the most valuable data for the early detection of water stress.

Out of the two methods of measuring NDVI, the camera system was determined to be significantly more sensitive to water stress than TCM 500 measurements using a confidence level of 95%. A response in the camera NDVI measurements occurred at a stress coefficient of 0.37, meaning that water stress was detected by the camera system before a response in visual quality was expected. However, partially due to a large range included in the 95% confidence level of the visual quality ratings as a result of the small sample size, the stress coefficient at

which visual quality degrades and the stress coefficient at which camera-based NDVI begins to decline cannot be significantly distinguished with 95% confidence.

The TCM 500 NDVI measurements was determined to be the least sensitive measurement to the water stress coefficient. The camera system responded to a decline to the stress coefficient at a less severe degree of stress than did the TCM 500 with 95% confidence. However, a relatively small sample size of available NDVI data collected by the TCM 500 may have contributed to the low calculated breaking point.

## Conclusions

Measurement data from several types of sensors used in turfgrass management were assessed for their utility in predicting water stress in turfgrass during drought periods. Predictive models were developed using soil moisture depletion, a pole mounted camera-based NDVI, and TCM 500 NDVI each as predictors for the daily turfgrass water stress coefficient. Soil moisture depletion was found to most strongly correlate with the stress coefficient ( $R = 0.93$ ), and a simple linear model was developed with a RMSE of 0.11. Of the two methods of measuring the NDVI of turfgrass plots, the camera system was determined to be the stronger predictor of water stress as measured by the  $R^2$  (0.63) and RMSE (0.162) of the developed models. During a consistent drought, these results indicate that soil moisture data gives the most accurate prediction of turf water stress. However, further research is encouraged broadening the scope of this research to include temporary wetting events. Because soil moisture is expected to recover more quickly in response to rewetting than evapotranspiration and visual quality after significant water stress, NDVI or some combination of sensor data may be a stronger predictor of the water stress coefficient than soil moisture following a rewetting event and during turfgrass recovery.

The sensitivity of each of these sensors to the water stress coefficient was also assessed by performing iterative partial regression to determine the no-effect range. From limited data, the decline in visual quality ratings was determined to be significant below stress coefficients of 0.34. Using **Equation 4.4**, this water stress coefficient relates to a percent soil moisture depletion of 77%. Soil moisture depletion was sensitive to declines in the water stress coefficient throughout its entire range. This suggests that the rate of turfgrass water use was restricted proportionate to the percentage of available water, even during the range of readily available water content. Camera-based NDVI was the second most sensitive measurement to water stress, although it could not be determined with 95% confidence that this measurement detected water stress before visible degradation of turfgrass quality occurred. The response of camera-based NDVI to a water stress became significant at a water stress coefficient of 0.37. Again using **Equation 4.4**, this coefficient is predicted at a percent soil moisture depletion of 74.5%. The TCM 500 NDVI meter was the least sensitive sensor to water stress, with a significant response occurring only below water stress coefficients of 0.24. This relates to a percent soil moisture depletion of 85%. Between the methods of NDVI sampling, it is likely that three NDVI measurements per plot using the TCM 500 did not provide sufficient spatial resolution of sampled turfgrass area, and that the camera-based method was advantaged by its measurement of nearly the entire plot areas.

Research was conducted on drought tolerant TifTuf turfgrass planted in a fine textured Cecil sandy loam soil. The impact of drought stress on turfgrass is significantly impacted by turfgrass physiology and soil type. Additional research is recommended especially using progressive segmented regression to compare the breaking points in the water stress coefficient at which turfgrass visual quality declines across multiple turfgrass species and soil types. Such

research may provide a valuable point of comparison of turfgrass drought tolerance across species and cultivars.

## REFERENCES

- Ahamed, T., Tian, L., Jiang, Y., Zhao, B., Liu, H., & Ting, K. C. (2012). Tower remote-sensing system for monitoring energy crops; image acquisition and geometric corrections. *Biosystems Engineering*, *112*(2), 93–107.  
<https://doi.org/10.1016/j.biosystemseng.2012.03.003>
- Allen, R. G., Pereira, L. S., Raes, D., & Smith, M. (1998a). Chapter 1. Introduction to evapotranspiration. *Crop Evapotranspiration—Guidelines for Computing Crop Water Requirements [Online]*. Food and Agriculture Organization of the United Nations (FAO). *Irrigation and Drainage Paper*, 56.
- Allen, R. G., Pereira, L. S., Raes, D., & Smith, M. (1998b). Chapter 08—ETc under soil water stress conditions. *Crop Evapotranspiration-Guidelines for Computing Crop Water Requirements-FAO Irrigation and Drainage Paper*, 56.
- Behmann, J., Steinrücken, J., & Plümer, L. (2014). Detection of early plant stress responses in hyperspectral images. *ISPRS Journal of Photogrammetry and Remote Sensing*, *93*, 98–111. <https://doi.org/10.1016/j.isprsjprs.2014.03.016>
- Berg, A., Byrne, J., & Rogerson, R. (1996). An Urban Water Balance Study, Lethbridge, Alberta: Estimation of Urban Lawn Overwatering and Potential Effects on Local Water Tables. *Canadian Water Resources Journal*, *21*(4), 355–365.  
<https://doi.org/10.4296/cwrj2104355>
- Bormann, F. H., Balmori, D., Geballe, G. T., & Geballe, P. G. T. (2001). *Redesigning the American Lawn: A Search for Environmental Harmony*. Yale University Press.
- Bradski, G. (2000). The OpenCV Library. *Dr. Dobb's Journal of Software Tools*.

- Bremer, D. J., Lee, H., Su, K., & Keeley, S. J. (2011a). Relationships between Normalized Difference Vegetation Index and Visual Quality in Cool-Season Turfgrass: I. Variation among Species and Cultivars. *Crop Science*, *51*(5), 2212–2218.  
<https://doi.org/10.2135/cropsci2010.12.0728>
- Bremer, D. J., Lee, H., Su, K., & Keeley, S. J. (2011b). Relationships between Normalized Difference Vegetation Index and Visual Quality in Cool-Season Turfgrass: II. Factors Affecting NDVI and its Component Reflectances. *Crop Science*, *51*(5), 2219–2227.  
<https://doi.org/10.2135/cropsci2010.12.0729>
- Christiansen, J. E. (1942). *Irrigation by sprinkling* (Vol. 4). University of California Berkeley.
- Clayton, S. (2007). Domesticated nature: Motivations for gardening and perceptions of environmental impact. *Journal of Environmental Psychology*, *27*(3), 215–224.  
<https://doi.org/10.1016/j.jenvp.2007.06.001>
- E. Fitz Rodríguez & C. Y. Choi. (2002). Monitoring Turfgrass Quality Using Multispectral Radiometry. *Transactions of the ASAE*, *45*(3). <https://doi.org/10.13031/2013.8839>
- Fenstermaker-Shaulis, L. K., Leskys, A., & Devitt, D. A. (1997). Utilization of Remotely Sensed Data to Map and Evaluate Turfgrass Stress Associated with Drought. *Journal of Turfgrass Management*, *2*(1), 65–81. [https://doi.org/10.1300/J099v02n01\\_06](https://doi.org/10.1300/J099v02n01_06)
- Haley, M. B., Dukes, M. D., & Miller, G. L. (2007). Residential Irrigation Water Use in Central Florida. *Journal of Irrigation and Drainage Engineering*, *133*(5), 427–434.  
[https://doi.org/10.1061/\(ASCE\)0733-9437\(2007\)133:5\(427\)](https://doi.org/10.1061/(ASCE)0733-9437(2007)133:5(427))
- Harris, P. B., & Brown, B. B. (1996). The Home and Identity Display: Interpreting Resident Territoriality from Home Exteriors. *Journal of Environmental Psychology*, *16*(3), 187–203. <https://doi.org/10.1006/jevpe.1996.0016>

- Henry, M. S. (1999). Landscape Quality and the Price of Single Family Houses: Further Evidence from Home Sales in Greenville, South Carolina. *Journal of Environmental Horticulture*, 17(1), 25–30. <https://doi.org/10.24266/0738-2898-17.1.25>
- Huffman, R. L., Fangmeier, D. D., Elliot, W. J., Workman, S. R., & Schwab, G. O. (2011). *Soil and water conservation engineering*. American Society of Agricultural and Biological Engineers St. Joseph.
- Ihab E Ghali, Garry L Grabow, Rodney L Huffman, & Grady L Miller. (2010). Comparing Digital Image Analysis and other Turf Quality Measurements in the Evaluation of “SMART” Irrigation Technologies. *2010 Pittsburgh, Pennsylvania, June 20 - June 23, 2010*. 2010 Pittsburgh, Pennsylvania, June 20 - June 23, 2010. <https://doi.org/10.13031/2013.30018>
- Jespersen, D., Leclerc, M., Zhang, G., & Raymer, P. (2019). Drought Performance and Physiological Responses of Bermudagrass and Seashore Paspalum. *Crop Science*, 59(2), 778–786. <https://doi.org/10.2135/cropsci2018.07.0434>
- Katuwal, K. B., Schwartz, B., & Jespersen, D. (2020). Desiccation avoidance and drought tolerance strategies in bermudagrasses. *Environmental and Experimental Botany*, 171, 103947. <https://doi.org/10.1016/j.envexpbot.2019.103947>
- Keskin, M., Dodd, R. B., Han, Y. J., & Khalilian, A. (2003). Predicting visual quality ratings of turfgrass research plots using spectral reflectance. *ASAE Annual International Meeting, Las Vegas, NV*, 27–30.
- Kim, Y., Glenn, D. M., Park, J., Ngugi, H. K., & Lehman, B. L. (2011). Hyperspectral image analysis for water stress detection of apple trees. *Computers and Electronics in Agriculture*, 77(2), 155–160. <https://doi.org/10.1016/j.compag.2011.04.008>

- Lee, H., Bremer, D. J., Su, K., & Keeley, S. J. (2011). Relationships between Normalized Difference Vegetation Index and Visual Quality in Turfgrasses: Effects of Mowing Height. *Crop Science*, *51*(1), 323–332. <https://doi.org/10.2135/cropsci2010.05.0296>
- Mellor, D. R. (2001). *Picture Perfect: Mowing Techniques for Lawns, Landscapes, and Sports*. John Wiley & Sons.
- Milesi, C., Running, S. W., Elvidge, C. D., Dietz, J. B., Tuttle, B. T., & Nemani, R. R. (2005). Mapping and Modeling the Biogeochemical Cycling of Turf Grasses in the United States. *Environmental Management*, *36*(3), 426–438. <https://doi.org/10.1007/s00267-004-0316-2>
- Miller, G., Peacock, C., Bruneau, A., Yelverton, F., Kerns, J., Brandenburg, R., Cooper, R., & Martin, M. (2021, July 2). *Carolina Lawns: A Guide to Maintaining Quality Turf in the Landscape*. <https://content.ces.ncsu.edu/carolina-lawns>
- Morris, K. N., & Shearman, R. C. (1998). NTEP turfgrass evaluation guidelines. *NTEP Turfgrass Evaluation Workshop, Beltsville, MD*, 1–5.
- Nemani, R., Elvidge, C., & Milesi, C. (2009). Assessing the Extent of Urban Irrigated Areas in the United States. In P. Thenkabail, C. Biradar, H. Turrall, & J. Lyon (Eds.), *Remote Sensing of Global Croplands for Food Security* (Vol. 20096579, pp. 217–236). CRC Press. <https://doi.org/10.1201/9781420090109.ch8>
- Nutter, F. W. J., Gleason, M. L., Jenco, J. H., & Christians, N. C. (1993). Assessing the accuracy, intra-rater repeatability, and inter-rater reliability of disease assessment systems. *Phytopathology (USA)*.
- Oosterbaan, R. J. (2017). *Determination of Formal Confidence Intervals of the Regression Lines in Case of Linear Regression with Breakpoint (BP)*. 6.

- Oosterbaan, R. J. (2018). Crop Tolerance to Soil Salinity, Statistical Analysis of Data Measured in Farm Lands. *International Journal of Agricultural Science*, 03.  
<https://www.iaras.org/iaras/home/caijas/crop-tolerance-to-soil-salinity-statistical-analysis-of-data-measured-in-farm-lands>
- Opitz, E. M., Kiefer, J. C., Davis, W. Y., Dziegielewski, B., & Nelson, J. O. (1999). *Residential End Uses of Water*. 18.
- Ozan, L. A., & Alsharif, K. A. (2013). The effectiveness of water irrigation policies for residential turfgrass. *Land Use Policy*, 31, 378–384.  
<https://doi.org/10.1016/j.landusepol.2012.08.001>
- Peacock, C. H., & Bruneau, A. H. (2006). *Water Requirements of North Carolina Turfgrasses: A Guide for Irrigation Technicians and Turfgrass Managers*. NC Cooperative Extension Service.
- Peñuelas, J., Filella, I., Biel, C., Serrano, L., & Savé, R. (1993). The reflectance at the 950–970 nm region as an indicator of plant water status. *International Journal of Remote Sensing*, 14(10), 1887–1905. <https://doi.org/10.1080/01431169308954010>
- Pinnix, G. D., & Miller, G. L. (2019a). Crop Coefficients for Tall Fescue and Hybrid Bermudagrass in the Transition Zone. *Crop, Forage & Turfgrass Management*, 5(1), 190013. <https://doi.org/10.2134/cftm2019.02.0013>
- Pinnix, G. D., & Miller, G. L. (2019b). Comparing evapotranspiration rates of tall fescue and bermudagrass in North Carolina. *Agricultural Water Management*, 223, 105725.  
<https://doi.org/10.1016/j.agwat.2019.105725>
- Reda, I., & Andreas, A. (2004). Solar position algorithm for solar radiation applications. *Solar Energy*, 76(5), 577–589. <https://doi.org/10.1016/j.solener.2003.12.003>

- Reza Aurasteh, M. Jafari, & L.S. Willardson. (1984). Residential Lawn Irrigation Management. *Transactions of the ASAE*, 27(2), 470–472. <https://doi.org/10.13031/2013.32812>
- Ritchie, G., Sullivan, D., Perry, C., Hook, J., & Bednarz, C. (2008). *Preparation of a Low-Cost Digital Camera System for Remote Sensing*. <https://doi.org/10.13031/2013.25359>
- Robbins, P., Polderman, A., & Birkenholtz, T. (2001). Lawns and Toxins: An Ecology of the City. *Cities*, 18(6), 369–380. [https://doi.org/10.1016/S0264-2751\(01\)00029-4](https://doi.org/10.1016/S0264-2751(01)00029-4)
- Ross, E. A., & Hardy, L. A. (1997). National Engineering Hand Book, Part 652 Irrigation Guide. *National Resource Conservation Service, National Cartography and Geospatial Center, Fort Worth, Texas, US.*
- Royer, J. M., & Vachaud, G. (1975). Field Determination of Hysteresis in Soil-Water Characteristics. *Soil Science Society of America Journal*, 39(2), 221–223. <https://doi.org/10.2136/sssaj1975.03615995003900020006x>
- Rumpf, T., Mahlein, A.-K., Steiner, U., Oerke, E.-C., Dehne, H.-W., & Plümer, L. (2010). Early detection and classification of plant diseases with Support Vector Machines based on hyperspectral reflectance. *Computers and Electronics in Agriculture*, 74(1), 91–99. <https://doi.org/10.1016/j.compag.2010.06.009>
- Sisser, J. M., Nelson, K. C., Larson, K. L., Ogden, L. A., Polsky, C., & Chowdhury, R. R. (2016). Lawn enforcement: How municipal policies and neighborhood norms influence homeowner residential landscape management. *Landscape and Urban Planning*, 150, 16–25. <https://doi.org/10.1016/j.landurbplan.2016.02.011>
- Stafford, B. (2021). *Pysolar Documentation*. 27.
- Sullivan, D., Zhang, J., Kowalewski, A. R., Peake, J. B., Anderson, W. F., Waltz, F. C., & Schwartz, B. M. (2017). Evaluating Hybrid Bermudagrass Using Spectral Reflectance

- under Different Mowing Heights and Trinexapac-ethyl Applications. *HortTechnology*, 27(1), 45–53. <https://doi.org/10.21273/HORTTECH03436-16>
- Thompson, G. L., & Kao-Kniffin, J. (2017). Applying Biodiversity and Ecosystem Function Theory to Turfgrass Management. *Crop Science*, 57(S1), S-238-S-248. <https://doi.org/10.2135/cropsci2016.05.0433>
- Trappe, J., Patton, A. J., & Richardson, M. (2008). Clipping yield and scalping tendency differ for bermudagrass and zoysiagrass cultivars. *Arkansas Turfgrass Rpt*, 56, 153–157.
- Trenholm, L. E., Carrow, R. N., & Duncan, R. R. (1999). Relationship of Multispectral Radiometry Data to Qualitative Data in Turfgrass Research. *Crop Science*, 39(3), [cropsci1999.0011183X003900030025x](https://doi.org/10.2135/cropsci1999.0011183X003900030025x). <https://doi.org/10.2135/cropsci1999.0011183X003900030025x>
- Williams, D. W., Powell, A. J., Vincelli, P., & Dougherty, C. T. (1996). Dollar Spot on Bentgrass Influenced by Displacement of Leaf Surface Moisture, Nitrogen, and Clipping Removal. *Crop Science*, 36(5), [cropsci1996.0011183X003600050039x](https://doi.org/10.2135/cropsci1996.0011183X003600050039x). <https://doi.org/10.2135/cropsci1996.0011183X003600050039x>
- Xiang, H., & Tian, L. (2011). An automated stand-alone in-field remote sensing system (SIRSS) for in-season crop monitoring. *Computers and Electronics in Agriculture*, 78(1), 1–8. <https://doi.org/10.1016/j.compag.2011.04.006>
- Zhang, Y., Yu, Q., Liu, C., Jiang, J., & Zhang, X. (2004). Estimation of Winter Wheat Evapotranspiration under Water Stress with Two Semiempirical Approaches. *Agronomy Journal*, 96(1), 159–168. <https://doi.org/10.2134/agronj2004.1590>